SHAPE OPTIMIZATION OF NOTCHED PARTS

FOR MAXIMUM FATIGUE LIFE

by

Volkan Erkol

B.S., Mechanical Engineering, Istanbul University, 2012

Submitted to the Institute for Graduate Studies in

Science and Engineering in partial fulfillment of

the requirements for the degree of

Master of Science

Graduate Program in Mechanical Engineering

Boğaziçi University

2016

SHAPE OPTIMIZATION OF NOTCHED PARTS

FOR MAXIMUM FATIGUE LIFE

APPROVED BY:

Prof. Fazıl Önder Sönmez   . . . .

(Thesis Supervisor)

Assoc. Prof. Nuri Ersoy   . . . .

Prof. Bülent Ekici   . . . .

DATE OF APPROVAL: 13.07.2016

ACKNOWLEDGEMENTS

I would like to express my gratitude to my thesis advisor Prof. Fazıl Önder Sönmez for his support, guidance and helpfulness during my thesis study.

I would like to thank to my family for their encouragements and supports for the challenges I encountered during my thesis study.

ABSTRACT

SHAPE OPTIMIZATION OF NOTCHED PARTS FOR MAXIMUM FATIGUE LIFE

The objective of the thesis study is to develop a shape optimization procedure to maximize fatigue life of notched components under in-phase or out-of-phase multiaxial loading conditions. Two critical-plane fatigue assessment models, Smith-Watson-Topper (SWT) and Fatemi-Socie (FS), are used to estimate the fatigue life of the parts. Two different notch geometry, fillet and groove, is considered. Considering that typical machine components under fluctuating loads are designed to endure long fatigue lives, no significant plastic deformation is expected to occur at the notch. Accordingly, the part is assumed to be linear elastic. Using ANSYS Parametric Design Language, codes are developed to carry out structural analysis of the parts, evaluate the fatigue life according to SWT and FS models, and optimize the notch shapes. First, the validity of the models for the particular notch geometries is investigated by comparing their predictions with the experimental results reported in the literature for circular notches. The results are generally accurate within acceptable limits. The boundary line of the notch is defined by spline curves passing through key points and the positions of the key points are selected as optimization variables. The objective function to be minimized is chosen as the SWT or FS damage parameter, which is inversely proportional to fatigue life. Using a modified simulated annealing algorithm, optimum notch shapes are obtained for notched shafts subjected to different combinations of torsional, bending, and axial loadings. Significant improvements are observed in fatigue life with the optimum notch shapes in comparison to circular notches.

ÖZET

MAKSİMUM YORULMA ÖMRÜ İÇİN ÇENTİKLİ PARÇALARIN ŞEKİL ENİYİLEMESİ

Bu tezde çalışmasında, aynı fazdaki ve farklı fazdaki çok eksenli yük durumları için, çentikli parçaların yorulma ömrünü arttırmak amacıyla şekil eniyileme yöntemi uygulanmıştır. Parçaların yorulma ömrünü tahmin etmek amacıyla, iki farklı kritik-düzlem yorulma değerlendirme modeli, Smith-Watson-Topper (SWT) ve Fatemi-Socie (FS) modelleri kullanılmıştır. İki farklı çentik içeren geometri, yuvarlatma ve oluk, düşünülmüştür. Tekrarlı yüklere maruz makine parçalarının uzun yorulma ömürleri için tasarlandığı düşünülerek, çentik bölgesinde önemli bir plastik deformasyon olmadığı varsayılmıştır. Bu nedenle, parçanın lineer elastik bir davranışta olduğu kabul edilmiştir. Parçaların yapısal analizini gerçekleştirmek, SWT ve FS modelleriyle yorulma ömrünü belirlemek ve eniyileme gerçekleştirmek için ANSYS Parametrik Tasarım Dili programında kodlar geliştirilmiştir. Literatürde dairesel çentikler için rapor edilmiş deneysel sonuçlar ile tahmini sonuçlar karşılaştırılarak, belirli tipteki çentikler için modellerin geçerliliği araştırılmıştır. Sonuçlar genellikle kabul edilebilir limit aralığındadır. Çentiğin sınır çizgisi, eğriden geçen anahtar noktaları ile tanımlanmıştır ve anahtar noktalarının konumları eniyileme değişkenleri olarak seçilmiştir. Azaltılması amaçlanan gaye fonksiyonu SWT ya da FS hasar parametresi olarak seçilmiştir ve hasar parametreleri yorulma ömrüyle ters orantılıdır. Değiştirilmiş bir tavlama simulasyonu algoritması kullanarak, burulma, eğme ve eksenel yüklemelerin değişik kombinasyonlarından oluşan yüklemelere maruz kalan çentikli şaftlar için ideal çentik şekilleri elde edilmiştir. Dairesel çentiklerle kıyaslandığında, ideal çentik şekilleri için yorulma ömürlerinde önemli ölçüde gelişmeler elde edilmiştir.

TABLE OF CONTENTS

LIST OF FIGURES

LIST OF TABLES

LIST OF SYMBOLS

A, A_t	Acceptability
A_{ijkl}	Elastic localization tensor
A_s	Search area
b	Axial fatigue strength exponent
b_0	Torsional fatigue strength exponent
c	Axial fatigue ductility exponent
c_0	Torsional fatigue ductiliy exponent
D	Damage
E	Modulus of elasticity
$E_e^{'}, E_f^{'}$	Axial fatigue strength, axial fatigue toughness
f_c, f_t	Cost function of a newly generated configuration
f_p	Previous cost function
f_h, f_l	The highest cost function, the lowest cost function
G	Shear modulus
K_f	Fatigue notch factor
K_t	Stress concentration factor
L_k	Length of a k th Markov chain
l_i, m_i, n_i	Direction cosines ($i = 1, 2, 3$)
m	Number of moving key points
n	Number of design varibles
N	Number of initial configurations
N_A	Number of cycles associated with axial loadings
N_f	Number of cycles to failure
N_T	Number of cycles associated with torsional loadings
N_w	Number of worst configurations
$P_{d,c}$	Damage parameter of current configuration
$P_{d,o}$	Damage parameter of original shaped component
R_{max}	Maximum moving distance

R_{max_i}	Initial moving distance
S_b, S_t	Normal fatigue strength, shear fatigue strength
t_A, t_B	Shear fatigue strength for case A, case B
T_k	Temperature parameter
$W_e{}', W_f{}'$	Shear fatigue strength, shear fatigue toughness
α_k	Temperature control parameter
β	Critical plane angle
$\varepsilon_1, \varepsilon_2, \varepsilon_3$	Principal strains
ε_a	Normal strain amplitude
$\varepsilon_f{}'$	Axial fatigue ductility coefficient
$\varepsilon_x, \varepsilon_y, \varepsilon_z, \gamma_{xy}, \gamma_{xz}, \gamma_{yz}$	Strain components
$\Delta\epsilon$	Total strain range
$\Delta\epsilon_e, \Delta\epsilon_p$	Elastic strain range, plastic strain range
γ_a	Shear strain amplitude
$\gamma_f{}'$	Torsional fatigue ductility coefficient
$\gamma_{max}, \Delta\varepsilon_{nm}$	Maximum shear strain amplitude
υ	Poisson's ratio
υ_e, υ_p	Elastic Poisson's ratio, plastic Poisson's ratio
$\sigma_1, \sigma_2, \sigma_3$	Principal stresses
σ_a, σ_m	Alternating stress, mean stress
σ_{eqv}	Equivalent stress
$\sigma_f{}'$	Axial fatigue strength coefficient
$\sigma_{H,a}$	Hydrostatic stress amplitude
$\sigma_h(t)$	Hydrostatic stress
$\sigma_{ij}(t)$	Microscopic stress tensor
σ_{max}	Maximum normal stress amplitude
$\sigma_{n,max}$	Maximum normal stress
$\sigma_x, \sigma_y, \sigma_z, \tau_{xy}, \tau_{xz}, \tau_{yz}$	Stress components
σ_t	Ultimate tensile strength
σ_y	Yield stress

τ_a	Shear stress amplitude
$\tau_f{}'$	Torsional fatigue strength coefficient
$\tau_{(t)}$	Local shear stress
ρ_{ij}	Local residual stress tensor

LIST OF ACRONYMS/ABBREVIATIONS

2D	Two Dimensional
3D	Three Dimensional
APDL	ANSYS Parametric Design Language
DSA	Direct Search Simulated Annealing
FE	Finite Element
FEM	Finite Element Modeling
FS	Fatemi-Socie
FS_{max}	Maximum Fatemi-Socie Parameter
SA	Simulated Annealing
SWT	Smith-Watson-Topper
SWT_{max}	Maximum Smith-Watson-Topper Parameter
VSE	Virtual Strain Energy

1. INTRODUCTION

Many engineering components are subjected to fluctuating loads; therefore they should be designed such that they are resistant to fatigue fracture. These components usually experience complex multiaxial stresses and strains. Fatigue evaluation should therefore be based on a generally applicable and reliable fatigue model, which can accurately predict fatigue life under multiaxial loading conditions. Loading may be proportional or non-proportional, where fluctuation of individual loads is out-of-phase. Engineering components such as axles, shafts, turbine blades unavoidably have notches such as fillets, grooves, holes, or other geometric discontinuities, which lead to stress concentrations. Because locally high stresses develop at the notches, fatigue cracks most likely initiate at these locations; for that reason, they are considered to be the most critical regions in fatigue design.

Fatigue strength of a component can significantly be enhanced by just optimizing the shapes of notches without using a stronger material or increasing the size of the component. In previous studies of notch shape optimization, fillets in plates [1-7] and bars [8-10], fillets in other types of structures [11-13], holes [4, 5, 7, 14-26], connecting rods [20, 27], grooves [25], gears [28] and notches in bars [24] were considered. The parts considered in those studies were under various loading conditions like pure axial loading [2-11, 13, 15, 17, 20, 22, 25-27], biaxial loading [1, 5, 7, 14, 16, 18, 19, 21, 23, 24], pure bending [3, 28], combination of tension and torsion [24], or pressure [12]. In the studies considering combined loading, proportional (in-phase) [5, 11, 18, 19, 21-23, 27] and non-proportional (out-of-phase) torsion-tension or biaxial [24] loading conditions were taken into account. The notch shapes were optimized with the objective of minimizing the area or volume of the part [2, 20, 27], the stress concentration factor, K_t, [3], the stress intensity factor, K, [4, 17, 19], fatigue stress concentration factor (fatigue notch factor), K_f, [8], the peak equivalent stress [1, 6, 7, 9, 10, 12, 24], the peak tensile stress [26, 28], the peak compressive stress [13], the maximum principal stress [14, 17, 23], the damage [10], maximizing fracture strength [14] or maximizing the fatigue life [5, 11, 15- 19, 21-23, 25, 26]. In shape optimization studies, the notch shapes were defined in terms of optimization variables, which were the coordinates of the boundary nodes in the FE models of the parts

[1-5, 7, 9-11, 13-17, 21, 24, 26], the key points of spline curves defining the boundary [6, 8, 22], or the geometric parameters of parts such as dimensions [12, 18-20, 23, 25, 27, 28]. Effectiveness of an optimization method depends on the search algorithm used to locate the optimum configuration. Some researchers employed stochastic global search algorithms like genetic algorithms [11, 12, 20, 23], direct search-simulated annealing algorithm [6], some others used gradient [1, 2, 7, 9, 10, 17-19, 21, 24, 25, 28] or non-gradient [3-5, 8, 11, 13-18, 21, 22, 26, 27] based local search algorithms.

In the previous studies, either unidirectional or proportional combined loading cases were considered. In the thesis, the models to be optimized are subjected to multiaxial in-phase or out-of-phase loadings. Unlike most of the previous studies, the objective is directly to maximize the fatigue life of the notched parts. The fatigue assessment models used to estimate the fatigue life of the part are verified for the particular notch geometries considered in this study.

In multiaxial fatigue design problems, notch geometries, loading histories and stress-strain states are usually complex. Even in the case of uniaxial loading, a multiaxial stress state develops at a notch. In case of uniaxial and proportional loading, fatigue life prediction can be performed using S-N curve (Wöhler curve). However, many engineering structures are generally subjected to multiaxial and proportional or non-proportional loading conditions. The usage of S-N curve is not appropriate for these loading conditions. Critical plane-based fatigue models are preferred as in the present study to account for the effect of multiaxiality and proportionality or non-proportionality.

In this thesis study, notches are considered as critical zones for fatigue crack initiation in engineering parts and their shapes are optimized. Notch boundary is defined by spline curves passing through key points. A modified simulated annealing algorithm is used to find the optimum positions of the key points so that the fatigue life will be maximum. In each iteration, the search algorithm generates new positions for the key points, thus a new shape. Whenever the shape is varied during optimization, the fatigue life needs to be evaluated. Considering that SWT or FS damage parameter is inversely proportional to fatigue life, maximizing fatigue life yields the same result as minimizing the damage parameter. In order to avoid unnecessary calculations during iterations, the

objective function to be minimized is selected as the maximum damage parameter (SWT or FS) in the part. Based on the stress and strain states determined via finite element analysis, the maximum damage parameter value is evaluated for each new shape generated according to the decision criteria of the algorithm. Applicability of the critical plane models to the parts with a particular notch geometry, fillet or groove, under the given multiaxial loading is investigated by comparing their predictions to experimental results obtained in previous studies for circular notch shapes.

The fatigue assessment models that require a geometry factor for the notch such as fatigue stress concentration factor, K_f, cannot be incorporated into general shape optimization procedures, considering that shape of the notch changes in each iteration and geometry factors of free-formed shapes are not readily available. Critical plane models have also a limited use, considering that they are local approaches, that means fatigue life is evaluated based on the state of a single material point. It is known that not only peak stress or strain level affects the fatigue life but also the stress gradient and size of the notch [29]. The effect of notch size can be taken into account by notch sensitivity factor, q. According to Neuber, q depends on a material parameter, ρ, as well as the radius of curvature at the notch root, r, as $q = 1/\left(1 + \sqrt{\rho/r}\right)$ and $K_f = 1 + (K_t - 1)q$ [30]. Accordingly, if the notch radius, r, is large, i.e for blunt notches, the value of q approaches 1.0, and then the difference between the fatigue notch factor, K_f, and the stress concentration factor, K_t, becomes very small. In that case, evaluation of fatigue life based on local stress and/or strain state yields accurate results. On the other hand, for sharp notches, q takes a small value as the formula implies; K_f will then take a value much smaller than K_t; in that case a fatigue assessment method using local stresses, e.g. $K_t \sigma_{nom}$, will highly underestimate the fatigue life. Considering that shape optimization of notches results in very smooth curves, in other words a very high radius of curvature at the critical point, use of a local approach like critical plane methods is justifiable.

There are many critical plane-based approaches about fatigue failure in the literature [31-36]. The critical plane is defined as the plane where a damage parameter takes the maximum value at a material point, which is subjected to a fluctuating load. It is assumed that fatigue cracks initiate and grow in the critical plane. Critical plane models are

characteristically evaluated in the maximum normal stress/strain plane or the maximum shear stress/strain plane. There are stress-based critical plane models for high cycle fatigue. For low cycle fatigue in which significant plastic deformations occur, strain-based models were proposed. Besides, there is the third category of critical plane models in which both stress and strain terms are included such as the Smith-Watson-Topper [SWT] parameter [37] for tensile-dominated fatigue failure and the Fatemi-Socie [FS] parameter [38] for shear-dominated fatigue failure. The SWT parameter-life and FS parameter-life equations can be solved to obtain fatigue life of an engineering component subjected to cyclic loading. Therefore, in the thesis study, the SWT and FS parameters are used for tensile and shear dominant fatigue failure, respectively.

2. MULTIAXIAL FATIGUE MODEL

Many engineering components are subjected to multiaxial cyclic loadings throughout their lifetimes. Multiaxial fatigue damage can be evaluated using the criteria in which the damage is expected to occur due to the normal/shear stresses or strains. Accordingly, the multiaxial fatigue models can be divided into three categories, namely, stress, strain and energy-based damage models. Stress-based models are usually developed for high-cycle fatigue in which plastic deformations can be neglected, while strain-based models preferred for low-cycle fatigue take into account the plasticity.

2.1. Stress-Based Fatigue Damage Model

McDiarmid [39] proposed a multiaxial high cycle fatigue damage criterion choosing the critical plane as the plane of having the maximum shear stress amplitude. The maximum normal stress on that plane is included in the criterion.

$$\frac{\tau_a}{t_{A,B}} + \frac{\sigma_{n,max}}{2\sigma_t} = 1 \tag{2.1}$$

where τ_a is the shear stress amplitude, t_A or t_B is the shear fatigue strength selected depending on the cracking mode, case A and case B, respectively. $\sigma_{n,max}$ is the maximum normal stress on the plane of maximum shear stress plane, σ_t is the ultimate tensile strength.

Dang Van [40] proposed a fatigue limit criterion considering that fatigue cracks occurs in microscopic (local) scale after local plastic deformation of grains. Because of the difference between the microscopic and macroscopic stress-strain state, the model was divided into two scales. In macroscopic scale, an elementary volume was presented to obtain homogeneous macroscopic stress-strain state. In microscopic scale, the grain size was considered to formulate the parameter where microscopic stresses and strains are not homogeneous.

$$D = max\left(\frac{\tau_{(t)}}{\alpha - \beta\sigma_h(t)}\right) \tag{2.2}$$

where $\tau_{(t)}$ is local (microscopic) shear stress, $\sigma_h(t)$ is hydrostatic stress and α, β are constants. When the variable D is greater than 1 ($D > 1$), the fatigue failure happens.

There is a relation between the microscopic and macroscopic stresses and it is used to obtain the local shear stress $\tau_{(t)}$. The relation is given by the following equation:

$$\sigma_{ij}(t) = A_{ijkl}\Sigma_{kl}(t) + \rho_{ij} \tag{2.3}$$

where $\sigma_{ij}(t)$ is the microscopic stress tensor, A_{ijkl} is the elastic localization tensor and ρ_{ij} is the local residual stress tensor. According to the Tresca maximum shear stress theory, the local shear stress is obtained by the following equation:

$$\tau_{(t)} = max|\sigma_i(t) - \sigma_j(t)| \tag{2.4}$$

where σ_i and σ_j are the principal stresses.

Carpinteri and Spagnoli [41] proposed a damage criterion including the maximum normal stress and maximum shear stress amplitude terms on the critical plane. The fatigue damage criterion is given by the following equation:

$$\left(\frac{\sigma_{n,max}}{S_b}\right)^2 + \left(\frac{\tau_a}{S_t}\right)^2 \leq 1 \tag{2.5}$$

where $\sigma_{n,max}$ is the maximum normal stress and τ_a is the shear stress amplitude, S_t is shear stress fatigue limit, S_b is the normal stress fatigue limit for fully reversed loadings. Mean stress effect, σ_m is included in the maximum normal stress term as

$$\sigma_{n,max} = \sigma_m + \sigma_a \tag{2.6}$$

Liu and Mahadevan [42] proposed a multiaxial high cycle fatigue criterion and life prediction model. Firstly, the damage parameter was presented under fully reversed bending-torsion loading condition.

$$\sqrt{\left(\frac{\sigma_a}{S_b}\right)^2 + \left(\frac{\tau_a}{S_t}\right)^2 + \alpha\left(\frac{\sigma_{H,a}}{S_b}\right)^2} = \beta \tag{2.7}$$

where σ_a, τ_a, $\sigma_{H,a}$ are the normal, shear and hydrostatic stress amplitude, respectively. S_t, S_b is shear stress fatigue limit and the normal stress fatigue limit for fully reversed loadings, respectively. α and β are material parameters. In case I, the angle between the critical plane where the most damage is expected to occur and the fatigue fracture plane where macro cracks actually occur was assumed to be zero. Then, the parameters α, β were found as a function of fatigue limit ratio (S_t/S_b).

$$\alpha = 9\left[\left(\frac{S_t}{S_b}\right)^2 - 1\right] \tag{2.8}$$

$$\beta = \frac{S_t}{S_b} \tag{2.9}$$

In case II, the angle was $45°$ and the parameters were also derived for this condition.

In a general case, a critical plane should be obtained for zero effect of the hydrostatic stress amplitude. Therefore, the damage parameter was rewritten in general form.

$$\sqrt{\left(\frac{\sigma_a}{S_b}\right)^2 + \left(\frac{\tau_a}{S_t}\right)^2} = \beta \tag{2.10}$$

After substitution and solving of equations, the following equations were obtained for the material parameter, β and the orientation angle, θ.

$$\beta = (\cos^2(2\theta)a^2 + \sin^2(2\theta))^{1/2} \tag{2.11}$$

$$\cos(2\theta) = \frac{-2 + \sqrt{4 - 4(1/a^2 - 3)(5 - 1/a^2 - 4a^2)}}{2(5 - 1/a^2 - 4a^2)} \tag{2.12}$$

where $a = S_t/S_b$

2.2. Strain-Based Fatigue Damage Model

Socie *et al.* [43] proposed modifications for two strain-based fatigue parameters to include mean stress effects. Uniaxial and biaxial fatigue tests were conducted. In axial tests of solid smooth specimens, fatigue lives were obtained for both 0.1 and 1.0 mm crack lengths and the strain life equations was fitted for both of them.

For 1.0 mm crack length, the modified strain-life equation takes the following form

$$\frac{\Delta\epsilon}{2} = \frac{\sigma'_f}{E}\left(2N_f\right)^b + 0.9\epsilon'_f\left(2N_f\right)^c \tag{2.13}$$

where $\Delta\epsilon/2$ is the axial strain amplitude, σ'_f is the fatigue strength coefficient, ϵ'_f is the fatigue ductility coefficient, b, c are the fatigue strength, ductility exponents, respectively. N_f is the life up to the given crack lengths (1.0 mm). The modified curves are shown in Figure 2.1. As shown in the figure, there is a small difference between the life for 1.0 mm crack length and for failure.
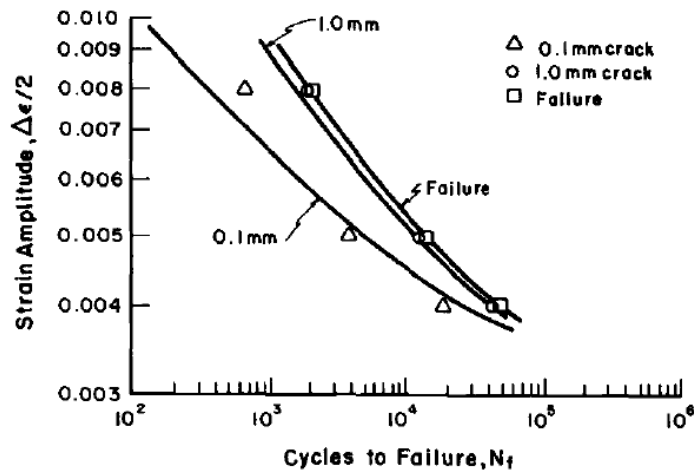
Figure 2.1. Strain-life relationship for uniaxial loadings [43].

The modification of the parameters was obtained including mean stress effects and the parameters versus the life up to 1.00 mm crack were shown in the paper.

The modification to the first parameter was given by the following equation:

$$\gamma^*{}_p + 0.4\epsilon^*{}_{p,n} + \frac{\sigma^*{}_n}{E} = 1.6\epsilon'{}_f \left(2N_f\right)^c \tag{2.14}$$

The modification to the second parameter takes the following form

$$\hat{\gamma}_p + \hat{\epsilon}_{p,n} + \frac{\hat{\sigma}_n}{E} = 1.75\epsilon'{}_f \left(2N_f\right)^c \tag{2.15}$$

where $\gamma^*{}_p$ and $\hat{\gamma}_p$ are plastic shear strain amplitudes on γ^* and $\hat{\gamma}$ planes, respectively, $\epsilon^*{}_{p,n}$ and $\hat{\epsilon}_{p,n}$ are normal plastic strain amplitudes on γ^* and $\hat{\gamma}$ planes, respectively, $\sigma^*{}_n$ and $\hat{\sigma}_n$ are normal mean stresses on γ^* and $\hat{\gamma}$ planes, respectively. E is the elastic modulus.

Brown and Miller [44] proposed a theory for multiaxial fatigue damage in which fatigue life was presented as a function of strain. According to the fatigue crack growth mechanics, which is determined by the direction of shear crack growth, case A for growth along the surface and case B for growth into surface, the maximum shear strain, γ_{max} and the normal strain in the plane of maximum shear strain, ε_n were related in the model as

$$\gamma_{max} = f(\varepsilon_n) \tag{2.16}$$

Using the equation, the relation between the maximum shear strain amplitude and the normal strain amplitude in the maximum shear plane was represented at different constant lives.

Fatemi and Socie [38] proposed a multiaxial fatigue damage parameter by changing the normal strain term in the Brown and Miller model by the normal stress term to predict fatigue life for both in-phase and out-of phase loadings. The parameter includes both the maximum shear strain amplitude and the maximum normal stress on the shear plane. Tests

were performed using hot-rolled 1045 steel thin-walled tubular specimens subjected to in-phase and out-of-phase loadings. Cracks were observed to initiate on the maximum shear strain planes and propagate perpendicular to the maximum normal stress direction under pure axial loads, while both initiation and propagation observed on the maximum shear strain planes under pure torsional loads. For in-phase tension-torsion loadings, initiation and early crack growth were observed on the maximum shear strain planes. Propagation continued on the plane perpendicular to the maximum principal stress direction after about half of the life. Fatemi-Socie parameter, FS, is defined as

$$FS = \Delta\varepsilon_{nm}\left[1 + k\frac{\sigma_{n,max}}{S_y}\right] \tag{2.17}$$

where k is a material constant obtained from uniaxial and torsional test data, $\Delta\varepsilon_{nm}$ is the amplitude of shear strain directed along $\boldsymbol{e_m}$ direction acting on a plane with unit normal $\boldsymbol{e_n}$, $\sigma_{n,max}$ is the peak normal stress on this plane, S_y is the yield stress, which is introduced to make the dimensions of the terms compatible. In this model, fatigue cracks are expected to occur on the plane in which FS takes its maximum value. The maximum FS parameter is related to fatigue life by the following equation [45]:

$$FS_{max} = \frac{\tau'_f}{G}(2N_f)^{b_0} + \gamma'_f(2N_f)^{c_0} \tag{2.18}$$

where $\tau_f{}'$ is torsional fatigue strength coefficient, G is shear modulus, b_0 is torsional fatigue strength exponent, $\gamma_f{}'$ is torsional fatigue ductility coefficient, c_0 is torsional fatigue ductility exponent, and N_f is the number of cycles to failure. For fully reversed torsion loading, $\sigma_{n,max}$ is zero; the left hand side of the equation then becomes equal to the alternating shear strain.

The FS parameter can also be related to fatigue life using uniaxial fatigue data [38] as:

$$\gamma_{max}\left(1 + k\frac{\sigma_{n,max}}{\sigma_y}\right)$$

$$= (1 + v_e)\frac{\sigma'_f}{E}(2N_f)^b + \frac{k}{2}(1 + v_e)\frac{\sigma'^2_f}{E\sigma_y}(2N_f)^{2b} \qquad (2.19)$$

$$+ (1 + v_p)\varepsilon'_f(2N_f)^c + \frac{k}{2}(1 + v_p)\frac{\varepsilon'_f\sigma'_f}{\sigma_y}(2N_f)^{b+c}$$

where σ'_f is the fatigue strength coefficient, ε'_f is the fatigue ductility coefficient, v_e and v_p are the elastic and plastic Poisson's ratios, respectively.

This model accounts for the effect of mean stress, because the peak normal stress term, $\sigma_{n,max}$, can be expressed as the sum of alternating ($\sigma_{a,n}$) and mean ($\sigma_{m,n}$) normal stress. An increase in $\sigma_{m,n}$ results in increase in the FS parameter and thus decrease in fatigue life.

2.3. Energy-Based Fatigue Damage Model

Smith *et al.* [37] introduced a fatigue damage parameter given by

$$SWT = \sigma_{max}\varepsilon_a \qquad (2.20)$$

where σ_{max} is the peak normal stress, or the maximum tensile principle stress in multiaxial loading, ε_a is the alternating normal strain, or the maximum alternating normal strain in multiaxial loading. Knowing that $\sigma_{max} = \sigma_m + \sigma_a$, the model includes the mean stress effect. According to the model, the fatigue cracks initiate at the plane where the SWT parameter is maximum.

The Basquin equation relating alternating elastic stress, σ_a, to fatigue life, N_f, for fully reversed pure axial loading is given by

$$\sigma_a = \sigma'_f(2N_f)^b \qquad (2.21)$$

Coffin-Manson equation [46] relates uniaxial alternating strain, which is sum of alternating elastic and plastic strains, to fatigue life as

$$\varepsilon_a = \varepsilon_a^e + \varepsilon_a^p = \frac{\sigma'_f}{E}(2N_f)^b + \varepsilon'_f(2N_f)^c \qquad (2.22)$$

where ε_a^e the alternating elastic strain, and ε_a^p is the alternating plastic strain. Multiplying both sides of Equations (2.21) and (2.22) one obtains

$$\sigma_a \varepsilon_a = \frac{(\sigma'_f)^2}{E}(2N_f)^{2b} + \sigma'_f \varepsilon'_f(2N_f)^{b+c} \qquad (2.23)$$

where σ'_f is axial fatigue strength coefficient, E is modulus of elasticity, b is axial fatigue strength exponent, ε'_f is axial fatigue ductility coefficient and c is axial fatigue ductility exponent. Equation (2.23) is valid for uniaxial loading. Smith *et al.* [37] replaced alternating elastic stress, σ_a, by peak tensile stress σ_{max}. For fully-reversed fatigue loading conditions, where mean stresses are zero, σ_{max} becomes equal to the normal stress amplitude, σ_a. In this formulation, multiaxial stress state is accounted for as well as the effect of mean stress. The maximum SWT parameter is then related to fatigue life as

$$SWT_{max} = \frac{(\sigma'_f)^2}{E}(2N_f)^{2b} + \sigma'_f \varepsilon'_f(2N_f)^{b+c} \qquad (2.24)$$

Based on the experimental results, the validity of the proposed model was evaluated for various metallic materials which were small and smooth specimens [37]. The model was found to be applicable for crack initiation and early crack propagation.

Liu [47] proposed a virtual strain energy (VSE)-based multiaxial fatigue model associated with the critical plane concept. For Mode I tensile failure, the critical plane was determined by the maximum normal (principal) stress and strain. For Mode II shear failure, the critical plane was associated with the one experiencing the maximum shear stress and strain. Two VSE parameters were introduced according to the type of failure. The validity of proposed model evaluated with the experimental results of two materials, Type 304

stainless steel and SAE 1045 steel. The strain-life relation can be expressed by the Coffin-Manson equation as

$$\Delta\varepsilon = \Delta\varepsilon_p + \Delta\varepsilon_e = A\left(N_f\right)^{-a} + B(N_f)^{-b} \tag{2.25}$$

where $\Delta\epsilon$, $\Delta\varepsilon_p$, $\Delta\varepsilon_e$ are the total, plastic and elastic strain ranges, respectively, A, B, a, b are the material constants. The virtual strain energy parameter was defined as

$$\Delta W = \Delta\sigma\Delta\varepsilon = E\Delta\varepsilon_e\left(\Delta\varepsilon_p + \Delta\varepsilon_e\right), \qquad (\Delta\sigma = E\Delta\varepsilon_e) \tag{2.26}$$

Substituting Equation (2.25) into Equation (2.26), the following virtual strain energy parameter can be obtained as

$$\Delta W = EAB(N_f)^{a+b} + EB^2(N_f)^{2b} \tag{2.27}$$

For Mode I failure, the parameter (ΔW_I) was given as the combination of two quantities in the plane of maximum normal strain energy quantity

$$\Delta W_I = (\Delta W)_{n,max} + (\Delta W)_s \tag{2.28}$$

For Mode II failure, the parameter (ΔW_{II}) was given as the combination of two quantities in the plane of maximum shear strain energy quantity

$$\Delta W_{II} = (\Delta W)_n + (\Delta W)_{s,max} \tag{2.29}$$

Pan *et al.* [48] proposed a modified strain energy density parameter based on the critical plane for prediction of multiaxial fatigue life. The comparison between proposed model and existing test results was made for SAE 1045 and 304 stainless steel. They noticed that the effect of shear-based strain energy is different from the effect of axial-based strain energy on the fatigue life of specimen. Therefore, they modified Glinka's model adding two material constants, β_1 and β_2 to the strain energy term in normal direction of formulation.

$$W^* = \frac{\Delta\gamma_{12}}{2}\frac{\Delta\sigma_{12}}{2} + \beta_1\beta_2\frac{\Delta\varepsilon_{22}}{2}\frac{\Delta\sigma_{22}}{2} \tag{2.30}$$

The material constants can be determined from uniaxial and pure torsional fatigue tests.

$$\beta_1 = \frac{\gamma_f{}'}{\varepsilon_f{}'} \qquad \text{and} \qquad \beta_2 = \frac{\sigma_f{}'}{\tau_f{}'} \tag{2.31}$$

where $\varepsilon_f{}'$ and $\gamma_f{}'$ are the axial and torsional fatigue ductility coefficients, respectively and $\sigma_f{}'$ and $\tau_f{}'$ are the axial and torsional fatigue strength coefficients, respectively.

Varvani-Farahani [49] proposed a multiaxial fatigue parameter included both the normal and shear strain energies that there is no need of using an experimental fitting parameter. Both in-phase and out-of-phase loading conditions were considered. Additional hardening resulting from out-of-phase loadings was taken into account through stress range. Besides, mean stress term normal to the maximum shear plane was included in the formulation. The parameter consists of the combination of normal and shear strain energy range terms.

$$\frac{1}{\left(\sigma_f{}'\varepsilon_f{}'\right)}(\Delta\sigma_n\Delta\varepsilon_n) + \frac{(1 + \sigma_{n,mean}/\sigma_f{}')}{\left(\tau_f{}'\gamma_f{}'\right)}\left(\Delta\tau_{max}\Delta\left(\frac{\gamma_{max}}{2}\right)\right) = f(N_f) \tag{2.32}$$

Jahed and Varvani-Farahani [50] proposed an energy-based fatigue model considering the upper and lower life limits. Two different parameters were introduced for each case of cracking which are Case A in which shear crack growth occurs along the surface and Case B in which shear crack growths into the surface. The upper limit of fatigue life was obtained from the parameter of Case A cracking, while the lower limit of that was obtained from the other parameter that is for Case B cracking. The existing test results of various metals including SAE 1045 were used to compare the predicted and measured fatigue lives.

The strain-life equations were given for both axial and shear strains by the following Coffin-Manson equations:

$$\frac{\Delta\varepsilon}{2} = \frac{\sigma'_f}{E}\left(2N_f\right)^b + \varepsilon'_f\left(2N_f\right)^c \tag{2.33}$$

$$\frac{\Delta\gamma}{2} = \frac{\tau'_f}{G}\left(2N_f\right)^{b_0} + \gamma'_f\left(2N_f\right)^{c_0} \tag{2.34}$$

Considering the strain-life equations, the energy-fatigue life curves were generated calculating the strain energies at the points of curve. Then, the two parameters were given as

$$\Delta E_A = E_e{}'(N_A)^B + E_f{}'(N_A)^C \tag{2.35}$$

$$\Delta E_T = W_e{}'(N_T)^{B_0} + W_f{}'(N_T)^{C_0} \tag{2.36}$$

where ΔE_A and ΔE_T are the pure tensile energy and the pure torsional energy, respectively. $E_e{}'$ and $W_e{}'$ are the axial and shear fatigue strengths, respectively. $E_f{}'$ and $W_f{}'$ are the axial and shear fatigue toughness, respectively. B, B_0, C, C_0 are the axial and shear energy-based fatigue strength exponents and the axial and shear fatigue toughness exponents, respectively. The lives, N_A and N_T are associated with pure axial and pure torsional loadings. It is suggested that the fatigue life of specimen should be within the upper and lower bounds. The life prediction model was given by the following equation:

$$N_f = \frac{\Delta E_A}{\Delta E}N_A + \frac{\Delta E_T}{\Delta E}N_T \tag{2.37}$$

where ΔE is the total energy obtained from elastic-plastic analysis.

3. FATIGUE LIFE PREDICTION

The notched components may exhibit different types of cracking modes under multiaxial fatigue loadings, which may be tensile-dominated or shear-dominated cases [29]. Therefore, both SWT parameter for tensile-dominated cracking and FS parameter for shear-dominated cracking (as indicated in refs. [29, 51, 52, 53]) were considered to determine the critical plane in which crack initiation occurs. SWT and FS parameters can be associated with the Basquin-Coffin-Manson life equations [53, 54] for the determination of crack initiation life of notched components [54, 55, 56, 57]. The life equations are used to evaluate failure of smooth and small specimens. However, for notched components, the equations usually correspond to the crack initiation life at the notch [29, 58].

3.1. SWT Parameter

The multiaxial fatigue life prediction model can be expressed by the following SWT-life relation [37]:

$$SWT_{max} = \sigma_{MAX}\varepsilon_a = \frac{(\sigma'_f)^2}{E}(2N_f)^{2b} + \sigma'_f\varepsilon'_f(2N_f)^{b+c} \qquad (3.1)$$

where ε_a is the normal strain amplitude given as

$$\varepsilon_a = \frac{\varepsilon_{max} - \varepsilon_{min}}{2} \qquad (3.2)$$

where ε_{max}, ε_{min} are the maximum and minimum normal strains during a loading cycle. σ_{MAX} is the maximum normal stress. For fully-reversed fatigue loading, σ_{MAX} is equal to σ_a.

The maximum normal stress and strain at a given point, which are used to calculate SWT parameter, can be determined from tensor transformation rules [59] (as explained in APPENDIX A and B).

The plane having the maximum damage parameter value is the principal plane in which shear components vanish and only normal components exist. Therefore, the largest amplitude principal stress, $\sigma_{1,a}$ and strain, $\varepsilon_{1,a}$ are used to SWT parameter as

$$SWT_{max} = \sigma_{1,a}\varepsilon_{1,a} \tag{3.3}$$

After obtaining eigenvalues of B matrix (Equation (B.8)), which are the principal strains, the nine direction cosines of principal planes are calculated from Equation (B.12). Then, using Equations (B.1), (B.2), and (B.3), the normal strains corresponding to the principal strains can also be obtained. The normal stresses in the principal orientation, which correspond to the principal stresses, are obtained from Equations (A.7), (A.8), (A.9) using the direction cosines of those planes.

3.2. FS Parameter

The FS parameter-life equation used for crack initiation life calculations of notched components can be expressed by the following equation [45, 53, 54, 60]:

$$FS_{max} = \Delta\varepsilon_{nm}\left[1 + k\frac{\sigma_{n,max}}{S_y}\right] = \frac{\tau'_f}{G}(2N_f)^{b_0} + \gamma'_f(2N_f)^{c_0} \tag{3.4}$$

The material constant k obtained from the axial and torsional fatigue tests can be approximated as the ratio of S_y to σ'_f [61].

In FS critical plane model, the critical plane is considered as the maximum shear strain plane. The maximum shear strains develop on the planes obtained via rotation of principal axes by 45^0. The planes obtained by 45^0 rotation around second principal axis are shown in Figure 3.1. This representation is made for the maximum shear stress, but the same representation can be done for the maximum shear strain replacing σ by ε.
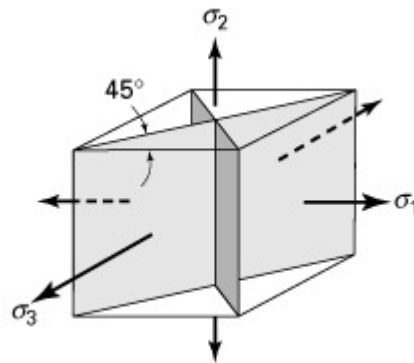
Figure 3.1. Planes of maximum shear strain [59].

Three principal directions are rotated separately. In each rotation, the new direction cosines are obtained and using Equations (B.4), (B.5), (B.6) the shear strains are selected as the largest ones. The maximum shear strain is then determined through three shear strains obtained from three separate rotation.

4. OPTIMIZATION PROCEDURE

A modified SA optimization algorithm proposed by Akbulut and Sonmez [62] is used as search algorithm to find the optimum shape. The notch shape is defined by spline curves passing through key points. x and y coordinates of the moving key points are taken as design variables. Accordingly, the number of design variables can be expressed as

$$n = 2m \tag{4.1}$$

where m is the number of moving keypoints. Whenever the positions of the key points are changed a new shape is obtained. During the optimization process, a new configuration is generated by giving random displacements to the moving key points of a current configuration, which is randomly selected from the set of current configurations. The coordinates of kth moving key point x_k', y_k' of the new configuration are calculated as [6]

$$x_k' = x_k + c_r R_{max} \cos(\theta_r) \tag{4.2}$$

$$y_k' = y_k + c_r R_{max} \sin(\theta_r) \tag{4.3}$$

where x_k, y_k are the coordinates of the kth moving key point of the randomly selected configuration, c_r is a randomly selected number between 0.0 and 1.0, R_{max} is the maximum distance that key points can move, θ_r is a randomly selected value between 0 and 2π. Using two, or more moving key points, shape optimization can be performed. If a low number of key points is used, convergence to an optimal solution can quickly be obtained. A high number of key points requires more computational time; but the shape can be more precisely defined.

Initially, a number of configurations are generated by choosing random positions for the key points within the design space (search area) and drawing spline curves through them. These configurations constitute the set of current configurations, which is updated in each iteration during the optimization process. Their number, N, is selected based on the number of design variables, n, as

$$N = 8(n + 1) \tag{4.4}$$

In each iteration, the algorithm generates a new configuration; but always keeps the best configuration unlike the standard SA, in which single current configuration is replaced by an accepted configuration.

After initial configurations are randomly generated, their objective function values are calculated. The objective function is defined as a function of the damage parameter as

$$f_t = \frac{D}{D_o} \tag{4.5}$$

where D is the maximum value of the damage parameter for the generated configuration and D_o is the maximum value for the original component with a circular notch. After carrying out finite element structural analysis of the new configuration, stress and strain state in the part is obtained. The value of the damage parameter is calculated for each element around the notch and the largest one is taken as the value of D.

The objective function value of a newly generated configuration, f_t, is calculated using Equation (4.5). Its acceptability is evaluated according to the following criterion:

$$A_t = \begin{cases} 1, & f_t \leq f_h \\ \exp\left(-(f_t - f_h)/T_k\right), & f_t > f_h \end{cases} \tag{4.6}$$

where f_h is the objective function value of a current configuration randomly chosen among the worst $(n + 1)$ configurations in the current set. If a new configuration has a lower objective function value than f_h, it is accepted. Otherwise, acceptance of the configuration depends on the acceptability, A_t, calculated using Equation (4.6) and a number randomly generated between 0.0 and 1.0, R_t, as

$$\begin{matrix} Accepted, & if\ A_t \geq R_t, & when\ f_t > f_h \\ Not\ accepted, & if\ A_t < R_t, & when\ f_t > f_h \end{matrix} \tag{4.7}$$

If a new configuration is accepted, it replaces a configuration randomly chosen among the worst $(n + 1)$ configuration.

The temperature parameter, T_k controls the probability of acceptance. According to Equation (4.6), at high values of T_k, it is more likely that a worse configuration having a higher cost is accepted. At the initial stages of optimization corresponding to the melting process in the physical annealing, the temperature parameter, T_0, should be so high that almost any new configuration regardless of the cost value is accepted. In this way, the entire design domain is searched, not just some part of it. Trials made at a given value of the temperature parameter are called Markow chain. At the end of a Markow chain, the value of the temperature parameter is reduced. During the optimization process, the temperature parameter is slowly decreased by multiplying with a temperature reduction factor, α_k

$$T_{k+1} = \alpha_{k+1}\, T_k \tag{4.8}$$

where T_{k+1} and T_k are the values in the *(k+1)*th and *k*th Markov chains, respectively. If the reduction rate is fast, the optimization process may end with a high-cost configuration. Therefore, the reduction rate should be slow to prevent the algorithm be stuck at a worse locally optimum configuration. However, it should not be too slow, if excessive computational times are to be avoided. Towards the end of optimization corresponding to freezing in the physical annealing process, when the temperature parameter is reduced to a small value, a new configuration having a cost value higher than that of the current configuration is nearly never accepted.

The maximum moving distance, R_{max}, in Equations (4.2) and (4.3) is also reduced during the optimization process. Its initial value, R_{max_i}, is selected sufficiently large to allow the key points to move large distances and thus a thorough search of the design space can be achieved. The value of R_{max_i} depends on the size of the search domain, A_s, as

$$R_{max_i} = 0.1\,\sqrt{A_s} \tag{4.9}$$

Towards the end of the optimization, R_{max} becomes so small that only a close neighborhood of the current configurations is searched to precisely locate the optimum configuration. If the worse configuration (defined as the worst configuration in the current set excluding the worst $(n + 1)$ current configurations) is not improved after iterations in a Markow chain are completed, then R_{max} is reduced as

$$R_{max} = \mu R_{max} \tag{4.10}$$

where the constant parameter, μ, selected between 0 and 1 controls how quickly convergence is reached. Choosing a very high number increases the likelihood of locating the globally optimal design, but results in a long computational time. With a lower number, on the other hand, convergence is quickly achieved; but the likelihood of getting trapped at a high cost local optimum will be high. The value of μ is selected as 0.98 in this study.

The temperature reduction parameter, α_k takes a value between α_{max} and α_{min} according to the following equation [62]:

$$\alpha_{k+1} = \begin{cases} \alpha_{max}, & L_{k,a}/L_k < [R_{max}/R_{max_i}]^2 + 0.01 \\ \alpha_{min}, & L_{k,a}/L_k \geq [R_{max}/R_{max_i}]^2 + 0.01 \end{cases} \tag{4.11}$$

where α_{max} and α_{min} are selected as 0.9999 and 0.9 in this study, respectively. L_k is the number of new configurations tried in k^{th} Markov chain, $L_{k,a}$ is the number of accepted configurations in that Markov chain. The initial value of α_k, $\alpha_{k,initial}$ is given as

$$\alpha_{k,initial} = \frac{(\alpha_{max} + \alpha_{min})}{2} \tag{4.12}$$

The length of a Markov chain is defined as the number of iterations which are performed at a constant temperature T_k. In the thesis, a Markov chain length, L_k, at the kth level is expressed as [6, 63, 64]

$$L_k = L + L(1 - e^{-(f_h - f_l)}) \tag{4.13}$$

where $L = 10n$, n is the dimension of problem, namely, the number of design variables. For the determination of current Markov chain length, the highest and lowest cost values f_h and f_l, respectively, are selected from the N number of configurations. Since there are two coordinates of a moving key point in 2D (as in this study), the number, n can be calculated from Equation (4.1). A Markov chain length takes a value between L and $2L$. When the difference between f_h and f_l is high, the iterations executed in a Markov chain will be high, closer to $2L$. In the case where there is small difference between f_h and f_l, the length of the chain approaches to L. A Markow chain will be stopped if a new configuration having a cost less than f_l is generated or when all the iterations in the Markow chain are executed.

In case of acceptance, a newly generated configuration replaces the worst configuration in DSA. According to ref. [62], this replacement method creates a drawback that search domain is limited to a small portion of design space. After replacement, the location of the worst configuration is lost except that if the new configuration is generated by using the design variables of the worst one, which is a rare condition, especially in case of a high number of initial configurations. Therefore, during iterations, the design space may be restricted in a smaller region as a result of removing the worst configurations.

Considering this issue, the modified SA algorithm [62] was proposed to perform a different replacement method. Firstly, the $8(n + 1)$ initially generated configurations are ordered with respect to their cost values. Then, a number of worst configurations, N_w is selected from the set of current configurations as

$$N_w = n + 1 \tag{4.14}$$

If a randomly generated configuration is accepted, it replaces a current configuration which is randomly selected among N_w worst configurations. $7(n + 1)$ current configurations having lower cost values are kept in the set except that a new configuration having cost value better than one of the $7(n + 1)$ current configurations is generated. In this way, N_w number of current configurations instead of just the worst one become candidates for replacement. The highest cost function, f_h is defined as the best of the worst N_w configurations.

The flowchart of the optimization algorithm is presented in Figure 4.1.
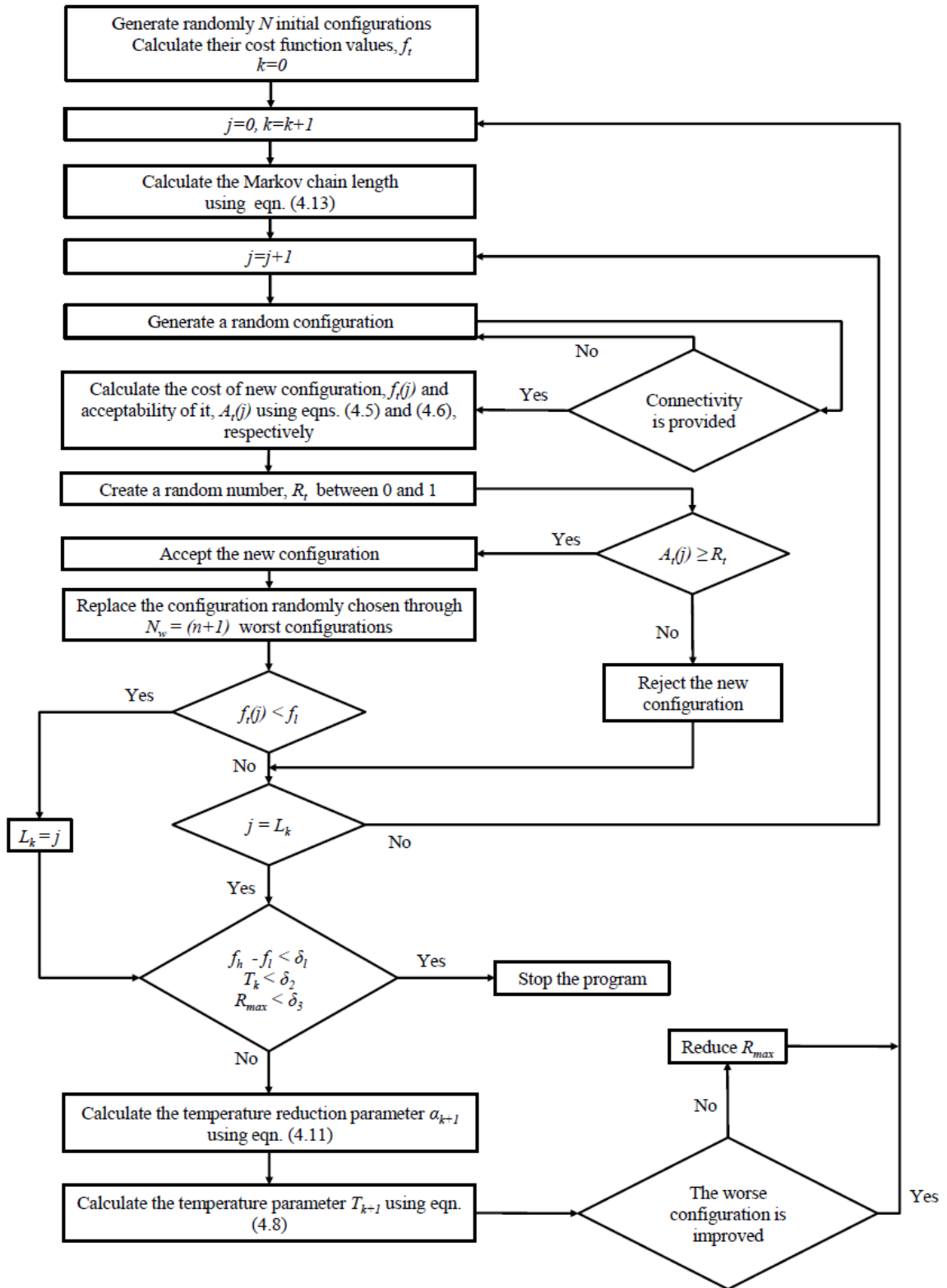
Figure 4.1. The flow chart for the optimization algorithm.

Iterations are continued until all the stopping criteria are satisfied. Three stopping criteria [64] are selected as

$$f_h - f_l < \delta_1 \tag{4.15}$$

$$T_k < \delta_2 \tag{4.16}$$

$$R_{max} < \delta_3 \tag{4.17}$$

where $\delta_1 = 0.0001$, $\delta_2 = 0.001$ and $\delta_3 = 0.000001$. δ_1 and δ_2 are small constants, δ_3 is a relatively small number compared to the first moving distance. During iterations, if connectivity of the part is lost due to the random movement of key points, the algorithm does not accept the current configuration and a new configuration is generated until the connectivity is provided.

5. NUMERICAL PROCEDURE

The analysis of stress and strain states of a shouldered shaft and a shaft with a groove is carried out by finite element modeling of ANSYS. Fatigue life calculations according to SWT and FS models are then performed by codes developed in ANSYS Parametric Design Language (APDL). After that, the shape optimization algorithm is implemented to maximize the fatigue life of the part by minimizing the maximum damage parameter. The algorithm iteratively searches to find the optimum shapes of the models.

5.1. Finite Element Modeling

Finite element modeling (FEM) of the shaft is done as follows:

(i)   Program initiation

(ii)   Entering the material properties

(iii)   Defining key points

(iv)   Creating the geometry by defining lines and areas

(v)   Creating the FE mesh in the areas

(vi)   Applying the boundary conditions

(vii)   Realization of the solution

Firstly, analysis type and material properties such as young modulus, Poisson's ratio are entered.

After the key points are generated, lines of the model are created. Since a 2D model is developed in the thesis, the definition of the geometry will be completed after the model area is defined. Area of the model is then meshed for a certain mesh size which is specified by the user. Subsequently, boundary conditions (boundary constraints and loadings) are applied to the lines and nodes.

After the FEM is developed and the structural analysis results are obtained, fatigue damage parameter is calculated by defining the necessary equations in APDL. The stress

and strain components obtained from FE analysis are substituted in the equations. Two separate codes are developed to calculate SWT and FS parameters.

After the damage parameter of original-shaped model is calculated, using moving key points, the optimization algorithm randomly generates configurations and calculates damage parameters of each configuration. Optimization continues until an optimum design is obtained.

5.1.1. Finite Element Analysis of the Shouldered Shaft

A shouldered shaft specimen made from the SAE 1045 steel is considered in this study. The geometry of the notched shaft is shown in Figure 5.1.
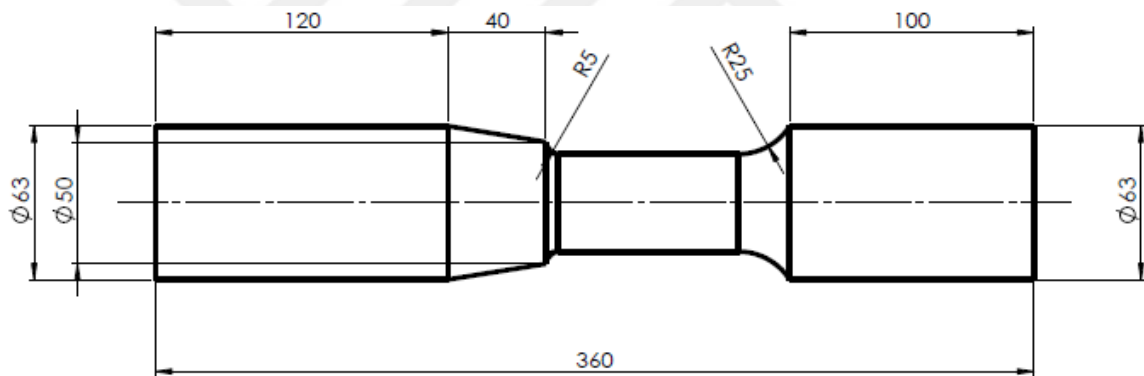
Figure 5.1. The SAE 1045 notched specimen.

The cross sectional area is circular; accordingly the geometry is axisymmetric. A 2D axisymmetric element that can take non-axisymmetric loads, PLANE83, is used to simulate the structural behavior of the specimen.

The most critical region of the specimen is the fillet with a smaller radius (5 millimeter). For this reason, a part of the specimen including the fillet having smaller radius is considered for the finite element analysis, which is shown in Figure 5.2. The length of the domain is chosen as 90 mm. If a longer portion is analyzed, no appreciable change occurs in the results.
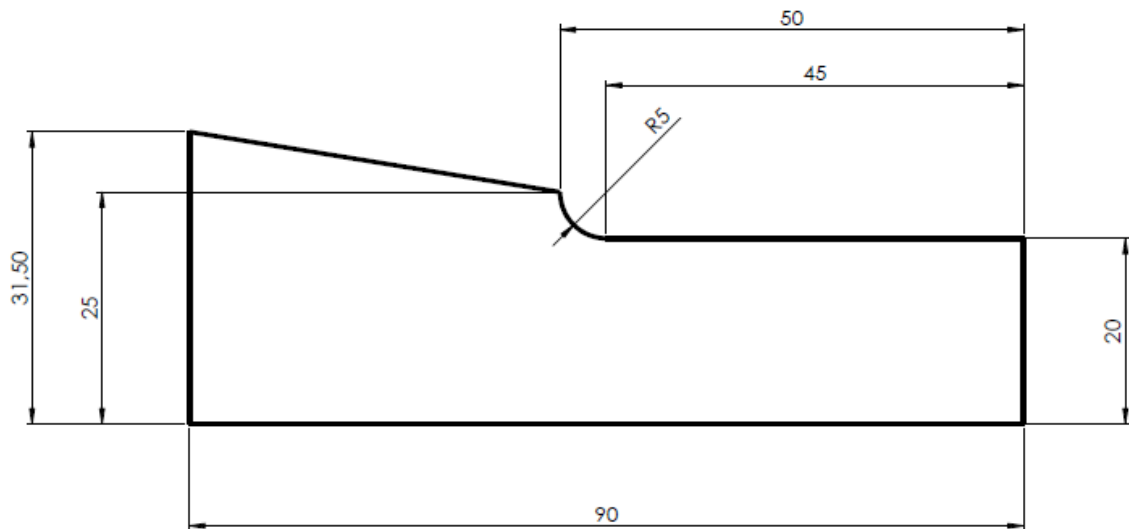
Figure 5.2. The domain of analysis for the shouldered shaft.

The fatigue damage parameter calculations of the specimen are carried out on this part since it includes the most critical region of the specimen.

5.1.2. The Model Creation using APDL

There is a feature of ANSYS that a 3D axisymmetric structure under non-axisymmetric loads can be modelled in 2D using axisymmetric elements of ANSYS. Because the specimen is axisymmetric, a 2D model of the notched part is created using the PLANE83 element type of ANSYS. PLANE83 element is 8-node axisymmetric-harmonic structural solid.

It is assumed that loads applied to the model do not create plastic deformations in the specimen and so, they are negligible. Therefore, the material is defined as linear elastic.

The material properties of SAE 1045 steel used in the analysis and fatigue life calculations are given in Table 5.1.

Table 5.1. The material properties of SAE 1045 steel [65].

Poisson's Ratio, ν	0.28
Modulus of Elasticity, E	202 GPa
Axial Fatigue Strength Coefficient, σ_f'	948 MPa
Axial Fatigue Strength Exponent, b	-0.092
Axial Fatigue Ductility Coefficient, ε_f'	0.26
Axial Fatigue Ductility Exponent, c	-0.445
Yield Stress, σ_y	380 MPa
Torsional Fatigue Strength Coefficient, τ_f'	505 MPa
Shear Modulus, G	79 GPa
Torsional Fatigue Strength Exponent, b_0	-0.097
Torsional Fatigue Ductility Coefficient, γ_f'	0.413
Torsional Fatigue Ductility Exponent, c_0	-0.445

The material parameter, k in FS parameter is approximated as 0.4 [61].

The analysis type and material properties are defined in the code using the commands shown in Table 5.2.

Table 5.2. The analysis type and material description commands.

Command	Description
MPTEMP,,,,,,,,, MPTEMP,1,0	Linear elastic isotropic material is defined.
MPDATA,EX,*MAT*,,E	Young modulus, *E,* is defined for the material numbered as *MAT*.
MPDATA,NUXY,*MAT*,, ν	Poisson's ratio, ν, is defined for the material numbered as *MAT*.

The notched part is modeled with two materials, which have the same material properties as shown in Figure 5.3.
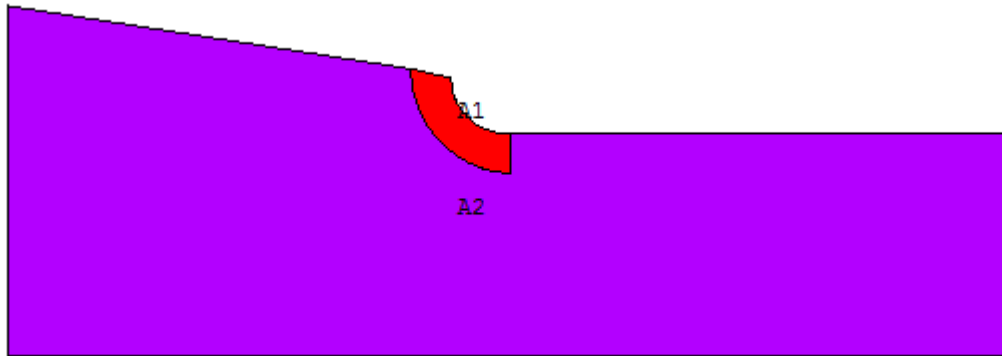
Figure 5.3. The formation of notched part with two same materials.

Because both maximum SWT and FS parameters are obtained at the critical point of the part, the critical region is separately characterized by material A1. Material A2 is not selected in post-processing. Thus, the calculations which are unnecessary for the non-critical region are not performed. In this way, the analysis time is reduced.

The commands creating key points and lines of the model are described in Table 5.3.

Table 5.3. The key point and line commands.

Command	Description
$x\%n\% = N$	The x coordinate of key point, n is defined where N is the value of x coordinate.
$y\%n\% = M$	The y coordinate of key point, n is defined where M is the value of y coordinate.
$k, n, x\%n\%, y\%n\%$	The key point, n is created.
l, n_1, n_2	The line between key points n_1 and n_2 is created.
$larc, n_1, n_2, n_3, R$	The circular arc line is defined between key points n_1 and n_2 around the key point n_3 with a radius of curvature R.
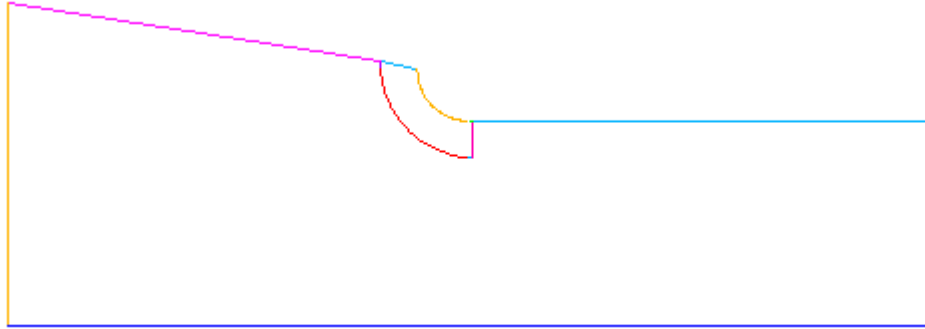
Figure 5.4. The lines of the part created between key points.

After the key points and the lines are created as shown in Figure 5.4, the areas of the model are created with the commands described in Table 5.4.

Table 5.4. The commands for creation of an area and combination of two areas.

Command	Description
al,l_1,,,l_k	The area is created combining k number of lines.
aglue,a_1,a_2	The area of the part is formed by the combination of areas *A1* and *A2*.

Where loads are applied to the nodes of the FE model, locally high stresses develop at the point of application of concentrated forces. In order to smoothly and realistically apply the loads, the notched part is loaded through and intermediate part defined by Area 3 (A3) as indicated in Figure 5.5. The same material properties are assigned to this part with a different material number and this material is unselected in post-processing.
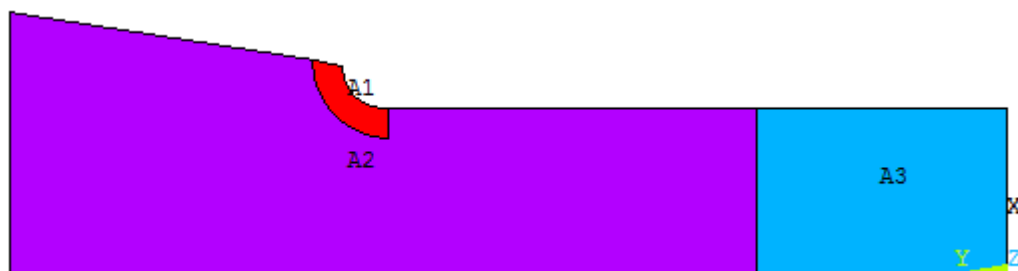
Figure 5.5. The representation of the combined areas.

The free mapped meshing process is performed after the generation of areas. According to a user defined mesh size, PLANE83 elements with axisymmetric option are created on the areas. Element size should be small enough so that the results of the FE analysis are accurate. Besides, a mesh refinement is applied to the boundaries around which high stresses develop. The commands are given in Table 5.5.

Table 5.5. The mesh and refinement commands.

Command	Description
aesize, all, S amesh,A	The area, A is meshed for a defined element size, S.
lsel, s, line, , l_m, l_n	The lines between l_m and l_n are selected for mesh refinement.
lrefine, all, , , r	Refinement is performed where the quantity of refinement, r takes a value from 1 (minimum refinement) to 5 (maximum refinement).

The notched component is subjected to bending moment and torsional loadings. Bending moment is created by a force couple applied in the global X direction. Torsional loading is applied via concentrated forces acting in the global Z direction. The bending and torsional loadings applied to the model create stresses in the bar away from the notch having almost the same values as predicted by the beam theory. The notched part (shown in Figure 5.2) was also modeled in the study [66] applying the same boundary conditions.

Boundary conditions (constraints of displacements and loadings) are applied to lines and nodes as indicated in Table 5.6.

Table 5.6. The boundary condition commands.

Command	Description
dl, l_n, , u_y, 0	The displacement of line, l_n in Y direction is fixed to zero.
dl, l_n, , u_z, 0	The displacement of line, l_n in Z direction is fixed to zero.
F, n, Fx, F_k	The load, F_k is applied to the node, n in the X direction.
F, n, Fz, F_k	The load, F_k is applied to the node, n in the Z direction.

The displacement boundary condition for bending is defined as zero displacement in the y direction for the bottom line and zero displacement in the y and z directions for the line in the left as shown in Figure 5.6. It is defined for torsion as zero displacement in the z direction for the bottom line and zero displacement in the y and z directions for the line in the left as shown in Figure 5.7. The bending and torsion loadings with their displacement boundary conditions are separately created and two *SOLVE* commands for each loading are used. After, they are superposed.
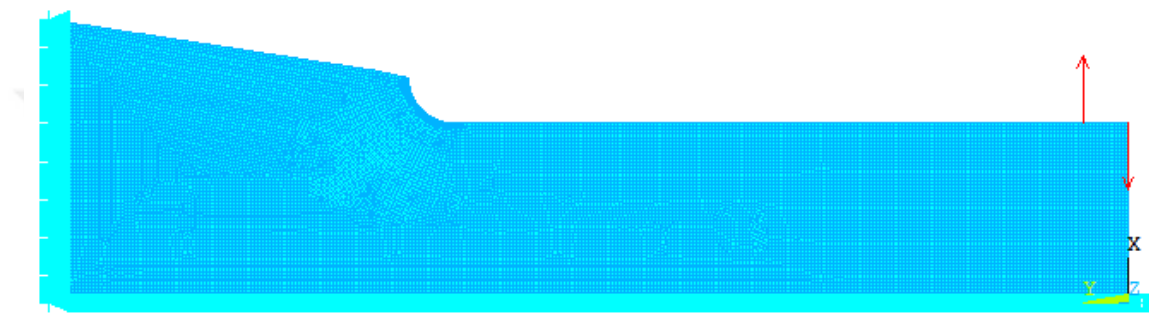
Figure 5.6. The bending moment and displacement boundary conditions.

Figure 5.7. The concentrated torsional loadings and displacement boundary conditions.

5.1.3. Finite Element Analysis of the Groove Model

A circular shaft with a groove made of an Al-Si alloy is considered in this study. The geometric features of the specimen are given in Figure 5.8. The material properties are given in Table 5.7.
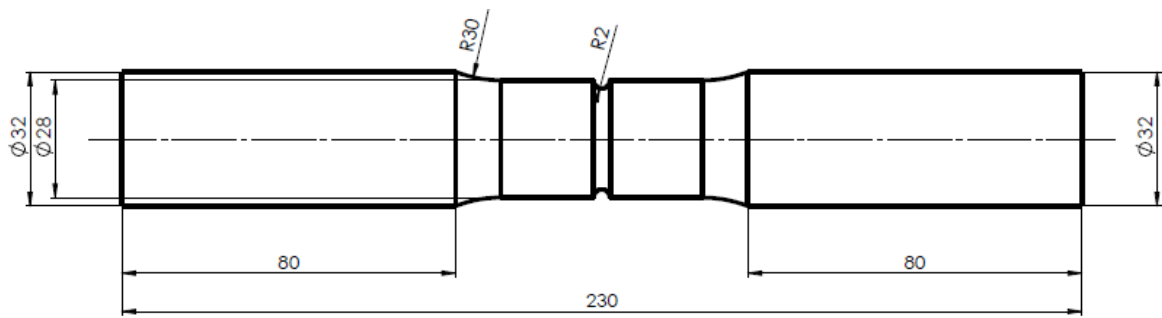
Figure 5.8. The Al-Si alloy notched specimen.

Table 5.7. The material properties of Al-Si alloy [67, 68].

Poisson's Ratio, v	0.3
Modulus of Elasticity, E	78 GPa
Axial Fatigue Strength Coefficient, $\sigma_f{}'$	398 MPa
Axial Fatigue Strength Exponent, b	-0.0843
Axial Fatigue Ductility Coefficient, $\varepsilon_f{}'$	0.028
Axial Fatigue Ductility Exponent, c	-0.6594

Similar to the previous model, the shaft is axisymmetric and therefore, a 2D model is used in ANSYS. Both axial load and torsion are applied to the model as shown in Figures 5.9 and 5.10. Except these, the same finite element analysis of the fillet model is performed for the groove model.
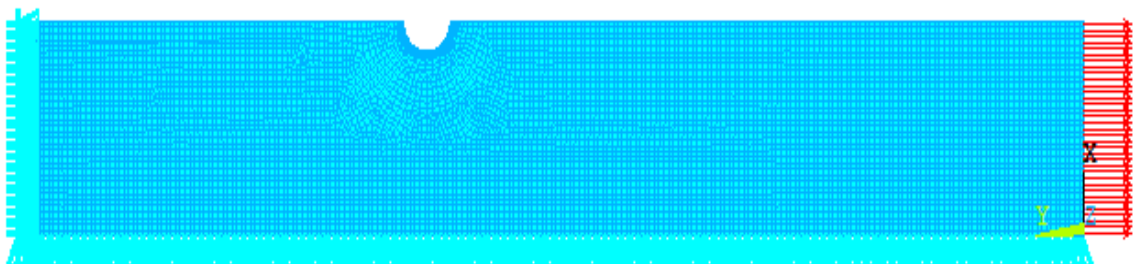
Figure 5.9. The axial load and displacement boundary conditions.

Figure 5.10. The torsional load and displacement boundary conditions.

A part of the specimen including the groove is modeled for finite element analysis. The dimensions of the axisymmetric section of the analyzed part are shown in Figure 5.11.
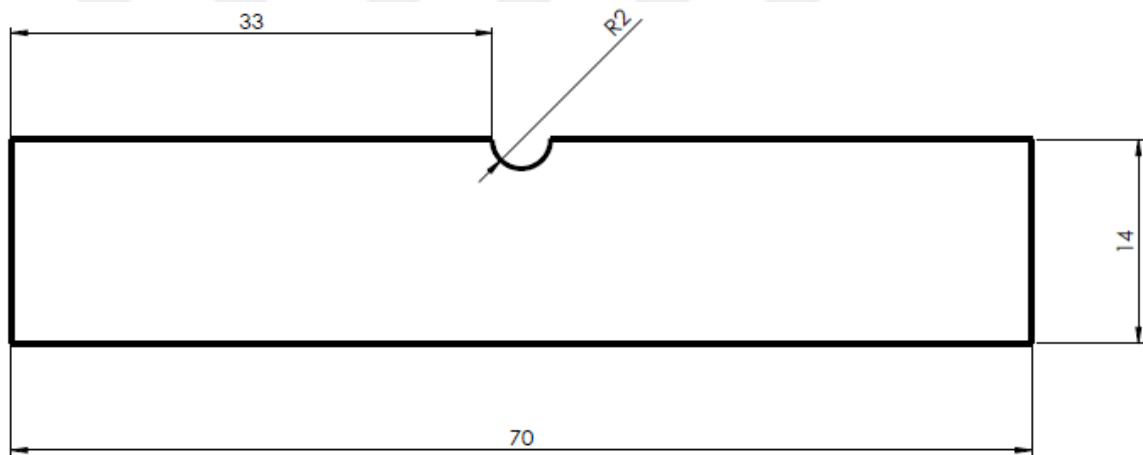
Figure 5.11. The axisymmetric part of the groove specimen analyzed by FEM.

As in the fillet model, in order to avoid unnecessary calculations, the damage parameter calculation is performed in the area A1 as shown in Figure 5.12 considering that the most critical region is in A1 around the groove.

Figure 5.12. The representation of combined three areas.

The SWT damage parameter calculation and shape optimization procedure of the specimen is carried out on this part.

5.2.   Fatigue Life Calculations

The model is created and boundary conditions are applied. Subsequently, the analysis of the notched component is performed. Specific results are obtained using the commands indicated in Table 5.8.

Table 5.8. The element table commands.

Command	Description
$\mathrm{ETABLE}, , \mathrm{S}, i$	The element tables of principal stresses are created where i takes a value from 1 to 3.
$\mathrm{ETABLE}, , \mathrm{EPTO}, i$	The element tables of principal strains are created where i takes a value from 1 to 3.
$\mathrm{esel}, \mathrm{u}, \mathrm{mat}, , n$	The material n is unselected ($n = 2$, $n = 3$)

The values of principal stresses and strains of kth element are then obtained by the commands given in Table 5.9.

Table 5.9. The commands for getting principal values.

Command	Description
$*\,\mathrm{get}, Psti, \mathrm{elem}, k, \mathrm{etab}, Si$	The principal stresses, $Psti$ of kth element are obtained for $S1$, $S2$, $S3$, respectively.
$*\,\mathrm{get}, Psni, \mathrm{elem}, k, \mathrm{etab}, EPTOi$	The principal strains, $Psni$ of kth element are obtained for $EPTO1$, $EPTO2$, $EPTO3$, respectively.

The SWT and FS parameters are separately calculated using both ANSYS and MATLAB programs. The ANSYS results are compared to the MATLAB results to demonstrate the accuracy of results.

The SWT parameter can be calculated from Equation (3.1) using principal values obtained from ANSYS. The procedure is expressed as

(i)   The principal stresses and strains are obtained for kth element of selected material.

(ii) The first possible SWT parameter is calculated by multiplying the first principal stress and strain.

(iii) The second possible SWT parameter is calculated by multiplying the second principal stress and strain.

(iv) The third possible SWT parameter is calculated by multiplying the third principal stress and strain.

(v)   The SWT damage parameter of kth element is selected as the maximum possible SWT parameter among the parameters stored in steps (ii) through (iv).

(vi) The operations from (i) to (v) are repeated for N number of elements of selected material. The N number of damage parameters is stored.

(vii) The maximum damage parameter is selected from the set.

The MATLAB code for SWT parameter is developed following the procedure explained in Section 3.

The FS parameter (Equation (3.4)) is calculated by a code developed using ANSYS Parametric Language. The procedure is explained as follows:

(i)   The principal stresses and strains are obtained for kth element of selected material.

(ii) Three principal axes are separately rotated 45^0 as shown in Figure 5.13, Figure 5.14 and Figure 5.15 to obtain the orientation of maximum shear strain plane. The rotation is carried out in positive or negative direction. The direction cosines of those orientations are given in Table 5.10, Table 5.11 and Table 5.12.

(a)

(b)
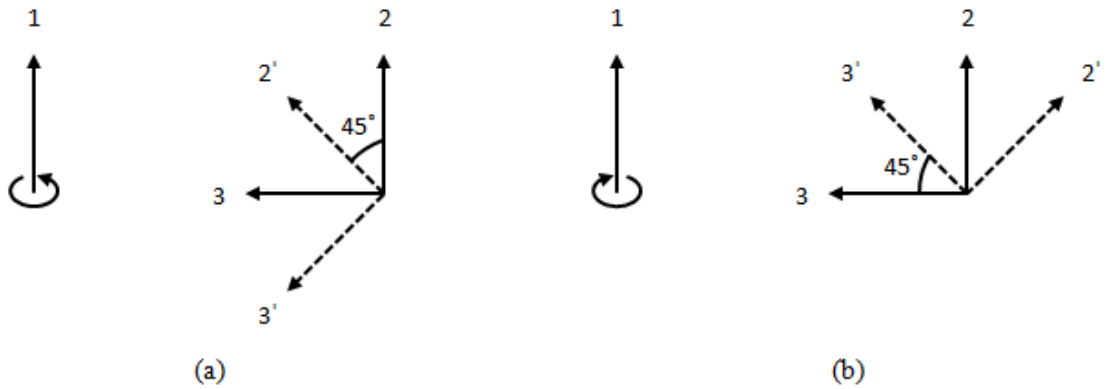
Figure 5.13. (a) $+45^0$ rotation about the 1st principal axis. (b) -45^0 rotation about the 1st principal axis.

Table 5.10. The direction cosine representation of the rotated 1st principal axis.

		$\theta = +45°$			$\theta = -45°$	
	1	2	3	1	2	3
1'	$l_1 = \cos(0)$	$m_1 = \cos(90)$	$n_1 = \cos(90)$	$l_1 = \cos(0)$	$m_1 = \cos(90)$	$n_1 = \cos(90)$
2'	$l_2 = \cos(90)$	$m_2 = \cos(45)$	$n_2 = \cos(45)$	$l_2 = \cos(90)$	$m_2 = \cos(45)$	$n_2 = \cos(135)$
3'	$l_3 = \cos(90)$	$m_3 = \cos(135)$	$n_3 = \cos(45)$	$l_3 = \cos(90)$	$m_3 = \cos(45)$	$n_3 = \cos(45)$

(a)

(b)
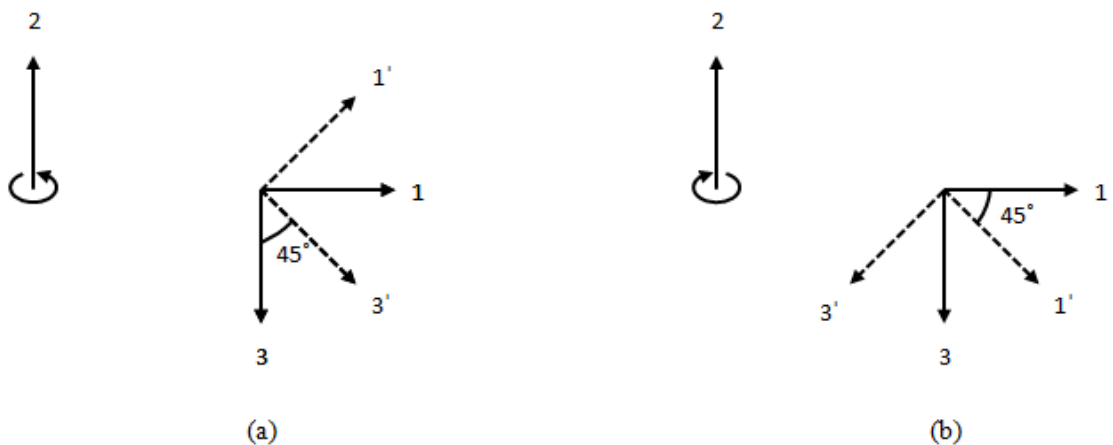
Figure 5.14. (a) $+45^0$ rotation about the 2nd principal axis. (b) -45^0 rotation about the 2nd principal axis.

Table 5.11. The direction cosine representation of the rotated 2nd principal axis.

	$\theta = +45°$			$\theta = -45°$		
	1	2	3	1	2	3
1'	$l_1 = \cos(45)$	$m_1 = \cos(90)$	$n_1 = \cos(135)$	$l_1 = \cos(45)$	$m_1 = \cos(90)$	$n_1 = \cos(45)$
2'	$l_2 = \cos(90)$	$m_2 = \cos(0)$	$n_2 = \cos(90)$	$l_2 = \cos(90)$	$m_2 = \cos(0)$	$n_2 = \cos(90)$
3'	$l_3 = \cos(45)$	$m_3 = \cos(90)$	$n_3 = \cos(45)$	$l_3 = \cos(135)$	$m_3 = \cos(90)$	$n_3 = \cos(45)$
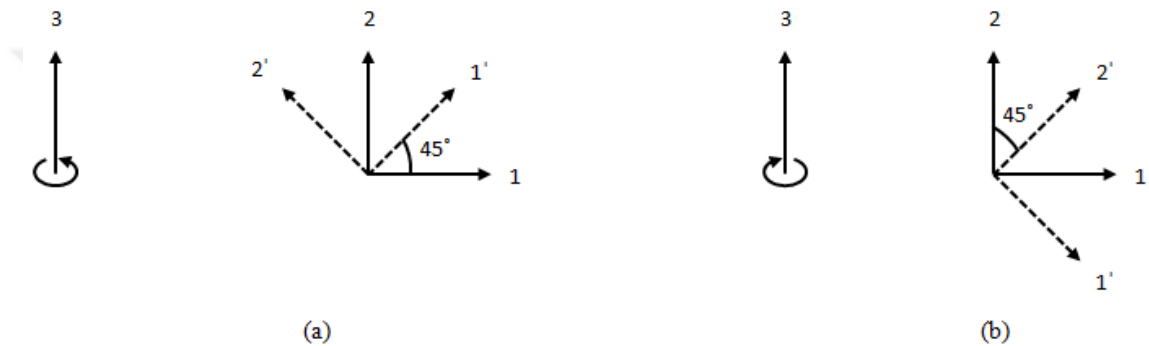
Figure 5.15. (a) +45^0 rotation about the 3rd principal axis. (b) -45^0 rotation about the 3rd principal axis.

Table 5.12. The direction cosine representation of the rotated 3rd principal axis.

	$\theta = +45°$			$\theta = -45°$		
	1	2	3	1	2	3
1'	$l_1 = \cos(45)$	$m_1 = \cos(45)$	$n_1 = \cos(90)$	$l_1 = \cos(45)$	$m_1 = \cos(135)$	$n_1 = \cos(90)$
2'	$l_2 = \cos(135)$	$m_2 = \cos(45)$	$n_2 = \cos(90)$	$l_2 = \cos(45)$	$m_2 = \cos(45)$	$n_2 = \cos(90)$
3'	$l_3 = \cos(90)$	$m_3 = \cos(90)$	$n_3 = \cos(0)$	$l_3 = \cos(90)$	$m_3 = \cos(90)$	$n_3 = \cos(0)$

(iii) Since there do not exist shear components of stresses and strains in the principal plane, Equations (A.7), (A.8), (A.9) and (B.4), (B.5), (B.6) can be rewritten by equating these shear components to zero. The normal components are equal to the principal values in this case.

(iv) The maximum shear strain is selected from the set of shear strains obtained by separately rotating the principal axes.

(v) The normal stress of the maximum shear strain plane is obtained using Equations (A.7), (A.8), (A.9) in which the normal stress components are the principal ones and the shear components are equal to zero.

(vi) The FS damage parameter of kth element is calculated from Equation (3.4).

(vii) The operations from (i) to (vi) are repeated for N number of elements of selected material. The N number of damage parameters is stored.

(viii) The maximum damage parameter is selected from the set.

The MATLAB code for FS parameter is developed following the procedure explained in Section 3.

5.3. Shape Optimization Procedure

The optimization algorithm [62] explained in Section 4 is adapted to the both fillet and groove models. The notched fillet shape with two moving key points (7th and 10th key points) that are used to define the spline curves for the fillet boundary is shown in Figure 5.16. The other key points are fixed, thus their positions do not change during shape optimization process. The positions of the moving key points are varied within a specified design space during optimization. The design spaces in which three, four and five moving key points are used for the shape optimization of the fillet boundary are also shown in Figures 5.17, 5.18 and 5.19, respectively. Outside the search domain, the boundary is not expected to be optimum. Each key point moves within its search area. The optimization of groove is performed with two moving key points, namely, 8th and 9th key points shown in Figure 5.20. Due to the symmetry, the movement of 5th and 6th key points depends on 9th and 8th key points, respectively. The 4th, 7th and 10th key points are fixed.
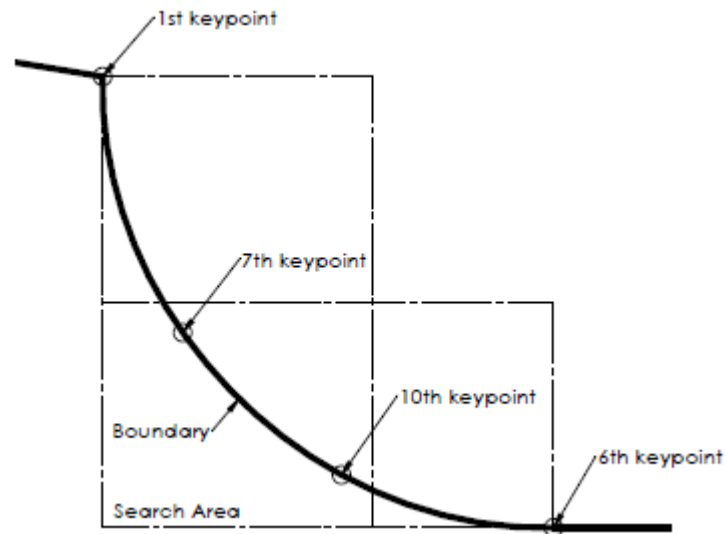
Figure 5.16. The design spaces of the two moving key points within which they are allowed to move during shape optimization of the fillet boundary.
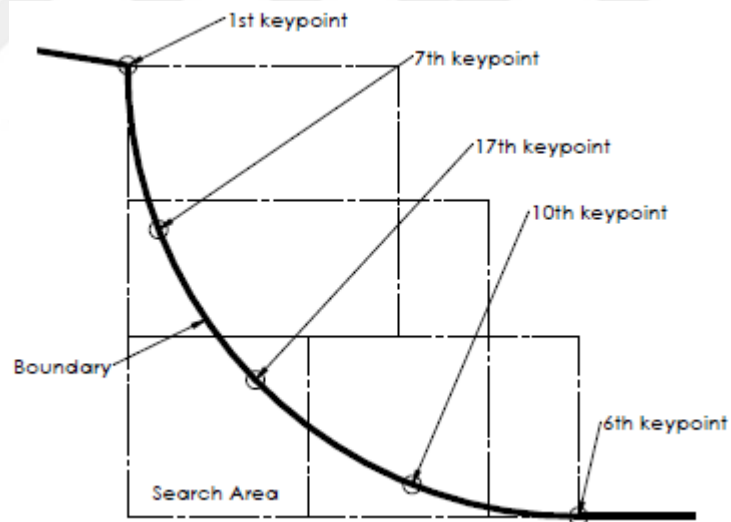
Figure 5.17. The design spaces of the three moving key points used to define the spline curves for the fillet boundary.
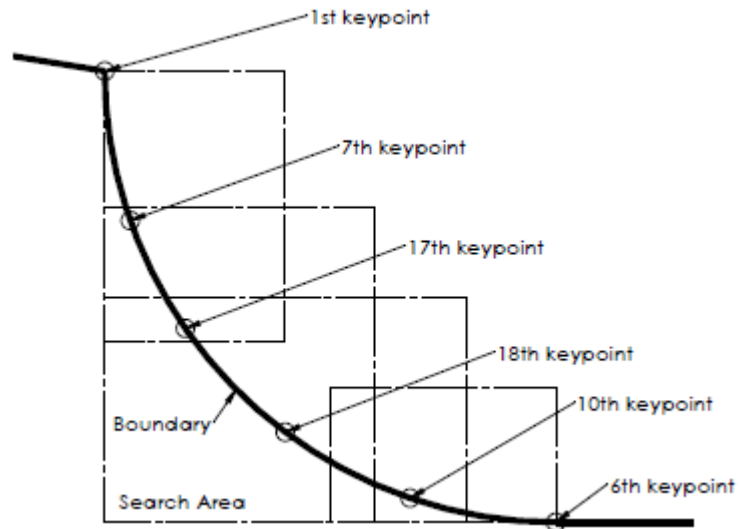
Figure 5.18. The design spaces of the four moving key points used to define the spline curves for the fillet boundary.
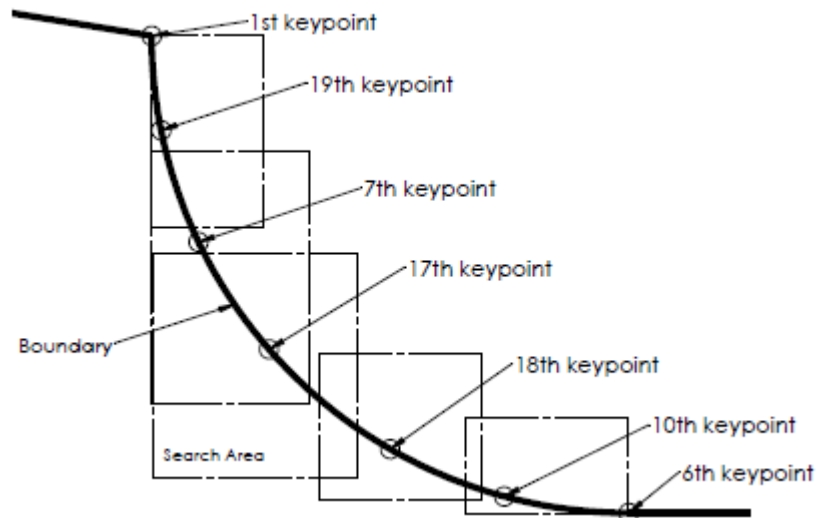
Figure 5.19. The design spaces of the five moving key points used to define the spline curves for the fillet boundary.
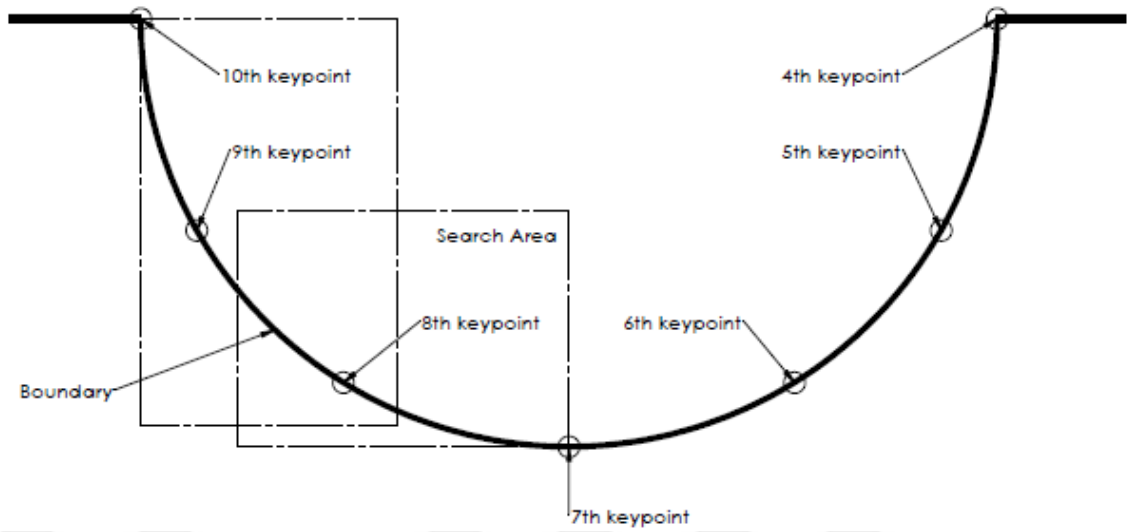
Figure 5.20. The design spaces of the two moving key points, 8th and 9th, within which they are allowed to move during shape optimization of the groove boundary. The other key points are fixed.

6. RESULTS AND DISCUSSION

6.1. The Shouldered Shaft

Firstly, the fatigue life results predicted by SWT and FS models are separately compared to the experimental results for shouldered shaft specimen with a circular fillet in order to validate the models for this geometry. Experiments were conducted [69, 70] on specimens under in-phase and out-of-phase combined loading of bending and torsional moments. The experimental crack initiation life was defined as the number of cycles until development of a crack with 1.0-mm length [69, 70].

In in-phase loading cases, during a loading cycle, bending and torsional moments reach their maximum and minimum values at the same time as shown schematically in Figure 6.1. Maximum and minimum stress, strain components (having the same magnitude $(\left|\sigma_{ij_{max}}\right| = \left|\sigma_{ij_{min}}\right|$ and $\left|\varepsilon_{ij_{max}}\right| = \left|\varepsilon_{ij_{min}}\right|)$ because of full-reversed loading case) occurring during a loading cycle are used to obtain the amplitude of stress and strain components. In in-phase loading cases, the maximum SWT or FS parameter values are obtained, when bending and torsional moments reach their maximum values.

In-phase bending, M_B and torsional, M_T moments fluctuate as

$$M_B = M_{B_a}\sin{(\omega t)} \tag{6.1}$$

$$M_T = M_{T_a}\sin{(\omega t)} \tag{6.2}$$

where M_{B_a} and M_{T_a} are the amplitudes of bending and torsional moments, respectively. In one cycle, ωt takes values between $2\pi n$ and $2\pi(n + 1)$.

In 90^0 out-of-phase loading cases, maximum of one load occurs at the time when the other load takes the lowest algebraic value as shown in Figure 6.2. In that case, SWT and FS parameters may reach their maximum values at any other time depending on the

relative magnitudes of out-of-phase loads. For this reason, the maximum values are searched through the whole load cycle.

In the case of 90^0 out-of –phase, bending and torsional moments are given as

$$M_B = M_{B_a} \sin(\omega t) \tag{6.3}$$

$$M_T = M_{T_a} \sin(\omega t + \pi/2) \tag{6.4}$$

In order to obtain the maximum value of SWT or FS parameter, ωt is increased in 1^0 intervals; each time the magnitudes of M_B and M_T are calculated according to Equations (6.3) and (6.4) and the stress and strain states and the peak value of SWT or FS parameter is evaluated. After that, the maximum value of SWT or FS parameter is selected for fatigue life calculation.
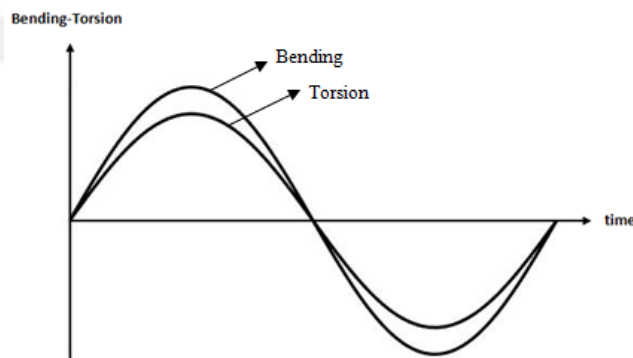
Figure 6.1. In-phase bending-torsional moments.
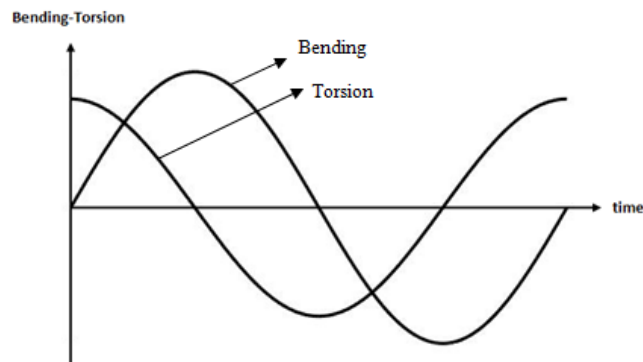
Figure 6.2. 90^0 out-of-phase bending-torsional moments.

6.1.1. Comparison of the Fatigue Life Predictions with Experimental Results

As mentioned before, SWT and FS parameters are evaluated only in the critical region designated by A1. As seen in Figures 6.3, 6.4, 6.5 and 6.6, the most stressed point is at the notched boundary within A1. Away from the notch, a uniform stress distribution is obtained along the axial direction.

The experimental fatigue life results [69, 70], the calculated maximum damage parameters and the crack initiation lives of the specimens predicted according to FS and SWT models under in-phase and 90^0 out-of-phase loading conditions are presented in Tables 6.1, 6.2, 6.3 and 6.4. The numerical results are obtained using the developed APDL codes. The plots in Figures 6.7, 6.8, 6.9 and 6.10 graphically show the comparison between the predicted results with the experimental ones. In order to validate the results obtained using ANSYS, two MATLAB codes are developed for SWT and FS parameter calculations. The MATLAB results for two different loading cases are shown in Table 6.5. As can be seen in Tables 6.1, 6.2 and 6.5, ANSYS and MATLAB yield the same results.

The equivalent (von Mises) and first principal stress distributions in both total part and critical region are shown in Figures 6.3, 6.4, 6.5 and 6.6.
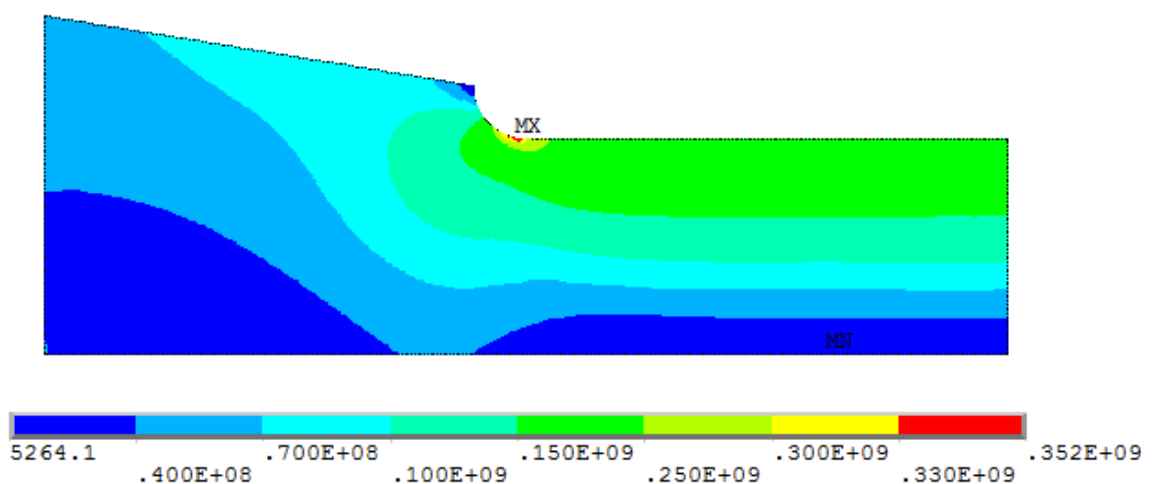
Figure 6.3. von Mises stress distribution in the part (A1+A2).
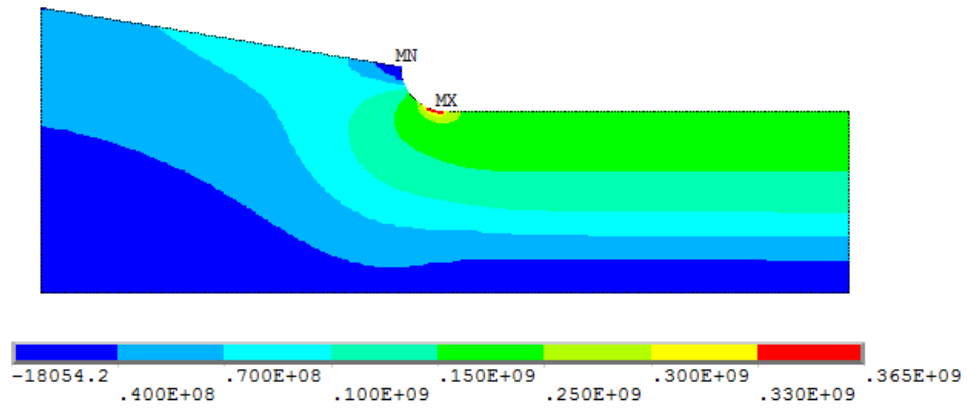
Figure 6.4. 1st principal stress distribution in the part (A1+A2).
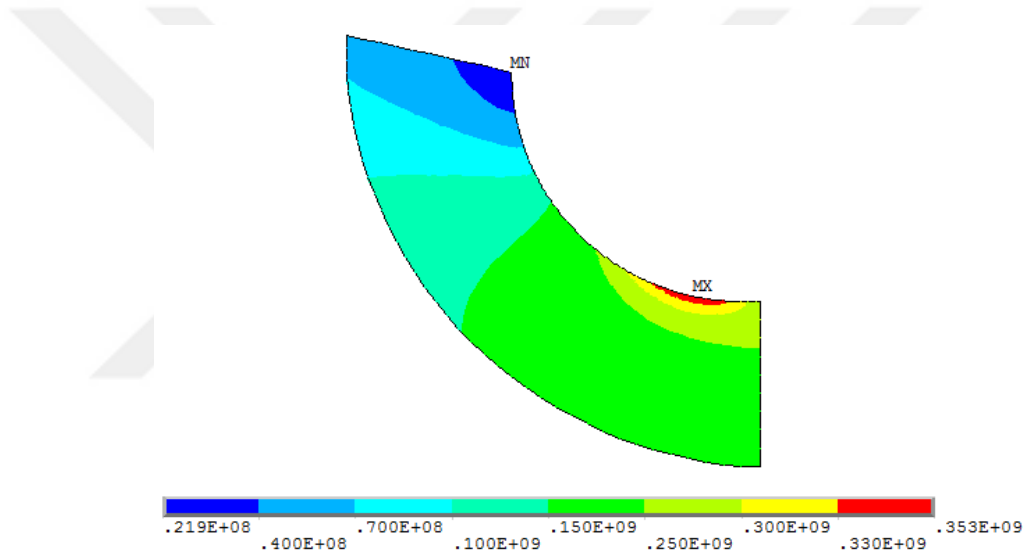
Figure 6.5. von Mises stress distribution in the critical region (A1).

Figure 6.6. 1st principal stress distribution in the critical region (A1).

Table 6.1. Experimental fatigue life results [69, 70] and the results predicted by SWT
parameter for in-phase loading cases.

Loading Case	Bending Moment (N·m)	Torsional Moment (N·m)	Exp. Crack Initiation Life (up to 1mm) $N_{i(\text{exp})}$	Exp. Final Fracture Life $N_{f(\text{exp})}$	Predicted Initiation Life by SWT Parameter $N_{i(\text{SWT})}$	The Ratio of Predicted Life to Measured Life $N_{R(\text{SWT})}$	Maximum SWT Parameter P_{SWT}	Max. Von Mises Stress (MPa) σ_{eq}
1	1850	2550	2,200	5,113	8,877	4.04	2023114	660
2	2800	0	2,571	8,262	5,191	2.02	2529466	674
3	2000	2100	5,998	12,050	9,520	1.59	1966276	632
4	1250	2700	6,402	10,420	22,414	3.50	1403225	588
5	1150	2700	3,000	12,700	27,249	9.08	1303350	574
6	2325	1350	2,905	11,735	8,321	2.86	2077460	625
7	2600	0	6,347	15,043	7,395	1.17	2181019	626
8	2586	0	14,000	17,450	7,590	0.54	2157594	623
9	0	3000	5,529	12,124	249,912	45.20	612361	538
10	1355	2550	5,500	11,630	21,383	3.89	1428686	580
11	1850	2100	5,740	11,565	12,455	2.17	1764556	603
12	851	2700	9,000	17,730	51,186	5.69	1035295	539
13	840	2700	10,000	24,540	52,462	5.25	1026280	538
14	1720	1350	19,260	58,790	29,909	1.55	1258774	494
15	0	2400	70,350	132,585	1,183,353	16.82	391911	431
16	780	2180	70,340	156,100	138,105	1.96	738697	446
17	570	2180	87,830	182,250	266,432	3.03	600453	423
18	1220	1710	89,750	160,900	78,626	0.88	891359	439
19	1680	960	30,000	65,049	45,467	1.52	1080054	451
20	1220	1700	60,800	124,500	79,688	1.31	887279	438
21	1875	0	48,180	112,200	39,702	0.82	1134267	452
22	1680	900	84,950	153,800	47,580	0.56	1062612	446
23	1550	1090	88,750	190,200	59,778	0.67	980112	433
24	1300	1400	84,680	226,000	92,551	1.09	843343	415
25	0	2000	1,011,333	1,843,666	4,999,874	4.94	272160	359
26	845	1800	259,900	396,800	226,037	0.87	631664	393
27	1730	0	67,300	157,125	62,378	0.93	965617	417
28	1708	0	163,800	249,900	67,137	0.41	941214	411
29	460	1760	2,688,500	> 10e6	1,190,454	0.44	391283	342
30	990	1390	641,500	890,500	285,803	0.45	587742	357
31	1150	1090	2,337,500	> 10e6	247,343	0.11	614311	350
32	1475	0	347,500	556,400	161,781	0.47	701934	355
33	0	1700	2,324,000	> 10e6	20,642,879	8.88	196635	305
34	1250	880	462,500	734,750	219,253	0.47	637679	349
35	1460	0	430,000	764,000	172,476	0.40	687730	352
36	1400	0	4,494,000	> 10e6	225,230	0.05	632366	337
37	725	1390	2,000,000	> 10e6	943,401	0.47	416680	314
38	0	1500	1,515,000	> 10e6	66,491,842	43.89	153090	269
39	920	880	3,473,000	> 10e6	1,148,731	0.33	395044	281

Table 6.2. Experimental fatigue life results [69, 70] and the results predicted by FS parameter for in-phase loading cases.

Loading Case	Bending Moment (N·m)	Torsional Moment (N·m)	Exp. Crack Initiation Life (up to 1mm)	Exp. Final Fracture Life	Predicted Initiation Life by FS Parameter	The Ratio of Predicted Life to Measured Life	Maximum FS Parameter	Max. Von Mises Stress (MPa)
			$N_{i\,(exp)}$	$N_{f\,(exp)}$	$N_{i\,(FS)}$	$N_{R\,(FS)}$	P_{FS}	σ_{eq}
1	1850	2550	2,200	5,113	23,781	10.81	0.56730E-02	660
2	2800	0	2,571	8,262	15,843	6.16	0.64417E-02	674
3	2000	2100	5,998	12,050	28,858	4.81	0.53487E-02	632
4	1250	2700	6,402	10,420	38,939	6.08	0.48933E-02	588
5	1150	2700	3,000	12,700	43,139	14.38	0.47496E-02	574
6	2325	1350	2,905	11,735	24,857	8.56	0.55966E-02	625
7	2600	0	6,347	15,043	21,384	3.37	0.58621E-02	626
8	2586	0	14,000	17,450	21,860	1.56	0.58222E-02	623
9	0	3000	5,529	12,124	84,230	15.23	0.39397E-02	538
10	1355	2550	5,500	11,630	40,546	7.37	0.48359E-02	580
11	1850	2100	5,740	11,565	34,751	6.05	0.50599E-02	603
12	851	2700	9,000	17,730	58,371	6.49	0.43575E-02	539
13	840	2700	10,000	24,540	59,011	5.90	0.43442E-02	538
14	1720	1350	19,260	58,790	74,429	3.86	0.40741E-02	494
15	0	2400	70,350	132,585	201,254	2.86	0.31518E-02	431
16	780	2180	70,340	156,100	126,619	1.80	0.35390E-02	446
17	570	2180	87,830	182,250	164,220	1.87	0.33136E-02	423
18	1220	1710	89,750	160,900	135,000	1.50	0.34814E-02	439
19	1680	960	30,000	65,049	101,735	3.39	0.37464E-02	451
20	1220	1700	60,800	124,500	136,997	2.25	0.34684E-02	438
21	1875	0	48,180	112,200	86,215	1.79	0.39151E-02	452
22	1680	900	84,950	153,800	105,043	1.24	0.37150E-02	446
23	1550	1090	88,750	190,200	129,733	1.46	0.35170E-02	433
24	1300	1400	84,680	226,000	184,869	2.18	0.32179E-02	415
25	0	2000	1,011,333	1,843,666	441,967	0.44	0.26265E-02	359
26	845	1800	259,900	396,800	218,036	0.84	0.30913E-02	393
27	1730	0	67,300	157,125	124,459	1.85	0.35547E-02	417
28	1708	0	163,800	249,900	132,080	0.81	0.35009E-02	411
29	460	1760	2,688,500	> 10e6	438,553	0.16	0.26310E-02	342
30	990	1390	641,500	890,500	366,082	0.57	0.27393E-02	357
31	1150	1090	2,337,500	> 10e6	426,331	0.18	0.26475E-02	350
32	1475	0	347,500	556,400	267,571	0.77	0.29444E-02	355
33	0	1700	2,324,000	> 10e6	957,727	0.41	0.22325E-02	305
34	1250	880	462,500	734,750	370,797	0.80	0.27314E-02	349
35	1460	0	430,000	764,000	281,594	0.65	0.29094E-02	352
36	1400	0	4,494,000	> 10e6	348,233	0.08	0.27705E-02	337
37	725	1390	2,000,000	> 10e6	669,541	0.33	0.24022E-02	314
38	0	1500	1,515,000	> 10e6	1,837,643	1.21	0.19698E-02	269
39	920	880	3,473,000	> 10e6	1,460,439	0.42	0.20563E-02	281

Table 6.3. Experimental fatigue life results [69, 70] and the results predicted by SWT parameter for 90^0 out-of-phase loading cases.

Loading Case	Bending Moment (N·m)	Torsional Moment (N·m)	Exp. Crack Initiation Life (up to 1mm) $N_{i_{(exp)}}$	Exp. Final Fracture Life $N_{f_{(exp)}}$	Predicted Initiation Life by SWT Parameter $N_{i_{(SWT)}}$	Maximum SWT Parameter P_{SWT}
1	1150	2700	10,600	13,110	187,471	669785
2	1850	2100	12,660	27,470	42,175	1109701
3	1800	2100	21,600	24,620	49,064	1051022
4	1698	2242	6,725	10,840	67,132	941242
5	2300	1325	17,720	23,980	13,544	1706744
6	770	2180	151,900	157,100	1,137,473	396090
7	1295	1710	25,580	45,580	361,894	547479
8	1220	1710	165,400	240,000	530,640	489537
9	985	1400	1,000,000	> 10e6	2,587,271	319924

Table 6.4. Experimental fatigue life results [69, 70] and the results predicted by FS parameter for 90^0 out-of-phase loading cases.

Loading Case	Bending Moment (N·m)	Torsional Moment (N·m)	Exp. Crack Initiation Life (up to 1mm) $N_{i_{(exp)}}$	Exp. Final Fracture Life $N_{f_{(exp)}}$	Predicted Initiation Life by FS Parameter $N_{i_{(FS)}}$	Maximum FS Parameter P_{FS}
1	1150	2700	10,600	13,110	111,893	0.36541E-02
2	1850	2100	12,660	27,470	90,946	0.38595E-02
3	1800	2100	21,600	24,620	102,883	0.37353E-02
4	1698	2242	6,725	10,840	133,996	0.34880E-02
5	2300	1325	17,720	23,980	35,524	0.50272E-02
6	770	2180	151,900	157,100	284,033	0.29036E-02
7	1295	1710	25,580	45,580	515,525	0.25396E-02
8	1220	1710	165,400	240,000	676,908	0.23967E-02
9	985	1400	1,000,000	> 10e6	2,061,265	0.19288E-02
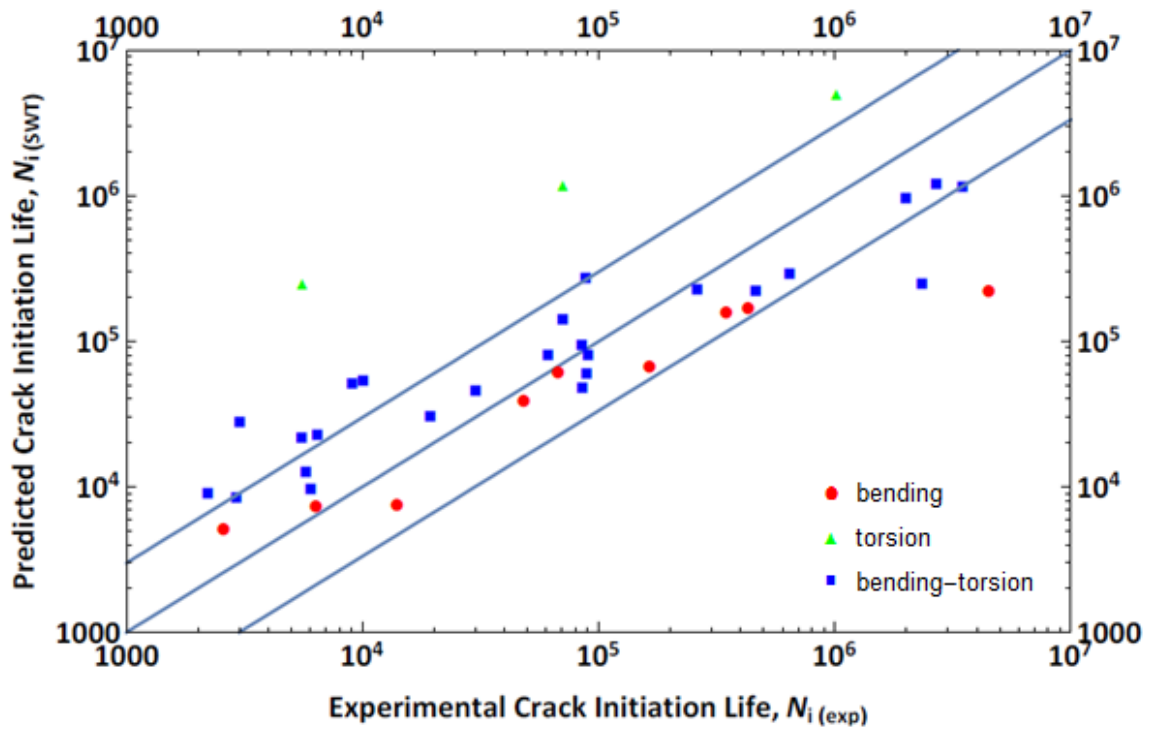
Figure 6.7. Predicted crack initiation life by SWT parameter versus experimental crack initiation life for in-phase loading cases.
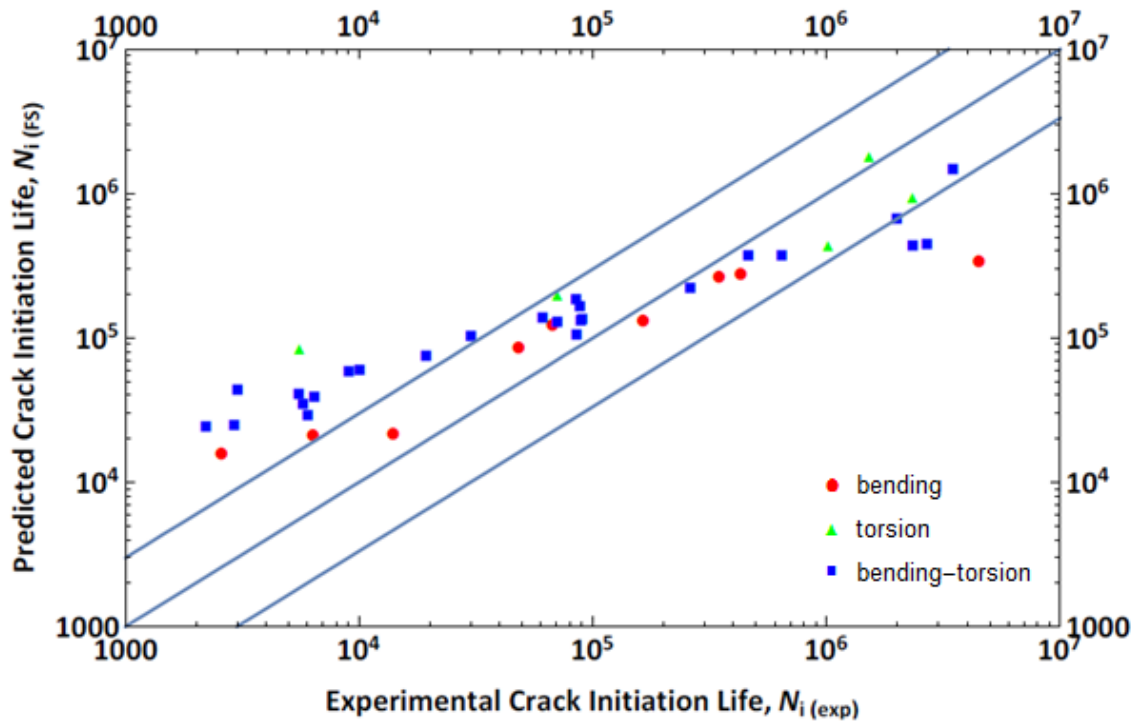
Figure 6.8. Predicted crack initiation life by FS parameter versus experimental crack initiation life for in-phase loading cases.
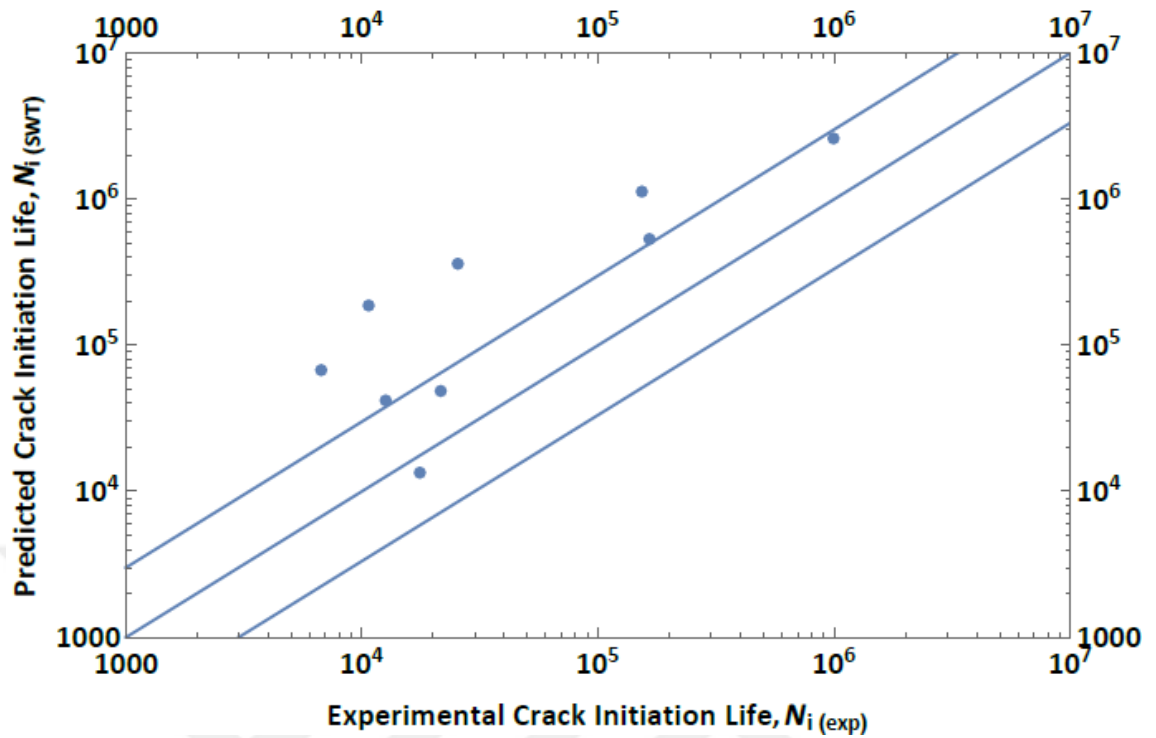
Figure 6.9. Predicted crack initiation life by SWT parameter versus experimental crack initiation life for 90^0 out-of-phase loading cases.
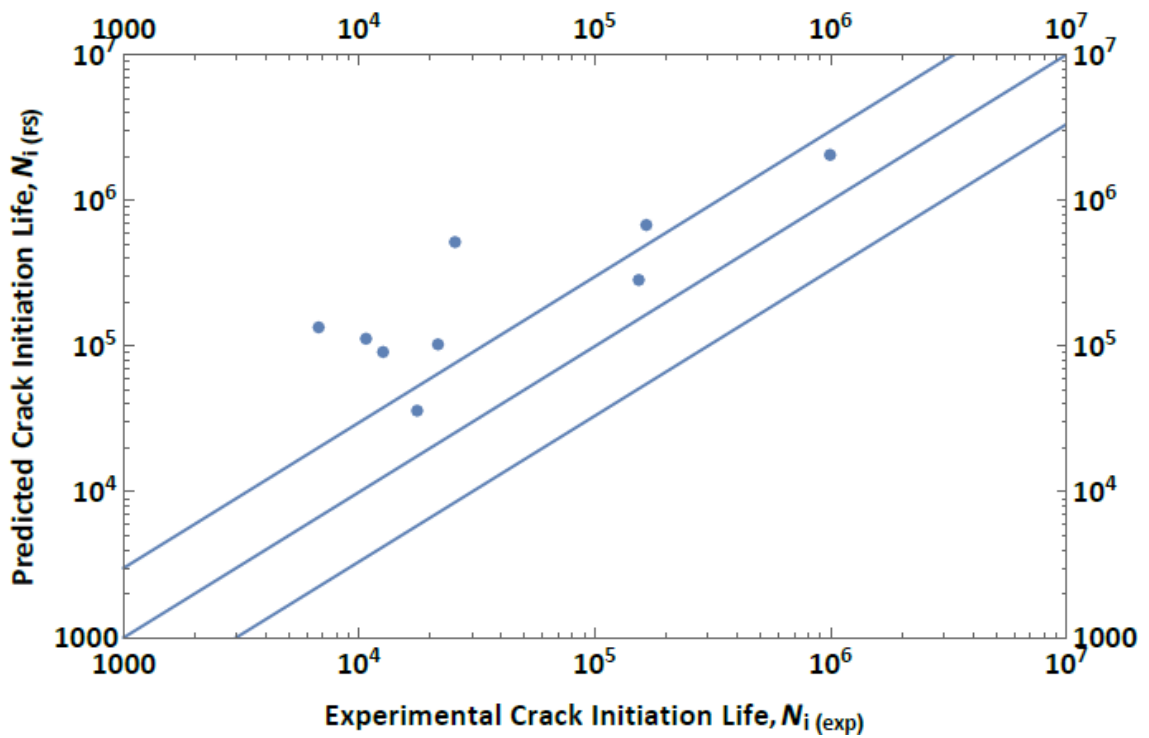
Figure 6.10. Predicted crack initiation life by FS parameter versus experimental crack initiation life for 90^0 out-of-phase loading cases.

Table 6.5. The maximum SWT and FS parameters obtained from MATLAB.

Loading Case	Bending Moment (N·m)	Torsional Moment (N·m)	Maximum SWT Parameter P_{SWT}	Maximum FS Parameter P_{FS}
1	1850	2550	2023114	0.5673E-02
2	2800	0	2529466	0.6442E-02

The results obtained for in-phase loading cases by SWT parameter are consistent with the experimental results. For most of the predictions, the ratio of the predicted life to the measured fatigue life falls within the range of $1/3$ and 3.0, especially for lives longer than 10^4 cycles as seen in Figure 6.7. Under pure torsion loadings, there are large differences between the experimental results and the results predicted by SWT model as can be noticed in Table 6.1. The reason for this may be the fact that the critical plane is the one at which the maximum principal stress develops according to SWT model while the experimental observation indicate that cracks initiate and grow at the maximum-shear-stress plane under pure torsion [38]. Besides, the material constants in the model (Equation 3.1) are obtained from fatigue tests on specimens under pure axial loading.

FS model highly overestimates fatigue lives shorter than 10^4 cycles as shown in Figure 6.8; otherwise the predictions are generally consistent with the experimental results. Unlike SWT model, FS predictions for pure torsion cases are accurate. This may be because FS model assumes that the maximum-shear-stress plane is the critical plane and the material constants are obtained from pure torsion tests.

The reason that both SWT and FS models fail to estimate the fatigue lives accurately in the low cycle range may be the plastic deformation occurring at low cycle. Because a linear elastic analysis is performed in ANSYS, plastic deformations are neglected. However, at low cycles, plastic deformations may be significant and so, stress and strain states may not be accurately determined. The maximum von Mises (equivalent) stress for each loading case is given in Tables 6.1 and 6.2. As seen in the tables, in most of the load cases, the maximum von Mises stress exceeds the yield strength of the material, which is 380 MPa; therefore plastic deformations occur in those cases. If local yielding occurs in the part, linear elastic analysis overestimates stresses; but underestimates strains. Because

SWT parameter is a product of stress and strain terms, the errors in their values somewhat compensate the error in the resulting value of the SWT parameter; for this reason, the accuracy of SWT model predictions for low cycle fatigue may still be acceptable. Because the dominant term in FS parameter is strain, FS model overestimates the life at low cycle

The fillet in this shouldered shaft is a mild notch. The stress concentration factor of the notch, K_t, is 1.56, the fatigue stress concentration factor, K_f, is 1.48. Because their values are close to each other, the predictions of the critical plane models based on the local stress and strains states are accurate. Considering that the notch with the optimum shape is milder, i.e. with a larger radius of curvature, the predictions of the models for the optimum shape are expected to be also accurate.

Comparison of the predictions with the experimental results obtained for the shouldered shaft shows that the critical plane models estimate the fatigue life with an acceptable accuracy. If the loading is predominantly torsion, FS model can provide a reliable evaluation of fatigue behavior as opposed to SWT model. On the other hand, SWT model is more reliable for low cycle fatigue.

In both SWT and FS results of 90^0 out-of phase loading cases, most of the predictions are outside the prediction limits as shown in Figures 6.9 and 6.10. It should be noted that there are only nine experimental results for out-of-phase loadings and in the experiments, eight of them were tested only once. Whereas, 18 of 39 in-phase fatigue tests were performed at least twice under the same loading cases.

6.1.2. Shape Optimization Results

Two different types of shape optimization are performed: One is for in-phase loading cases and the other is for 90^0 out-of-phase loading cases. For 90^0 out-of-phase shape optimization, it is not possible to find the parameter, ωt for each current configuration since it will take so much time. For this reason, the parameter, ωt of the current configuration having lowest cost function in the set is examined and this parameter is accepted for all current configurations. At the end of every five chains, the parameter of

the current lowest cost function is replaced with the previous one and the costs of the current configurations are updated. The process continues to the end of algorithm.

Because SWT or FS parameter is inversely proportional to fatigue life, maximizing fatigue life yields the same result as minimizing the damage parameter. Because fatigue life calculation at each iteration increases the computational burden, the objective function is chosen as the damage parameter. Optimum shapes are separately obtained using SWT and FS models. The optimization algorithm tries to find the optimum coordinates of the moving key points for the minimum objective function value, i.e. minimum SWT or FS damage parameter value. For in-phase loading cases, optimum shapes are obtained using two, three, four and five moving key points. One of the optimization processes in which four moving key points are used is performed by choosing the objective function as FS parameter. All others are performed by taking the objective function as SWT parameter. For 90^0 out-of-phase loading, shape optimization is performed using four moving key points and the objective function is chosen as SWT parameter.

Two optimization parameters, maximum moving distance and temperature parameters are used in the algorithm. The initial maximum moving distance parameters of fillet model calculated from Equation (4.9) are 0.45 mm, 0.45 mm, 0.42 mm and 0.34 mm for two, three, four and five moving key points, respectively. The initial temperature parameter of fillet model is 1.0E7.

Table 6.6 presents the shape optimization results obtained using two moving key points for the in-phase loading cases of $M = 1550$ Nm, $T = 1090$ Nm and $M = 845$ Nm, $T = 1800$ Nm. One of the loading cases is bending-moment dominated and the other is torsional-moment dominated. Although the loading cases are different, the optimum shapes are quite similar. At the end of each optimization process, two optimum shapes are obtained and the objective function values of the loading cases of $M = 1550$ Nm, $T = 1090$ Nm and $M = 845$ Nm, $T = 1800$ Nm dropped to 0.7852 and 0.8264, respectively. According to SWT model, under the same loading condition, fatigue lives of the optimum parts are 121,821 and 121,369 for these two loading cases, respectively, which are 104 % and 103 % higher than that of the parts with circular fillets.

The optimization process is repeated using three and four moving key points for the in-phase loading case of $M = 1550$ Nm, $T = 1090$ Nm. At the end, fatigue lives of the optimum parts are 127,903 and 137,659 for three and four moving key points, respectively, which are 114 % and 130 % higher than that of the part with circular fillet. The results are given in Tables 6.7 and 6.8.

Optimization is also conducted using FS model for fatigue assessment with four moving key points for the in-phase loading case of $M = 1550$ Nm, $T = 1090$ Nm. The fatigue life of the optimum part is 137,301, which is 130 % higher than that of the part with circular fillet. The results are given in Table 6.9.

Another optimization is performed using five moving key points and SWT model for the in-phase loading case of $M = 1550$ Nm, $T = 1090$ Nm. The fatigue life of the optimized part is 138,055, which is 131 % higher than that of the parts with circular fillets. The results are given in Table 6.10.

The results obtained with four moving key points for 90^0 out-of-phase loading case of $M = 1220$ Nm, $T = 1710$ Nm, are presented in Table 6.11. The fatigue life of the optimum part is 1,376,754, which is 159 % higher than that of the parts with circular fillets.

Table 6.6. The results obtained with two moving key points for two in-phase loading cases using SWT parameter as the objective function.

	$M = 1550$ Nm, $T = 1090$ Nm		$M = 845$ Nm, $T = 1800$ Nm	
	7th key point	10th key point	7th key point	10th key point
The x coordinate (mm)	23.5028	21.6230	23.4989	21.6243
The y coordinate (mm)	79.9826	79.9819	79.9972	79.9742

Table 6.7. The results obtained with three moving key points for an in-phase loading case using SWT parameter as the objective function.

	$M = 1550$ Nm, $T = 1090$ Nm		
	7th key point	10th key point	17th key point
The x coordinate (mm)	22.7381	20.5184	21.7265
The y coordinate (mm)	79.9996	77.9391	79.9868

Table 6.8. The results obtained with four moving key points for an in-phase loading case using SWT parameter as the objective function.

	$M = 1550$ Nm, $T = 1090$ Nm			
	7th key point	10th key point	17th key point	18th key point
The x coordinate (mm)	22.4694	20.1300	21.5313	20.5700
The y coordinate (mm)	79.9541	76.3507	79.7672	78.1434

Table 6.9. The results obtained with four moving key points for an in-phase loading case using FS parameter as the objective function.

	$M = 1550$ Nm, $T = 1090$ Nm			
	7th key point	10th key point	17th key point	18th key point
The x coordinate (mm)	22.5462	20.1461	21.5449	20.5721
The y coordinate (mm)	79.9782	76.4318	79.7968	78.1361

Table 6.10. The results obtained with five moving key points for an in-phase loading case using SWT parameter as the objective function.

	$M = 1550$ Nm, $T = 1090$ Nm				
	7th key point	10th key point	17th key point	18th key point	19th key point
The x coordinate (mm)	22.5396	20.1429	21.5402	20.5677	23.6867
The y coordinate (mm)	79.9973	76.4304	79.7984	78.1276	79.9916

Table 6.11. The results obtained with four moving key points for a 90^0 out-of-phase loading case using SWT parameter as the objective function.

	$M = 1220$ Nm, $T = 1710$ Nm			
	7th key point	10th key point	17th key point	18th key point
The x coordinate (mm)	24.7781	20.4016	23.3830	21.7124
The y coordinate (mm)	79.9958	77.4962	79.9954	79.9765

ANSYS generates a spline curve through the key points at the boundary and the optimum shapes are obtained as shown in Figures 6.11, 6.12, 6.13, 6.14, 6.15, 6.16, and 6.17.
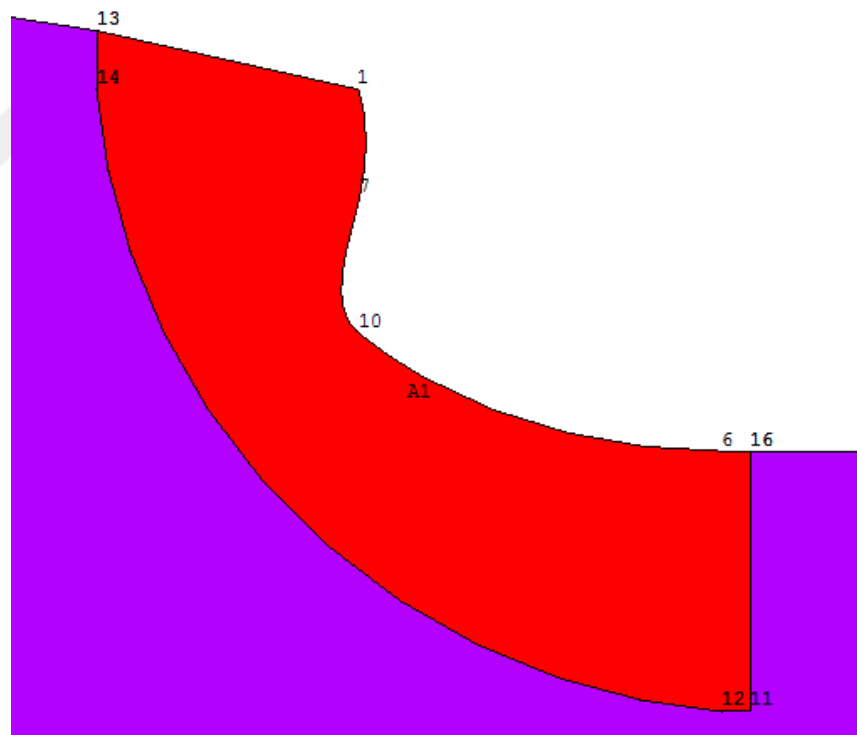
Figure 6.11. The optimum fillet boundary obtained with two moving key points for the in-phase loading case of $M = 1550$ Nm, $T = 1090$ Nm using SWT model.
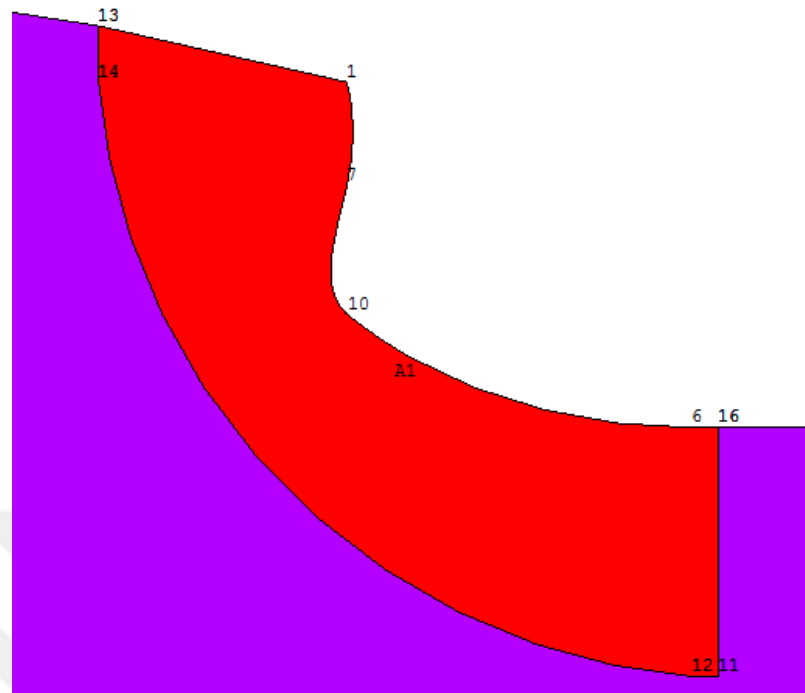
Figure 6.12. The optimum fillet boundary obtained with two moving key points for the in-phase loading case of $M = 845$ Nm, $T = 1800$ Nm using SWT model.
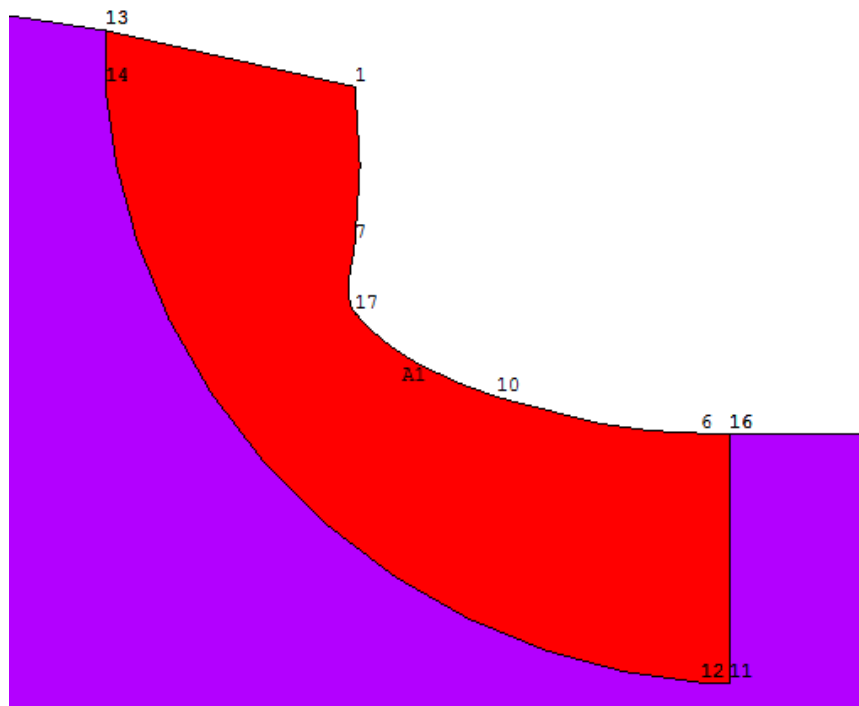
Figure 6.13. The optimum fillet boundary obtained with three moving key points for the in-phase loading case of $M = 1550$ Nm, $T = 1090$ Nm using SWT model.
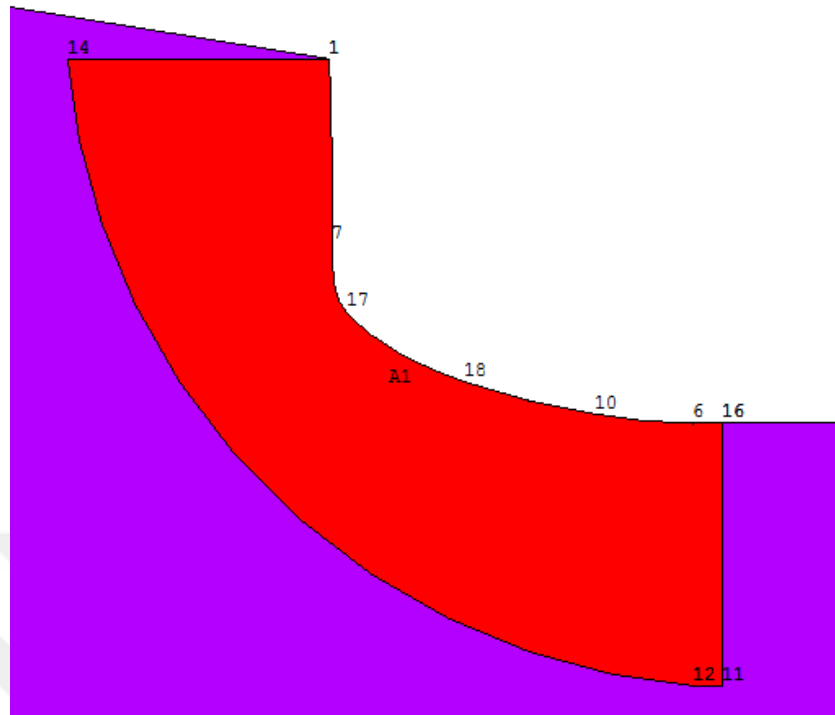
Figure 6.14. The optimum fillet boundary obtained with four moving key points for the in-phase loading case of $M = 1550$ Nm, $T = 1090$ Nm using SWT model.
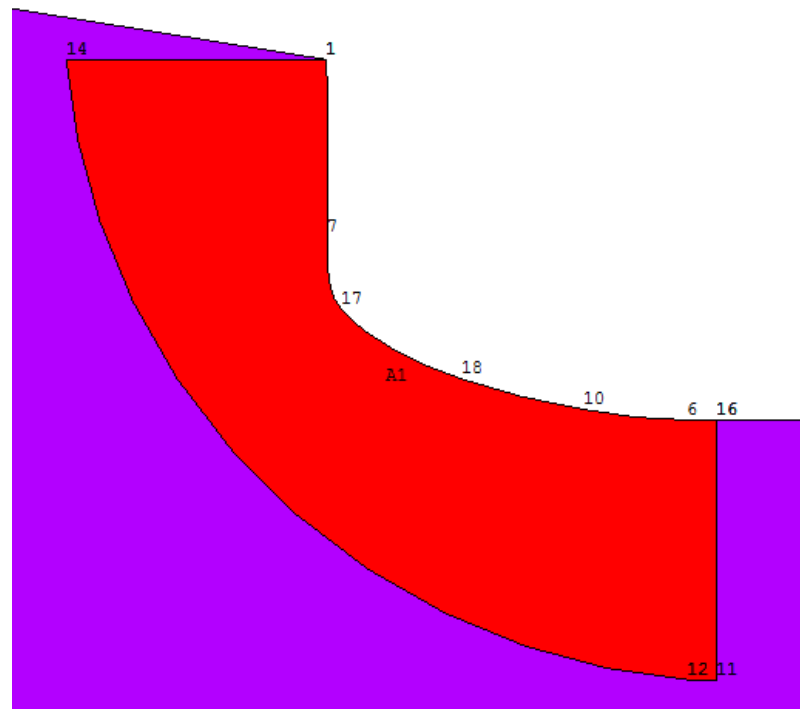
Figure 6.15. The optimum fillet boundary obtained with four moving key points for the in-phase loading case of $M = 1550$ Nm, $T = 1090$ Nm using FS model.

Figure 6.16. The optimum fillet boundary obtained with five moving key points for the in-phase loading case of $M = 1550$ Nm, $T = 1090$ Nm using SWT model.
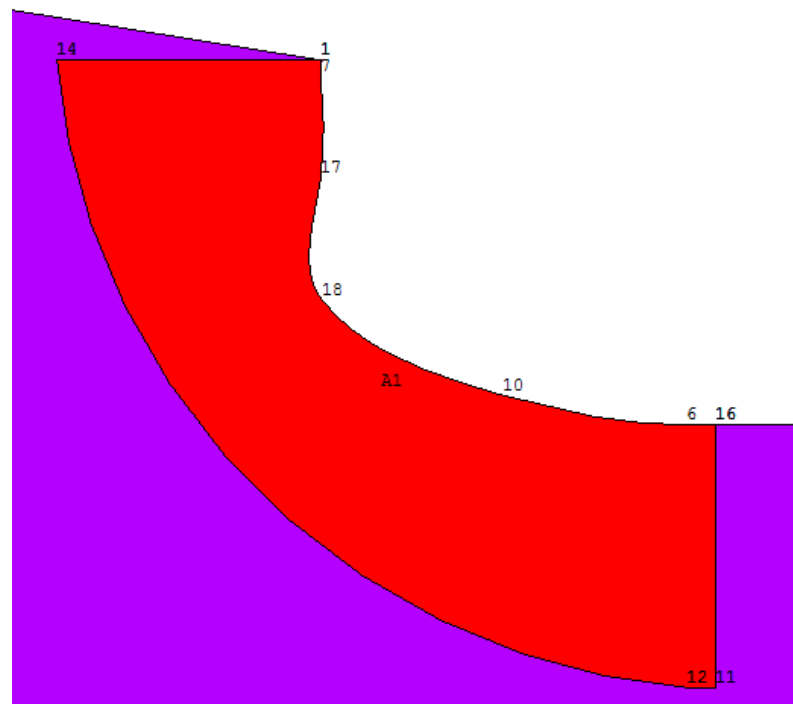
Figure 6.17. The optimum fillet boundary obtained with four moving key points for the 90^0 out-of-phase loading case of $M = 1220$ Nm, $T = 1710$ Nm using SWT model.

The SWT parameter distributions for the circular fillet and the optimized shapes obtained with two, three, four and five moving key points are shown in Figures 6.18, 6.19, 6.20, 6.21 and 6.22.
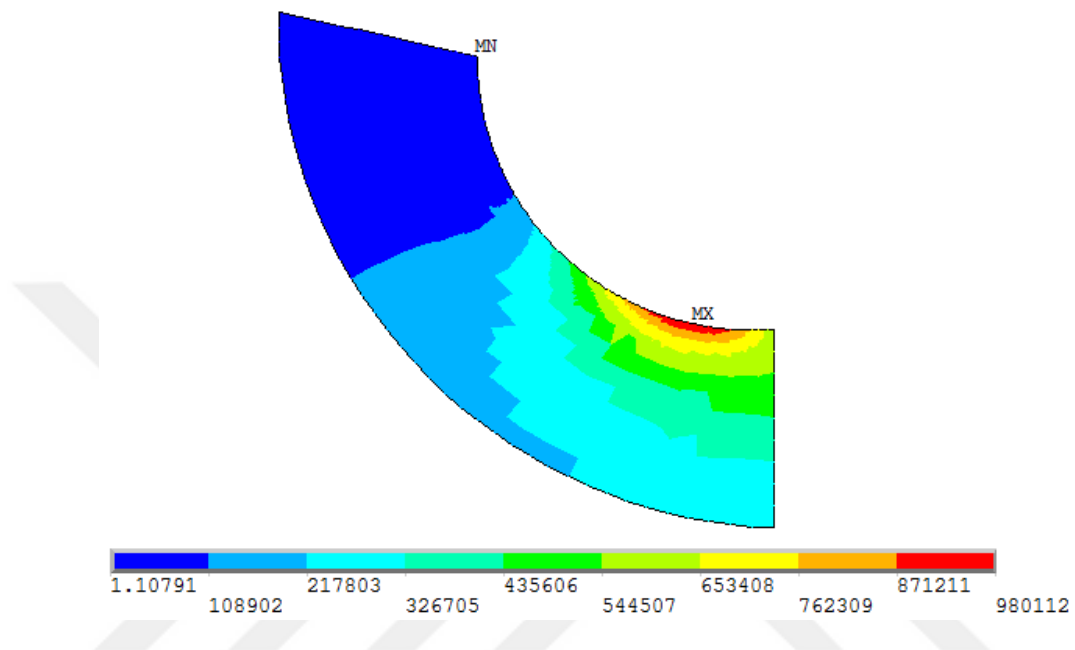
Figure 6.18. SWT parameter distribution of the part with circular fillet.
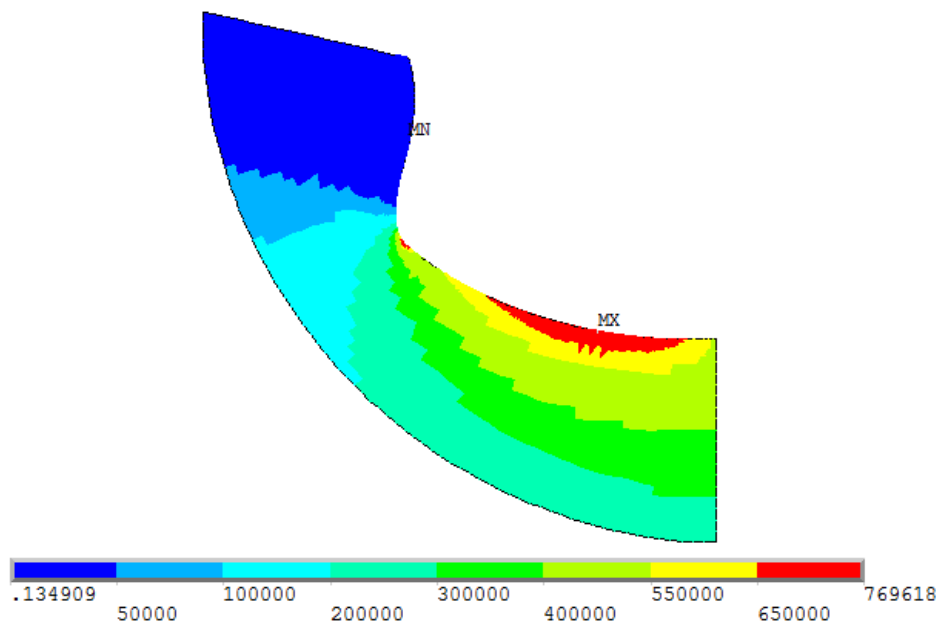
Figure 6.19. SWT parameter distribution of the optimized part with two moving key points.
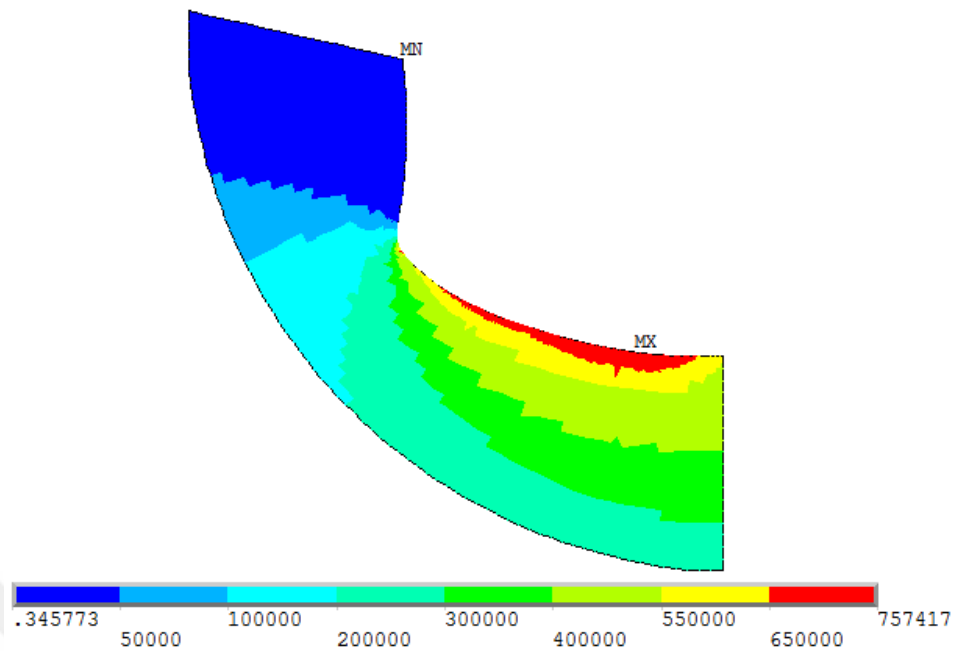
Figure 6.20. SWT parameter distribution of the optimized part with three moving key points.
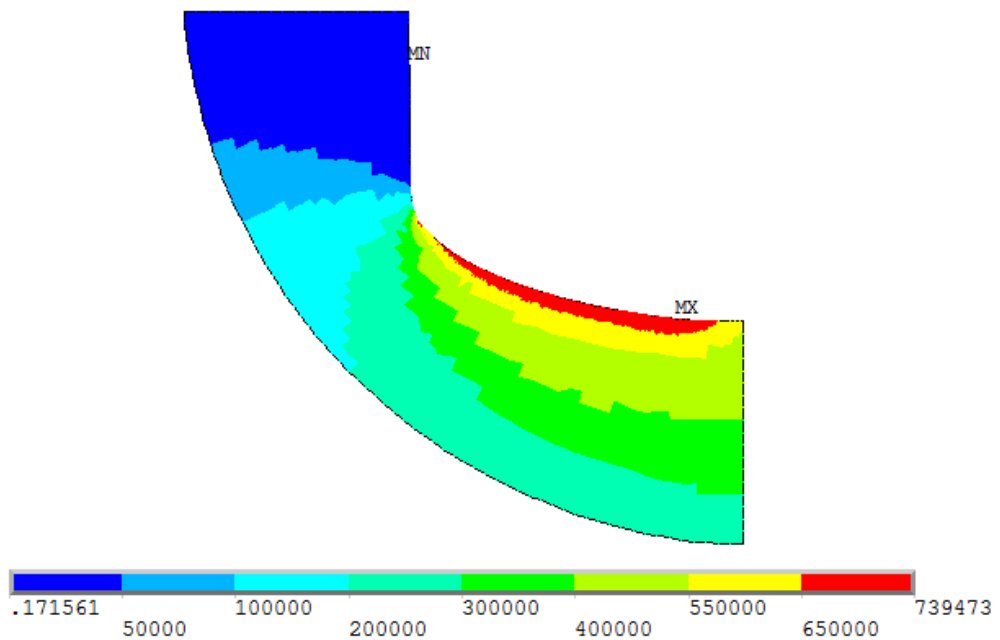
Figure 6.21. SWT parameter distribution of the optimized part with four moving key points.
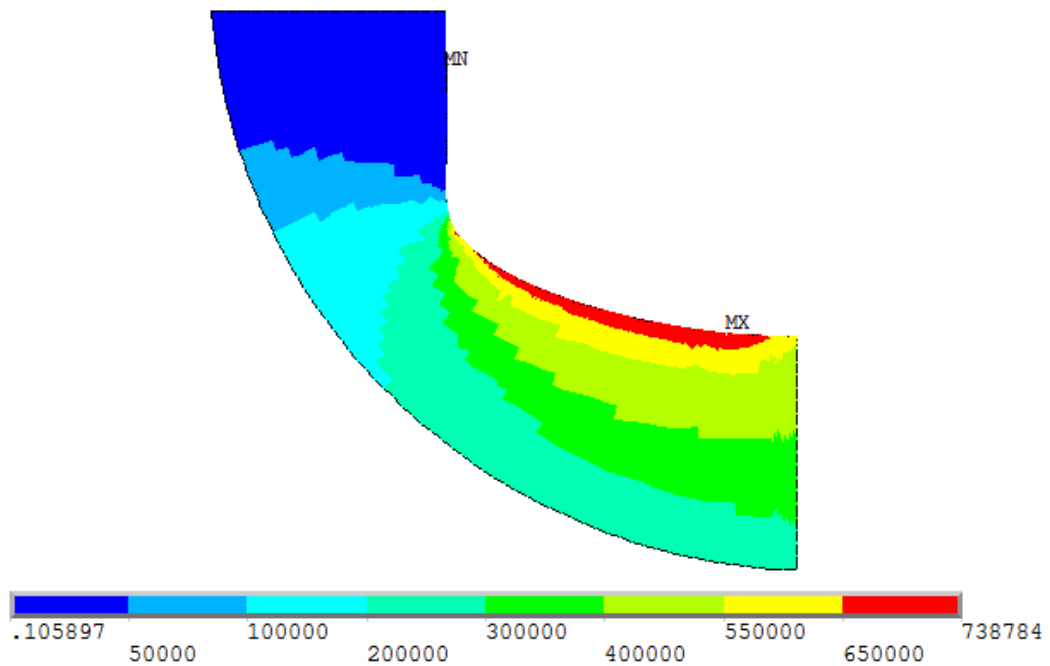
Figure 6.22. SWT parameter distribution of the optimized part with five moving key points.

For in-phase shape optimization performed using SWT or FS parameter, six different optimized shapes are obtained and all the optimized shapes created by two, three, four and five moving key points are analyzed for some loading cases.

The maximum SWT and FS parameter results and fatigue life results of the optimized parts are given in Tables 6.12, 6.13, 6.14, 6.15, 6.16, 6.17, 6.18, 6.19, 6.20, 6.21, 6.22 and 6.23. In addition, the theoretical percentage increases in fatigue life for each loading case using the optimized part compared to the original shaped part are shown in the tables. Sorting is performed according to the percentage increase in fatigue life.

For all optimized shapes obtained for an in-phase loading case, the percentage increases for the loading cases in which bending moment is higher than the torsional moment are generally more than the ones in which torsional moment dominates.

For the case in which two moving key points are used, the results are given in Tables 6.12, 6.13, 6.14 and 6.15. As can be seen from the results, there is little difference between

the shapes and results of two optimized parts (obtained by use of loading cases of $M = 1550$ Nm, $T = 1090$ Nm and $M = 845$ Nm, $T = 1800$ Nm), less than or equal to one percent in fatigue life. Accordingly, the optimized shapes are obtained not depending on the loading case used in the algorithm.

The in-phase results of the optimized shapes obtained by three and four moving key points are given in Tables 6.16, 6.17, 6.18, 6.19, 6.20 and 6.21. As in the results obtained by two moving key points, the percentage increases in fatigue life are higher in bending moment-dominated cases. The objective function decreases and hence fatigue life increases with the increasing number of moving key points. The highest increases in fatigue life are obtained for the shape optimized by four moving key points. As can be seen from Tables 6.18, 6.19, 6.20 and 6.21, there is not a significant difference between the fatigue life results of optimized shapes obtained by the use of SWT parameter and FS parameter as the objective function. Accordingly, the objective function can be selected as either one.

The results of the optimized shape obtained with five moving key points are given in Tables 6.22 and 6.23. Although the percentage increases in fatigue life are slightly better, the fatigue life results of optimized shape created by five moving key points are quite similar to that of optimized shape created by four moving key points. Besides, the use of five moving key points requires more computational effort and time. Therefore, the use of four moving key points is sufficient.

For 90^0 out-of-phase shape optimization, one optimized shape created by four moving key points is analyzed for nine 90^0 out-of-phase loading cases. The theoretical percentage increases in fatigue life of all 90^0 out-of-phase loading cases calculated by SWT and FS parameters are given in Tables 6.24 and 6.25, respectively. The highest increase in fatigue life is obtained for torsional moment-dominated cases for both SWT and FS models. However, only one of nine 90^0 out-of-phase loading cases is bending moment-dominated.

Table 6.12. The SWT parameter and life results of optimized part obtained with two moving key points for the in-phase loading case of $M = 1550$ Nm, $T = 1090$ Nm using SWT model.

|	Loading Case	Bending Moment (N·m)	Torsional Moment (N·m)	Maximum SWT Parameter (Optimized Part) $P_{o_{SWT}}$	Predicted Initiation Life by SWT Parameter (Optimized Part) $N_{i_{o(SWT)}}$	The Percentage Increase in Fatigue Life (Obtained by SWT Parameter) $N_{SWT_{\%}}$
1	39	920	880	312798	2,830,621	146 %
2	36	1400	0	487458	538,568	139 %
3	35	1460	0	530135	403,486	134 %
4	23	1550	1090	769618	121,821	104 %
5	19	1680	960	844300	92,241	103 %
6	3	2000	2100	1561440	16,986	78 %
7	10	1355	2550	1174739	36,064	69 %
8	4	1250	2700	1165434	36,857	64 %
9	15	0	2400	357816	1,670,397	41 %
10	9	0	3000	559088	337,317	35 %

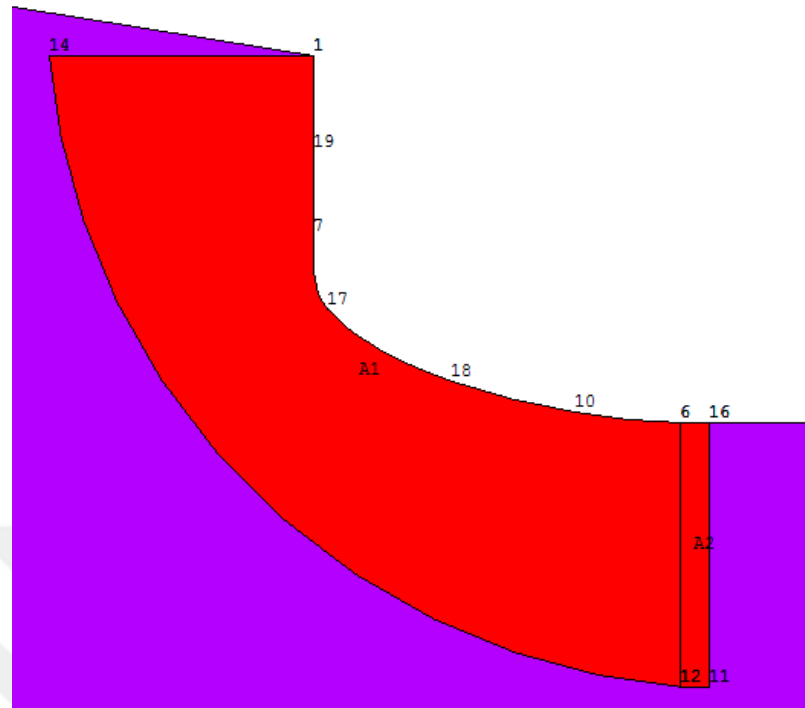Table 6.13. The FS parameter and life results of optimized part obtained with two moving key points for the in-phase loading case of $M = 1550$ Nm, $T = 1090$ Nm using SWT model.

|	Loading Case	Bending Moment (N·m)	Torsional Moment (N·m)	Maximum FS Parameter (Optimized Part) $P_{o_{FS}}$	Predicted Initiation Life by FS Parameter (Optimized Part) $N_{i_{o(FS)}}$	The Percentage Increase in Fatigue Life (Obtained by FS Parameter) $N_{FS_{\%}}$
1	36	1400	0	0.23799E-02	700,134	101 %
2	35	1460	0	0.24973E-02	557,386	98 %
3	39	920	880	0.18262E-02	2,800,068	92 %
4	23	1550	1090	0.30387E-02	234,215	81 %
5	19	1680	960	0.32259E-02	183,011	80 %
6	3	2000	2100	0.47209E-02	44,053	53 %
7	10	1355	2550	0.43577E-02	58,362	44 %
8	4	1250	2700	0.44407E-02	54,577	40 %
9	15	0	2400	0.30115E-02	243,227	21 %
10	9	0	3000	0.37644E-02	99,904	19 %

Table 6.14. The SWT parameter and life results of optimized part obtained with two moving key points for the in-phase loading case of $M = 845$ Nm, $T = 1800$ Nm using SWT model.

	Loading Case	Bending Moment (N·m)	Torsional Moment (N·m)	Maximum SWT Parameter (Optimized Part)	Predicted Initiation Life by SWT Parameter (Optimized Part)	The Percentage Increase in Fatigue Life (Obtained by SWT Parameter)
				$P_{o_{SWT}}$	$N_{i_{o}(SWT)}$	$N_{SWT\%}$
1	39	920	880	313176	2,816,968	145 %
2	36	1400	0	488132	535,978	138 %
3	35	1460	0	530869	401,595	133 %
4	23	1550	1090	770561	121,369	103 %
5	19	1680	960	845381	91,892	102 %
6	26	845	1800	521980	425,352	88 %
7	3	2000	2100	1563315	16,934	78 %
8	10	1355	2550	1170152	36,452	70 %
9	4	1250	2700	1160695	37,270	66 %
10	15	0	2400	355904	1,705,177	44 %
11	9	0	3000	556099	343,417	37 %

Table 6.15. The FS parameter and life results of optimized part obtained with two moving key points for the in-phase loading case of $M = 845$ Nm, $T = 1800$ Nm using SWT model.

	Loading Case	Bending Moment (N·m)	Torsional Moment (N·m)	Maximum FS Parameter (Optimized Part)	Predicted Initiation Life by FS Parameter (Optimized Part)	The Percentage Increase in Fatigue Life (Obtained by FS Parameter)
				$P_{o_{FS}}$	$N_{i_{o}(FS)}$	$N_{FS\%}$
1	36	1400	0	0.23817E-02	697,597	100 %
2	35	1460	0	0.24992E-02	555,412	97 %
3	39	920	880	0.18275E-02	2,788,719	91 %
4	23	1550	1090	0.30409E-02	233,506	80 %
5	19	1680	960	0.32283E-02	182,459	79 %
6	3	2000	2100	0.47244E-02	43,941	52 %
7	26	845	1800	0.28130E-02	325,762	49 %
8	10	1355	2550	0.43466E-02	58,895	45 %
9	4	1250	2700	0.44291E-02	55,085	41 %
10	15	0	2400	0.30035E-02	245,967	22 %
11	9	0	3000	0.37544E-02	100,916	20 %

Table 6.16. The SWT parameter and life results of optimized part obtained with three moving key points for the in-phase loading case of $M = 1550$ Nm, $T = 1090$ Nm using SWT model.

	Loading Case	Bending Moment (N·m)	Torsional Moment (N·m)	Maximum SWT Parameter (Optimized Part) $P_{o_{SWT}}$	Predicted Initiation Life by SWT Parameter (Optimized Part) $N_{i_{o(SWT)}}$	The Percentage Increase in Fatigue Life (Obtained by SWT Parameter) $N_{SWT_\%}$
1	39	920	880	308180	3,004,704	162 %
2	36	1400	0	478792	573,421	155 %
3	35	1460	0	520710	428,903	149 %
4	23	1550	1090	757417	127,903	114 %
5	19	1680	960	830491	96,875	113 %
6	3	2000	2100	1538990	17,631	85 %
7	10	1355	2550	1144550	38,729	81 %
8	4	1250	2700	1130501	40,067	79 %
9	15	0	2400	358183	1,663,845	41 %
10	9	0	3000	559660	336,166	35 %

Table 6.17. The FS parameter and life results of optimized part obtained with three moving key points for the in-phase loading case of $M = 1550$ Nm, $T = 1090$ Nm using SWT model.

	Loading Case	Bending Moment (N·m)	Torsional Moment (N·m)	Maximum FS Parameter (Optimized Part) $P_{o_{FS}}$	Predicted Initiation Life by FS Parameter (Optimized Part) $N_{i_{o(FS)}}$	The Percentage Increase in Fatigue Life (Obtained by FS Parameter) $N_{FS_\%}$
1	36	1400	0	0.23527E-02	740,030	113 %
2	35	1460	0	0.24686E-02	588,394	109 %
3	39	920	880	0.18200E-02	2,855,026	95 %
4	23	1550	1090	0.30067E-02	244,866	89 %
5	19	1680	960	0.31907E-02	191,382	88 %
6	3	2000	2100	0.46978E-02	44,809	55 %
7	10	1355	2550	0.43247E-02	59,968	48 %
8	4	1250	2700	0.43898E-02	56,856	46 %
9	15	0	2400	0.30131E-02	242,684	21 %
10	9	0	3000	0.37664E-02	99,703	18 %

Table 6.18. The SWT parameter and life results of optimized part obtained with four moving key points for the in-phase loading case of $M = 1550$ Nm, $T = 1090$ Nm using SWT model.

	Loading Case	Bending Moment (N·m)	Torsional Moment (N·m)	Maximum SWT Parameter (Optimized Part) $P_{o_{SWT}}$	Predicted Initiation Life by SWT Parameter (Optimized Part) $N_{i_{o(SWT)}}$	The Percentage Increase in Fatigue Life (Obtained by SWT Parameter) $N_{SWT_\%}$
1	39	920	880	301180	3,296,636	187 %
2	36	1400	0	466801	626,962	178 %
3	35	1460	0	507669	467,868	171 %
4	23	1550	1090	739473	137,659	130 %
5	19	1680	960	810429	104,220	129 %
6	3	2000	2100	1504599	18,690	96 %
7	10	1355	2550	1139462	39,206	83 %
8	4	1250	2700	1132802	39,844	78 %
9	15	0	2400	354916	1,723,520	46 %
10	9	0	3000	554556	346,628	39 %

Table 6.19. The FS parameter and life results of optimized part obtained with four moving key points for the in-phase loading case of $M = 1550$ Nm, $T = 1090$ Nm using SWT model.

	Loading Case	Bending Moment (N·m)	Torsional Moment (N·m)	Maximum FS Parameter (Optimized Part) $P_{o_{FS}}$	Predicted Initiation Life by FS Parameter (Optimized Part) $N_{i_{o(FS)}}$	The Percentage Increase in Fatigue Life (Obtained by FS Parameter) $N_{FS_\%}$
1	36	1400	0	0.23269E-02	780,722	124 %
2	35	1460	0	0.24414E-02	619,951	120 %
3	39	920	880	0.18053E-02	2,991,024	105 %
4	23	1550	1090	0.29652E-02	259,684	100 %
5	19	1680	960	0.31479E-02	202,281	99 %
6	3	2000	2100	0.46512E-02	46,388	61 %
7	10	1355	2550	0.42980E-02	61,313	51 %
8	4	1250	2700	0.43850E-02	57,078	47 %
9	15	0	2400	0.29993E-02	247,422	23 %
10	9	0	3000	0.37491E-02	101,458	20 %

Table 6.20. The SWT parameter and life results of optimized part obtained with four moving key points for the in-phase loading case of $M = 1550$ Nm, $T = 1090$ Nm using FS model.

	Loading Case	Bending Moment (N·m)	Torsional Moment (N·m)	Maximum SWT Parameter (Optimized Part) $P_{o_{SWT}}$	Predicted Initiation Life by SWT Parameter (Optimized Part) $N_{i_{o(SWT)}}$	The Percentage Increase in Fatigue Life (Obtained by SWT Parameter) $N_{SWT_{\%}}$
1	39	920	880	301412	3,286,384	186 %
2	36	1400	0	467338	624,418	177 %
3	35	1460	0	508254	466,019	170 %
4	23	1550	1090	740101	137,301	130 %
5	19	1680	960	811159	103,939	129 %
6	3	2000	2100	1505727	18,653	96 %
7	10	1355	2550	1123014	40,808	91 %
8	4	1250	2700	1110894	42,050	88 %
9	15	0	2400	349648	1,825,934	54 %
10	9	0	3000	546325	364,472	46 %

Table 6.21. The FS parameter and life results of optimized part obtained with four moving key points for the in-phase loading case of $M = 1550$ Nm, $T = 1090$ Nm using FS model.

	Loading Case	Bending Moment (N·m)	Torsional Moment (N·m)	Maximum FS Parameter (Optimized Part) $P_{o_{FS}}$	Predicted Initiation Life by FS Parameter (Optimized Part) $N_{i_{o(FS)}}$	The Percentage Increase in Fatigue Life (Obtained by FS Parameter) $N_{FS_{\%}}$
1	36	1400	0	0.23173E-02	796,623	129 %
2	35	1460	0	0.24313E-02	632,246	125 %
3	39	920	880	0.18064E-02	2,980,560	104 %
4	23	1550	1090	0.29625E-02	260,690	101 %
5	19	1680	960	0.31427E-02	203,663	100 %
6	3	2000	2100	0.46539E-02	46,294	60 %
7	10	1355	2550	0.42902E-02	61,714	52 %
8	4	1250	2700	0.43561E-02	58,438	50 %
9	15	0	2400	0.29770E-02	255,349	27 %
10	9	0	3000	0.37212E-02	104,378	24 %

Table 6.22. The SWT parameter and life results of optimized part obtained with five moving key points for the in-phase loading case of $M = 1550$ Nm, $T = 1090$ Nm using SWT model.

	Loading Case	Bending Moment (N·m)	Torsional Moment (N·m)	Maximum SWT Parameter (Optimized Part)	Predicted Initiation Life by SWT Parameter (Optimized Part)	The Percentage Increase in Fatigue Life (Obtained by SWT Parameter)
				$P_{o_{SWT}}$	$N_{i_{o(SWT)}}$	$N_{SWT_\%}$
1	39	920	880	300830	3,312,216	188 %
2	36	1400	0	466277	629,455	179 %
3	35	1460	0	507100	469,681	172 %
4	23	1550	1090	738784	138,055	131 %
5	19	1680	960	809483	104,586	130 %
6	3	2000	2100	1502854	18,746	97 %
7	10	1355	2550	1121012	41,010	92 %
8	4	1250	2700	1111283	42,009	87 %
9	15	0	2400	347829	1,863,196	57 %
10	9	0	3000	543483	370,931	48 %

Table 6.23. The FS parameter and life results of optimized part obtained with five moving key points for the in-phase loading case of $M = 1550$ Nm, $T = 1090$ Nm using SWT model.

	Loading Case	Bending Moment (N·m)	Torsional Moment (N·m)	Maximum FS Parameter (Optimized Part)	Predicted Initiation Life by FS Parameter (Optimized Part)	The Percentage Increase in Fatigue Life (Obtained by FS Parameter)
				$P_{o_{FS}}$	$N_{i_{o(FS)}}$	$N_{FS_\%}$
1	36	1400	0	0.23145E-02	801,342	130 %
2	35	1460	0	0.24283E-02	635,960	126 %
3	39	920	880	0.18043E-02	3,000,577	105 %
4	23	1550	1090	0.29591E-02	261,964	102 %
5	19	1680	960	0.31390E-02	204,653	101 %
6	3	2000	2100	0.46482E-02	46,492	61 %
7	10	1355	2550	0.42858E-02	61,941	53 %
8	4	1250	2700	0.43517E-02	58,649	51 %
9	15	0	2400	0.29692E-02	258,203	28 %
10	9	0	3000	0.37115E-02	105,420	25 %

Table 6.24. The SWT parameter and life results of optimized part obtained with four moving key points for the 90^0 out-of-phase loading case of $M = 1220$ Nm, $T = 1710$ Nm using SWT model.

	Loading Case	Bending Moment (N·m)	Torsional Moment (N·m)	Maximum SWT Parameter (Optimized Part) $P_{o_{SWT}}$	Predicted Initiation Life by SWT Parameter (Optimized Part) $N_{i_{o(SWT)}}$	The Percentage Increase in Fatigue Life (Obtained by SWT Parameter) $N_{SWT\%}$
1	9	985	1400	246413	7,613,769	194 %
2	8	1220	1710	376435	1,376,754	159 %
3	7	1295	1710	418825	925,841	156 %
4	4	1698	2242	720053	149,450	123 %
5	3	1800	2100	800783	108,037	120 %
6	2	1850	2100	844992	92,017	118 %
7	5	2300	1325	1298303	27,533	103 %
8	6	770	2180	330788	2,267,066	99 %
9	1	1150	2700	551188	353,780	89 %

Table 6.25. The FS parameter and life results of optimized part obtained with four moving key points for the 90^0 out-of-phase loading case of $M = 1220$ Nm, $T = 1710$ Nm using SWT model.

	Loading Case	Bending Moment (N·m)	Torsional Moment (N·m)	Maximum FS Parameter (Optimized Part) $P_{o_{FS}}$	Predicted Initiation Life by FS Parameter (Optimized Part) $N_{i_{o(FS)}}$	The Percentage Increase in Fatigue Life (Obtained by FS Parameter) $N_{FS\%}$
1	7	1295	1710	0.22149E-02	996473	93 %
2	3	1800	2100	0.31630E-02	198342	93 %
3	2	1850	2100	0.32659E-02	174095	91 %
4	4	1698	2242	0.29791E-02	254588	90 %
5	5	2300	1325	0.42310E-02	64877	83 %
6	9	985	1400	0.17682E-02	3,373,535	64 %
7	8	1220	1710	0.21880E-02	1,059,807	57 %
8	6	770	2180	0.26839E-02	400948	41 %
9	1	1150	2700	0.33643E-02	154547	38 %

6.2. The Al-Si Alloy Notched Shaft

The experimental fatigue life results [67], the calculated maximum damage parameters and the crack initiation lives of the groove specimen predicted by SWT model under in-phase loading conditions are presented in Tables 6.26. The axial and torsional loads are fully-reversed (R = −1) [67]. The plot in Figure 6.23 graphically shows the comparison between the predicted crack initiation life and the experimental fatigue life.

Table 6.26. Experimental fatigue life results [67] and the results predicted by SWT parameter.

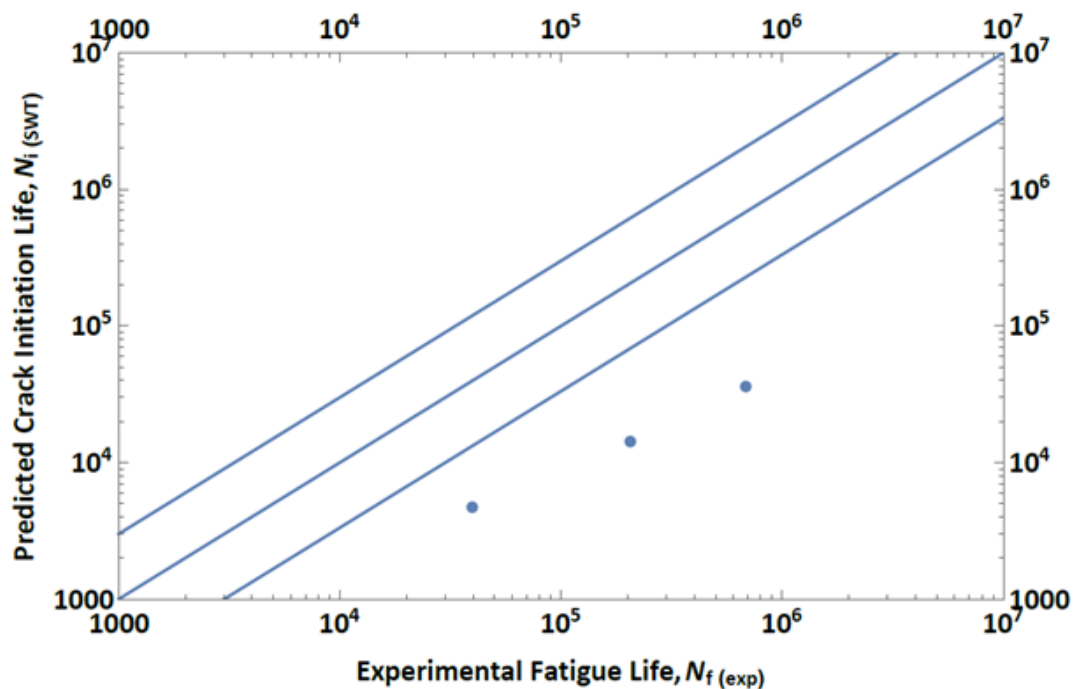| Loading Case	Axial Load (N)	Torsional Moment (N·m)	Exp. Fatigue Life N_f	Predicted Initiation Life by SWT Parameter $N_{i(SWT)}$	Maximum SWT Parameter P_{SWT}
1	34,461	63	39,413	4,660	447383
2	31,180	57	204,428	14,120	366246
3	28,741	52.5	683,147	35,803	311140

Figure 6.23. Predicted crack initiation life by SWT parameter versus experimental fatigue life for groove model.

6.2.1. Shape Optimization Results

The initial maximum moving distance parameter of groove model calculated from Equation (4.9) is 0.18 mm. The initial temperature parameter of groove model is 1.0E7.

The SWT parameter and fatigue life results of the optimized part are given in Table 6.27. The shape optimization is performed by an in-phase loading case as shown in Table 6.27. SWT parameter is selected as the objective function and two moving key points, namely, 9th and 8th key points are used. Due to the symmetry, 6th and 5th key points are located depending on the 8th and 9th key points, respectively. At the end, fatigue life of the optimum part is 286,694, which is 1930 % higher than that of the part with circular groove.

Since the circular groove has smaller radius, critical plane approaches underestimate fatigue life. In other words, the notch sensitivity factor, q, is 0.67 [71], the stress concentration factor of the notch, K_t, is 2.32, the fatigue stress concentration factor, K_f, is 1.88. There is a significant difference between the values of the factors and so, the critical plane models are not appropriate for circular groove. On the other hand, the optimized shape has larger a radius of curvature and therefore, critical plane approaches is expected to give accurate results. It may be the reason why there is a large increase in fatigue life of optimized groove compared to that of circular groove.

In comparison to the experimentally determined fatigue life, the increase in life by optimizing the shape is 40 percent. However, it is unclear whether the experimental fatigue life was measured for crack initiation or total failure [67].

The coordinates of the moving key points are given in Table 6.28. The optimized shape is shown in Figure 6.24. The SWT parameter distributions of both circular and optimized grooves are shown in Figure 6.25 and 6.26, respectively.
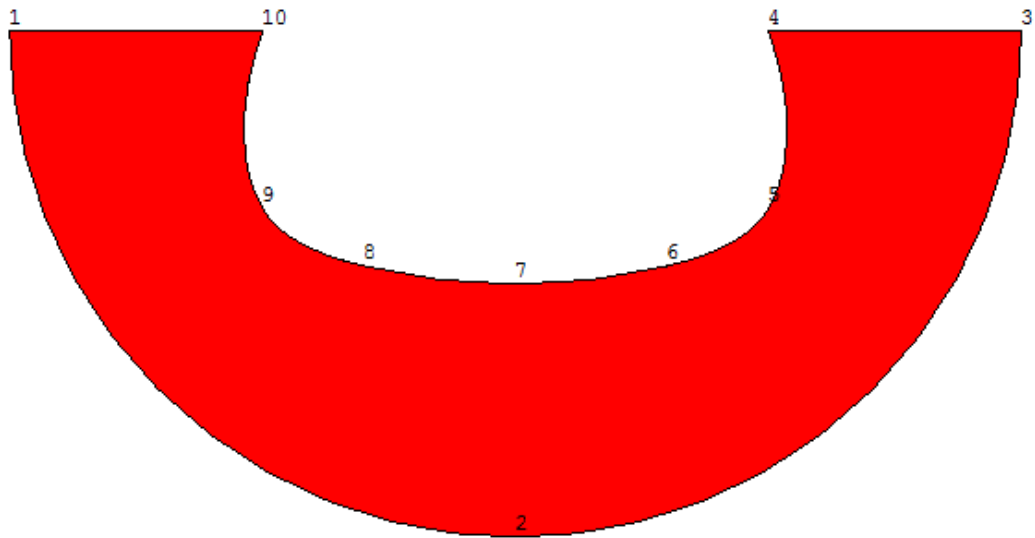
Figure 6.24. The optimized groove boundary.
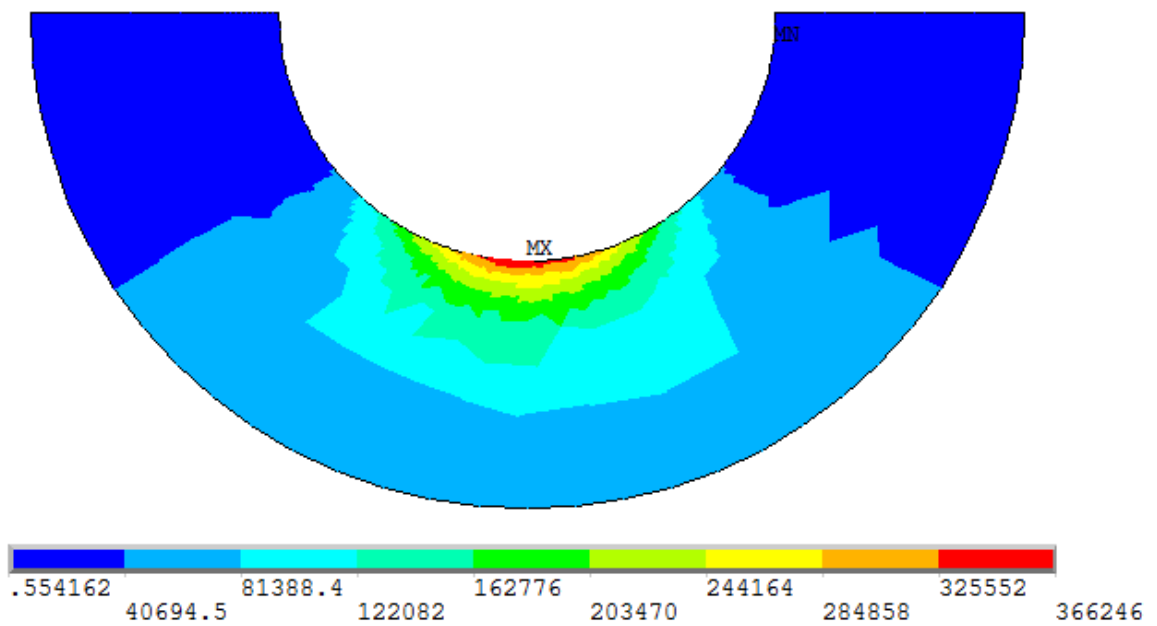
Figure 6.25. SWT parameter distribution of the circular groove part.
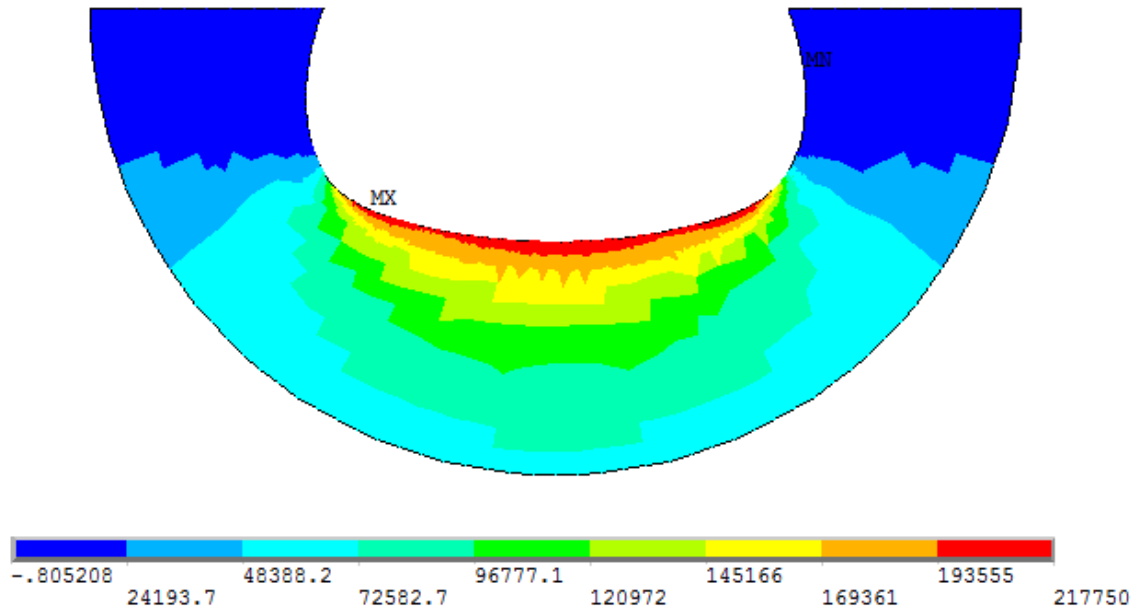
Figure 6.26. SWT parameter distribution of the optimized groove part.

Table 6.27. The SWT parameter and fatigue life results of the optimized part.

Axial Load (N)	Torsional Moment (N·m)	Maximum SWT Parameter (Optimized Part)	Predicted Initiation Life by SWT Parameter (Optimized Part)	The Percentage Increase in Fatigue Life
		$P_{o_{SWT}}$	N_o	$N_\%$
31,180	57	217750	286,694	1930 %

Table 6.28. The coordinates of moving key points of the optimized part.

	9th key point	8th key point	6th key point	5th key point
The x coordinate (mm)	12.6002	12.1451	12.1451	12.6002
The y coordinate (mm)	57.9999	57.2023	54.7977	54.0001

In the optimum shape, cavities develop at the sides. Considering that undercutting poses difficulties in manufacturing, the cavities are removed as shown in Figure 6.27 and the fatigue life is reevaluated. SWT parameter distribution of the flattened groove is shown

in Figure 6.28. The results are given in Table 6.29. Compared to the original optimized groove shape, there is a 40 % decrease in fatigue life. Therefore, if manufacturing difficulties are tolerated, the original optimized groove shape should be preferred for maximum fatigue life.
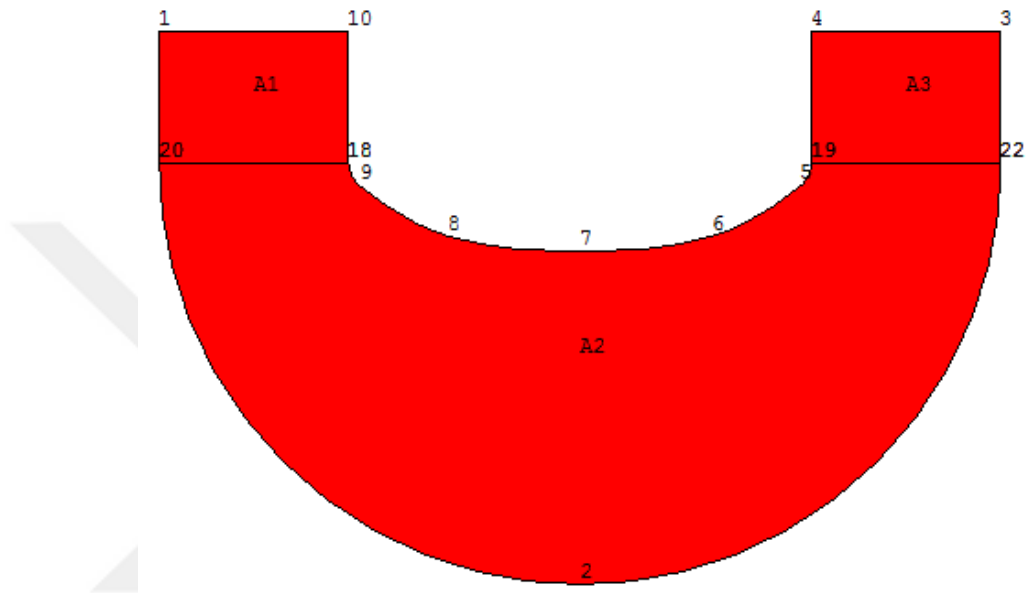
Figure 6.27. The flattened-optimized groove boundary.
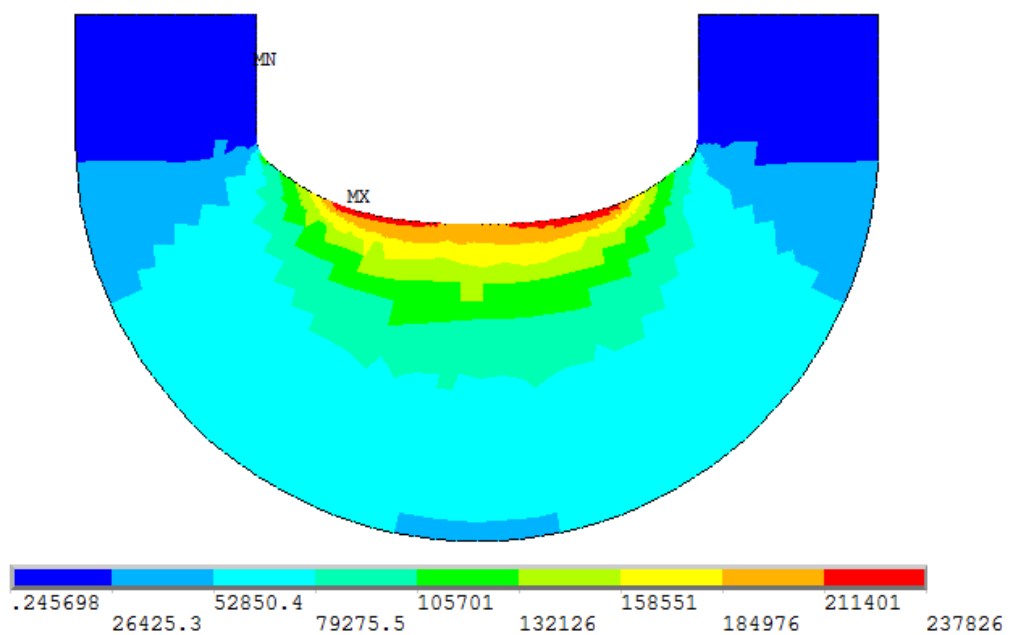
Figure 6.28. SWT parameter distribution of the flattened-optimized groove part.

Table 6.29. The SWT parameter and fatigue life results of flattened-optimized groove part.

Axial Load (N)	Torsional Moment (N·m)	Maximum SWT Parameter (Flattened-Optimized Part) $P_{FO_{SWT}}$	Predicted Initiation Life by SWT Parameter (Flattened-Optimized Part) N_o	The Percentage Increase in Fatigue Life $N_\%$
31,180	57	237826	170,856	1110 %

7. CONCLUSION

In this study, a shape optimization procedure is proposed to maximize the fatigue life of notched parts. SWT and FS models are used to estimate the fatigue life. The models are verified for the notched geometries by comparing their predictions with the empirical results reported in the literature for circular notch. The accuracy of the predictions is found to be within acceptable limits.

It is generally known that shape optimization problems involve numerous local optimums besides the globally optimal design. In this study, a modified simulated annealing algorithm is used as the search algorithm to obtain the globally optimal notch shapes. When the algorithm is used repeatedly starting from randomly chosen configurations, mostly similar results are obtained with smooth notch shapes. The modified SA algorithm searches the optimum shape having the minimum SWT or FS parameter value. Because the parameter is inversely proportional to the fatigue life, the shape with the maximum fatigue life is obtained at the end of the optimization. For both in-phase and 90^0 out-of-phase loading, a significant increase is achieved in fatigue life by shape optimization. As high as 187 percent increase in fatigue life is obtained for the shouldered shaft in comparison to circular fillets. There is no significant difference between the optimal shapes found for different loading cases. Besides, the optimal groove shape has 1930 percent increase in fatigue life; thereby, the fatigue life of the part is increased considerably.

REFERENCES

1. Kristensen, E. S. and N. F. Madsen, "On the Optimum Shape of Fillets in Plates Subjected to Multiple In-Plane Loading Cases", *International Journal for Numerical Methods in Engineering*, Vol. 10, pp. 1007-1019, 1976.

2. Parvizian, J. and R. T. Fenner, "Shape Optimization of Fillets by the Boundary Element Method", *Journal of Strain Analysis*, Vol. 37, No. 2, pp. 93-100, 2002.

3. Waldman, W., M. Heller and G. X. Chen, "Optimal Free-Form Shapes for Shoulder Fillets in Flat Plates under Tension and Bending", *International Journal of Fatigue*, Vol. 23, pp. 509-523, 2001.

4. Jones, R., P. Chaperon and M. Heller, "Structural Optimisation with Fracture Strength Constraints", *Engineering Fracture Mechanics*, Vol. 69, pp. 1403-1423, 2002.

5. Jones, R., D. Peng, P. Chaperon, S. Pitt, D. Abramson and T. Peachey, "Structural Optimisation with Damage Tolerance Constraints", *Theoretical and Applied Fracture Mechanics*, Vol. 43, pp. 133-155, 2005.

6. Sonmez, F. O., "Optimal Shape Design of Shoulder Fillets for Flat and Round Bars under Various Loadings", *Proc. IMechE*, Vol. 223, pp. 1741-1754, 2009.

7. Wilczynski, B., "Shape Optimisation for Stress Reduction around Single and Interacting Notches Based on the Fictitious Stress Method", *Engineering Analysis with Boundary Elements*, Vol. 19, pp. 117-128, 1997.

8. Hedia, H. S., "Shape Optimisation to Maximise Crack Initiation Time", *Bio-Medical Materials and Engineering*, Vol. 11, pp. 293-300, 2001.

9. Grunwald, J. and E. Schnack, "A Fatigue Model for Shape Optimization", *Structural Optimization*, Vol. 14, pp. 36-44, 1997.

10. Schnack, E. and W. Weikl, "Shape Optimization under Fatigue Using Continuum Damage Mechanics", *Computer-Aided Design*, Vol. 34, pp. 929-938, 2002.

11. Krishnapillai, K. and R. Jones, "Structural Optimization of 3D Damage Tolerant Components Comparing the Biological and Genetic Algorithm Solutions", *Engineering Failure Analysis*, Vol. 16, pp. 713-727, 2009.

12. Corriveau, G., R. Guilbault and A. Tahan, "Genetic Algorithms and Finite Element Coupling for Mechanical Optimization", *Advances in Engineering Software*, Vol. 41, pp. 422-426, 2010.

13. Heller, M., M. McDonald, M. Burchill and K. C. Watters, "Shape Optimization of Critical Stiffener Runouts for F-111 Airframe Life Extension", *Fatigue & Fracture of Engineering Materials & Structures*, Vol. 25, pp. 151-172, 2002.

14. Peng, D. and R. Jones, "An Approach Based on Biological Algorithm for Three-Dimensional Shape Optimisation with Fracture Strength Constraints", *Computer Methods in Applied Mechanics and Engineering*, Vol. 197, pp. 4383-4398, 2008.

15. Peng, D., R. Jones and S. Pitt, "Three-Dimensional Structure Optimal Design for Extending Fatigue Life by Using Biological Algorithm", *Theoretical and Applied Fracture Mechanics*, Vol. 49, pp. 26-37, 2008.

16. Peng, D. and R. Jones, "A CAD-based on Biological Method for Designing Optimal Fatigue Life", *Struct Multidisc Optim*, Vol. 37, pp. 295-304, 2009.

17. Das, R. and R. Jones, "Damage Tolerance Based Design Optimisation of a Fuel Flow Vent Hole in an Aircraft Structure", *Structural and Multidisciplinary Optimization*, Vol. 38, pp. 245-265, 2009.

18. Das, R. and R. Jones, "Fatigue Life Enhancement of Structures Using Shape Optimisation", *Theoretical and Applied Fracture Mechanics*, Vol. 52, pp. 165-179, 2009.

19. Das, R. and R. Jones, "Characteristics of the Design Surface of Damage Tolerance Parameters and their Relation to Shape Optimisation", *International Journal of Fatigue*, Vol. 70, pp. 490-502, 2015.

20. Zhang, Z. Q., J. X. Zhou, N. Zhou, X. M. Wang and L. Zhang, "Shape Optimization Using Reproducing Kernel Particle Method and an Enriched Genetic Algorithm", *Comput. Methods Appl. Mech. Engrg.*, Vol. 194, pp. 4048-4070, 2005.

21. Krishnapillai, K., R. Jones and D. Peng, "Fatigue Based Three-Dimensional Structural Design Optimisation Studies Implementing the Generalised Frost-Dugdale Crack Growth Law", *Theoretical and Applied Fracture Mechanics*, Vol. 50, pp. 30-48, 2008.

22. Krishnapillai, K., R. Jones and D. Peng, "Three-Dimensional Fatigue-Based Structural Design Optimization of Fuel Flow Vent Holes", *Engineering Failure Analysis*, Vol. 16, pp. 371-390, 2009.

23. Krishnapillai, K. and R. Jones, "Three-Dimensional Structural Design Optimisation Based on Fatigue Implementing a Genetic Algorithm and a Non-Similitude Crack Growth Law", *Finite Elements in Analysis and Design*, Vol. 45, pp. 132-146, 2009.

24. Ghelichi, R., A. Bernasconi and M. Guagliano, "Geometrical Optimization of Notches under Multi-axial Fatigue Loading", *International Journal of Fatigue*, Vol. 33, pp. 985-991, 2011.

25. Wilczynski, B. and Z. Mroz, "Optimal Design of Machine Components Using Notch Correction and Plasticity Models", *Computers and Structures*, Vol. 85, pp. 1382-1398, 2007.

26. McDonald, M. and M. Heller, "Robust Shape Optimization of Notches for Fatigue-life Extension", *Structural and Multidisciplinary Optimization*, Vol. 28, pp. 55-68, 2004.

27. Lee, T. H. and J. J. Jung, "Metamodel-based Shape Optimization of Connecting Rod Considering Fatigue Life", *Key Engineering Materials*, Vols. 306-308, pp. 211-216, 2006.

28. Andrews, J. D. and E. J. Hearn, "An Automatic Design Optimization Procedure to Minimize Fillet Bending Stresses in Involute Spur Gears", *International Journal for Numerical Methods in Engineering*, Vol. 24, pp. 975-991, 1987.

29. Rashed, G., R. Ghajar and S. J. Hashemi, "Evaluation of Multiaxial Fatigue Life Prediction Model Based on Critical Plane for Notched Specimens", *International Journal of Damage Mechanics*, Vol. 17, pp. 419-445, 2008.

30. Stephens, R. I., A. Fatemi, R. R. Stephens and H. O. Fuchs, *Metal Fatigue in Engineering*, Second Edition, John Wiley & Sons, Inc., USA, 2001.

31. Shang, D. and D. Wang, "A New Multiaxial Fatigue Damage Model Based on the Critical Plane Approach", *Int. J. Fatigue*, Vol. 20, No. 3, pp. 241-245, 1998.

32. Lagoda, T., E. Macha and W. Bedkowski, "A Critical Plane Approach Based on Energy Concepts: Application to Biaxial Random Tension-Compression High-Cycle Fatigue Regime", *International Journal of Fatigue*, Vol. 21, pp. 431-443, 1999.

33. Morel, F., "A Critical Plane Approach for Life Prediction of High Cycle Fatigue under Multiaxial Variable Amplitude Loading", *International Journal of Fatigue*, Vol. 22, pp. 101-119, 2000.

34. Shang, D., G. Sun, J. Deng and C. Yan, "Multiaxial Fatigue Damage Parameter and Life Prediction for Medium-Carbon Steel Based on the Critical Plane Approach", *International Journal of Fatigue*, Vol. 29, pp. 2200-2207, 2007.

35. Carpinteri, A., A. Spagnoli and S. Vantadori, "Multiaxial Fatigue Assessment Using a Simplified Critical Plane-Based Criterion", *International Journal of Fatigue*, Vol. 33, pp. 969-976, 2011.

36. Li, J., Z. Zhang, Q. Sun and C. Li, "Multiaxial Fatigue Life Prediction for Various Metallic Materials Based on the Critical Plane Approach", *International Journal of Fatigue*, Vol. 33, pp. 90-101, 2011.

37. Smith, K. N., P. Watson and T. H. Topper, "A Stress–Strain Function for the Fatigue of Metals", *Journal of Materials*, Vol. 5, No. 4, pp. 767-778, 1970.

38. Fatemi, A. and D. F. Socie, "A Critical Plane Approach to Multiaxial Fatigue Damage Including out-of-Phase Loading", *Fatigue Fract. Engng Mater. Struct.*, Vol. 11, No. 3, pp. 149-165, 1988.

39. McDiarmid, D. L., "A General Criterion for High Cycle Multiaxial Fatigue Failure", *Fatigue & Fracture of Engineering Materials & Structures*, Vol. 14, No. 4, pp. 429-453, 1991.

40. Dang-Van, K., "Macro-Micro Approach in High-Cycle Multiaxial Fatigue", *Advances in Multiaxial Fatigue, ASTM STP 1191, D. L. McDowell and R. Ellis, Eds., American Society for Testing and Materials, Philadelphia*, pp. 120-130, 1993.

41. Carpinteri, A. and A. Spagnoli, "Multiaxial High-Cycle Fatigue Criterion for Hard Metals", *International Journal of Fatigue*, Vol. 23, pp. 135-145, 2001.

42. Liu, Y. and S. Mahadevan, "Multiaxial High-Cycle Fatigue Criterion and Life Prediction for Metals", *International Journal of Fatigue*, Vol. 27, pp. 790-800, 2005.

43. Socie, D. F., L. A. Waill and D. F. Dittmer, "Biaxial Fatigue of Inconel 718 Including Mean Stress Effects", *Multiaxial Fatigue, ASTM STP 853, K. J. Miller and M. W. Brown, Eds., American Society for Testing and Materials, Philadelphia*, pp. 463-481, 1985.

44. Brown, M. W. and K. J. Miller, "A Theory for Fatigue Failure under Multiaxial Stress-Strain Conditions", *Proc Instn Mech Engrs*, Vol. 187, pp. 745-755, 1973.

45. Gates, N. and A. Fatemi, "Notched Fatigue Behavior and Stress Analysis under Multiaxial States of Stress", *International Journal of Fatigue*, Vol. 67, pp. 2-14, 2014.

46. Lee, Y., J. Pan, R. Hathaway and M. Barkey, *Fatigue Testing and Analysis (Theory and Practice)*, Elsevier, Inc., USA, 2005.

47. Liu, K. C., "A Method Based on Virtual Strain-Energy Parameters for Multiaxial Fatigue Life Prediction", *Advances in Multiaxial Fatigue, ASTM STP 1191, D. L. McDowell and R. Ellis, Eds., American Society for Testing and Materials, Philadelphia*, pp. 67-84, 1993.

48. Pan, W., C. Hung and L. Chen, "Fatigue Life Estimation under Multiaxial Loadings", *International Journal of Fatigue*, Vol. 21, pp. 3-10, 1999.

49. Varvani-Farahani, A., "A New Energy-Critical Plane Parameter for Fatigue Life Assessment of Various Metallic Materials Subjected to in-Phase and out-of-Phase Multiaxial Fatigue Loading Conditions", *International Journal of Fatigue*, Vol. 22, pp. 295-305, 2000.

50. Jahed, H. and A. Varvani-Farahani, "Upper and Lower Fatigue Life Limits Model Using Energy-Based Fatigue Properties", *International Journal of Fatigue*, Vol. 28, pp. 467-473, 2006.

51. Fatemi, A. and N. Shamsaei, "Multiaxial Fatigue: An Overview and Some Approximation Models for Life Estimation", *International Journal of Fatigue*, Vol. 33, pp. 948-958, 2011.

52. Reis, L., B. Li and M. Freitas, "Analytical and Experimental Studies on Fatigue Crack Path under Complex Multi-axial Loading", *Fatigue Fract Engng Mater Struct*, Vol. 29, pp. 281-289, 2006.

53. Han, C., X. Chen and K. S. Kim, "Evaluation of Multiaxial Fatigue Criteria under Irregular Loading", *International Journal of Fatigue*, Vol. 24, pp. 913-922, 2002.

54. Jen, Y. and W. Wang, "Crack Initiation Life Prediction for Solid Cylinders with Transverse Circular Holes under in-Phase and out-of-Phase Multiaxial Loading", *International Journal of Fatigue*, Vol. 27, pp. 527-539, 2005.

55. Vazquez, J., C. Navarro and J. Dominguez, "On the Estimation of Fatigue Life in Notches Differentiating the Phases of Crack Initiation and Propagation", *Fatigue Fract Engng Mater Struct*, Vol. 33, pp. 22-36, 2009.

56. Shang, D., W. Yao and D. Wang, "A New Approach to the Determination of Fatigue Crack Initiation Size", *Int. J. Fatigue*, Vol. 20, No. 9, pp. 683-687, 1998.

57. Harvey, W., "Biaxial Fatigue of the SAE Unnotched Shaft Test Specimen", *Multiaxial Fatigue: Analysis and Experiments AE-14, Gall E. Leese and Darrell Socie, Co-editors, Society of Automotive Engineers, Inc.*, pp. 107-119, 1989.

58. Ranganathan, N., H. Aldroe, F. Lacroix, F. Chalon, R. Leroy and A. Tougui, "Fatigue Crack Initiation at a Notch", *International Journal of Fatigue*, Vol. 33, pp. 492-499, 2011.

59. Ugural, A. and S. Fenster, *Advanced Strength and Applied Elasticity*, Third Edition, Prentice-Hall, Inc., New Jersey, USA, 1995.

60. Socie, D., "Critical Plane Approaches for Multiaxial Fatigue Damage Assessment", *Advances in Multiaxial Fatigue, ASTM STP 1191, D. L. McDowell and R. Ellis, Eds., American Society for Testing and Materials, Philadelphia*, pp. 7-36, 1993.

61. Navarro, C., J. Vazquez and J. Dominguez, "A General Model to Estimate Life in Notches and Fretting Fatigue", *Engineering Fracture Mechanics*, Vol. 78, pp. 1590-1601, 2011.

62. Akbulut, M. and F. O. Sonmez, "Design Optimization of Laminated Composites Using a New Variant of Simulated Annealing", *Computers and Structures*, Vol. 89, pp. 1712-1724, 2011.

63. Ali, M. M., A. Törn and S. Viitanen, "A Direct Search Variant of the Simulated Annealing Algorithm for Optimization Involving Continuous Variables", *Computers & Operations Research*, Vol. 29, pp. 87-102, 2002.

64. Sonmez, F. O., "Shape Optimization of 2D Structures Using Simulated Annealing", *Comput. Methods Appl. Mech. Engrg.*, Vol. 196, pp. 3279-3299, 2007.

65. Leese, G. E. and J. Morrow, "Low Cycle Fatigue Properties of a 1045 Steel in Torsion", *Multiaxial Fatigue, ASTM STP 853, K. J. Miller and M. W. Brown, Eds., American Society of Testing and Materials, Philadelphia*, pp. 482-496, 1985.

66. Karadeniz, C. Ö., *Strain Energy Based Fatigue Model for Notched Part Subjected to Multiaxial Loading*, M.S. Thesis, Boğaziçi University, 2013.

67. Liu, X., T. Su, Y. Zhang and M. Yuan, "A Multiaxial High-Cycle Fatigue Life Evaluation Model for Notched Structural Components", *International Journal of Fatigue*, Vol. 80, pp. 443-448, 2015.

68. Che, X., X. Liang, L. Chen, L. Chen and F. Li, "Microstructures and Low-Cycle Fatigue Behavior of Al-9.0%Si-4.0%Cu-0.4%Mg(-0.3%Sc) Alloy", *Jinshu Xuebao/Acta Metallurgica Sinica*, Vol. 50, No. 9, pp. 1046-1054, 2014.

69. Fash, J. W., *An Evaluation of Damage Development During Multiaxial Fatigue of Smooth and Notched Specimens*, Ph.D. Thesis, Department of Mechanical and Industrial Engineering, University of Illinois at Urbana-Champaign, 1985.

70. Fash, J. W., D. F. Socie and D. L. McDowell, "Fatigue Life Estimates for a Simple Notched Component under Biaxial Loading", *Multiaxial Fatigue, ASTM STP 853, K. J. Miller and M. W. Brown, Eds., American Society of Testing and Materials, Philadelphia*, pp. 497-513, 1985.

71. Bannantine, J. A., J. J. Comer and J. L. Handrock, *Fundamentals of Metal Fatigue Analysis*, Prentice-Hall, Inc., New Jersey, USA, 1990.

72. Kirkpatrick, S., C. D. Gelatt and M. P. Vecchi, "Optimization by Simulated Annealing", *Science*, Vol. 220, pp. 671-680, 1983.

APPENDIX A: THREE-DIMENSIONAL (3D) STRESS TRANSFORMATION

A small tetrahedron shown in Figure A.1 (a) subjected to stresses can be considered for the 3D transformation.
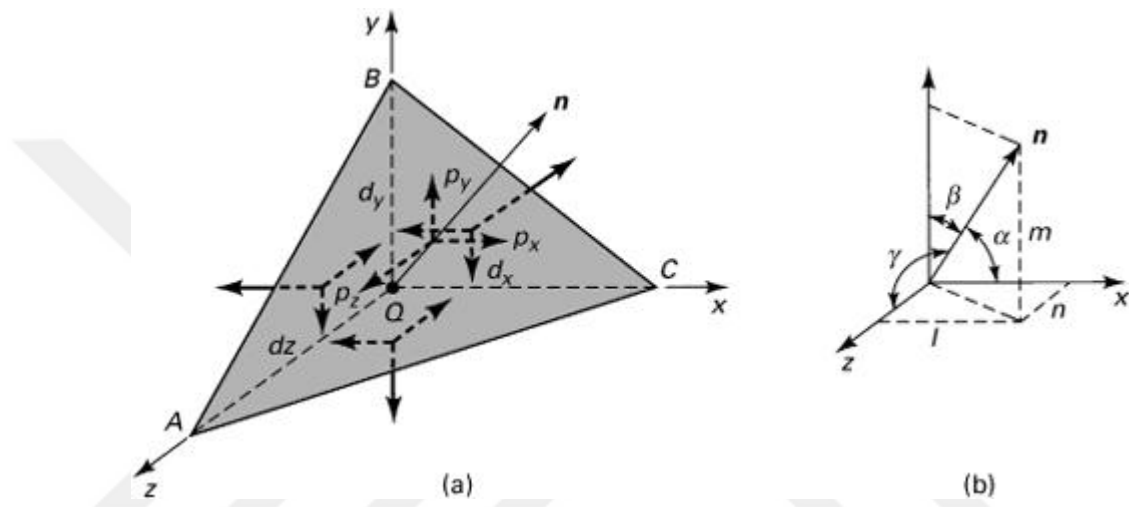
Figure A.1. (a) The representation of stress components. (b) The orientation of the oblique plane [59].

p_x, p_y, p_z are the stress components of stress resultant p on the ABC oblique plane. The orientation of the oblique plane can be expressed with the angles, α, β, γ between a unit normal n of the plane and the x, y, z directions as in Figure A.1 (b). The direction cosines are expressed as

$$\cos \alpha = \cos(n, x) = l \tag{A.1}$$

$$\cos \beta = \cos(n, y) = m \tag{A.2}$$

$$\cos \gamma = \cos(n, z) = n \tag{A.3}$$

Considering the three perpendicular planes *QAB, QAC, QBC* and the equilibrium of forces, the stress components are expressed as

$$p_x = \sigma_x l + \tau_{xy} m + \tau_{xz} n \qquad (A.4)$$

$$p_y = \tau_{xy} l + \sigma_y m + \tau_{yz} n \qquad (A.5)$$

$$p_z = \tau_{xz} l + \tau_{yz} m + \sigma_z n \qquad (A.6)$$

The direction cosine relations between the $x' y' z'$ system, where x' is coincided with the unit normal $\boldsymbol{n}$ while y', z' lie on the oblique plane, and the xyz system are given in Table A.1.

Table A.1. The direction cosine representation.

	x	y	z
x'	$l_1 = \cos(x', x)$	$m_1 = \cos(x', y)$	$n_1 = \cos(x', z)$
y'	$l_2 = \cos(y', x)$	$m_2 = \cos(y', y)$	$n_2 = \cos(y', z)$
z'	$l_3 = \cos(z', x)$	$m_3 = \cos(z', y)$	$n_3 = \cos(z', z)$

The 3D stress transformation equations are obtained by projecting p_x, p_y and p_z in the x', y', z' directions.

The normal stress components $\sigma_{x'}$, $\sigma_{y'}$, $\sigma_{z'}$ for any orientation can be obtained by the following equations

$$\sigma_{x'} = \sigma_x l_1^2 + \sigma_y m_1^2 + \sigma_z n_1^2 + 2(\tau_{xy} l_1 m_1 + \tau_{yz} m_1 n_1 + \tau_{xz} l_1 n_1) \qquad (A.7)$$

$$\sigma_{y'} = \sigma_x l_2^2 + \sigma_y m_2^2 + \sigma_z n_2^2 + 2(\tau_{xy} l_2 m_2 + \tau_{yz} m_2 n_2 + \tau_{xz} l_2 n_2) \qquad (A.8)$$

$$\sigma_{z'} = \sigma_x l_3^2 + \sigma_y m_3^2 + \sigma_z n_3^2 + 2(\tau_{xy} l_3 m_3 + \tau_{yz} m_3 n_3 + \tau_{xz} l_3 n_3) \qquad (A.9)$$

The shear stress components $\tau_{x'y'}$, $\tau_{x'z'}$, $\tau_{y'z'}$ are expressed as

$$\tau_{x'y'} = \sigma_x l_1 l_2 + \sigma_y m_1 m_2 + \sigma_z n_1 n_2 + \tau_{xy}(l_1 m_2 + m_1 l_2)$$
$$+ \tau_{yz}(m_1 n_2 + n_1 m_2) + \tau_{xz}(n_1 l_2 + l_1 n_2)$$

(A.10)

$$\tau_{x'z'} = \sigma_x l_1 l_3 + \sigma_y m_1 m_3 + \sigma_z n_1 n_3 + \tau_{xy}(l_1 m_3 + m_1 l_3)$$
$$+ \tau_{yz}(m_1 n_3 + n_1 m_3) + \tau_{xz}(n_1 l_3 + l_1 n_3)$$

(A.11)

$$\tau_{y'z'} = \sigma_x l_2 l_3 + \sigma_y m_2 m_3 + \sigma_z n_2 n_3 + \tau_{xy}(m_2 l_3 + l_2 m_3)$$
$$+ \tau_{yz}(n_2 m_3 + m_2 n_3) + \tau_{xz}(l_2 n_3 + n_2 l_3)$$

(A.12)

APPENDIX B: THREE-DIMENSIONAL (3D) STRAIN TRANSFORMATION

The strain transformation equations can be obtained from the stress expressions replacing σ and τ by ε and $\gamma/2$, respectively.

The normal strain components $\varepsilon_{x'}$, $\varepsilon_{y'}$, $\varepsilon_{z'}$ can be obtained for any specified orientation by the following equations

$$\varepsilon_{x'} = \varepsilon_x l_1{}^2 + \varepsilon_y m_1{}^2 + \varepsilon_z n_1{}^2 + \gamma_{xy} l_1 m_1 + \gamma_{yz} m_1 n_1 + \gamma_{xz} l_1 n_1 \tag{B.1}$$

$$\varepsilon_{y'} = \varepsilon_x l_2{}^2 + \varepsilon_y m_2{}^2 + \varepsilon_z n_2{}^2 + \gamma_{xy} l_2 m_2 + \gamma_{yz} m_2 n_2 + \gamma_{xz} l_2 n_2 \tag{B.2}$$

$$\varepsilon_{z'} = \varepsilon_x l_3{}^2 + \varepsilon_y m_3{}^2 + \varepsilon_z n_3{}^2 + \gamma_{xy} l_3 m_3 + \gamma_{yz} m_3 n_3 + \gamma_{xz} l_3 n_3 \tag{B.3}$$

The shear strain components $\gamma_{x'y'}$, $\gamma_{x'z'}$, $\gamma_{y'z'}$ are expressed as

$$\begin{aligned} \gamma_{x'y'} = 2(\varepsilon_x l_1 l_2 + \varepsilon_y m_1 m_2 + \varepsilon_z n_1 n_2) + \gamma_{xy}(l_1 m_2 + m_1 l_2) \\ + \gamma_{yz}(m_1 n_2 + n_1 m_2) + \gamma_{xz}(n_1 l_2 + l_1 n_2) \end{aligned} \tag{B.4}$$

$$\begin{aligned} \gamma_{x'z'} = 2(\varepsilon_x l_1 l_3 + \varepsilon_y m_1 m_3 + \varepsilon_z n_1 n_3) + \gamma_{xy}(l_1 m_3 + m_1 l_3) \\ + \gamma_{yz}(m_1 n_3 + n_1 m_3) + \gamma_{xz}(n_1 l_3 + l_1 n_3) \end{aligned} \tag{B.5}$$

$$\begin{aligned} \gamma_{y'z'} = 2(\varepsilon_x l_2 l_3 + \varepsilon_y m_2 m_3 + \varepsilon_z n_2 n_3) + \gamma_{xy}(m_2 l_3 + l_2 m_3) \\ + \gamma_{yz}(n_2 m_3 + m_2 n_3) + \gamma_{xz}(l_2 n_3 + n_2 l_3) \end{aligned} \tag{B.6}$$

For a given stress-strain state at any point of material, principal stresses or strains can be calculated as follows

$$A = \begin{bmatrix} \sigma_x & \tau_{xy} & \tau_{xz} \\ \tau_{xy} & \sigma_y & \tau_{yz} \\ \tau_{xz} & \tau_{yz} & \sigma_z \end{bmatrix} \tag{B.7}$$

$$B = \begin{bmatrix} \varepsilon_x & \frac{1}{2}\gamma_{xy} & \frac{1}{2}\gamma_{xz} \\ \frac{1}{2}\gamma_{xy} & \varepsilon_y & \frac{1}{2}\gamma_{yz} \\ \frac{1}{2}\gamma_{xz} & \frac{1}{2}\gamma_{yz} & \varepsilon_z \end{bmatrix} \tag{B.8}$$

Principal stresses σ_1, σ_2, σ_3 and principal strains ε_1, ε_2, ε_3 are the eigenvalues of stress tensor, A and strain tensor, B, respectively.

The orientation of a plane where principal values are observed is defined with direction cosines as indicated in Table A.1. Considering that strain state of a point is given, the direction cosines of principal orientation can be calculated as follows:

$$\left(\varepsilon_x - \varepsilon_{p,i}\right)l_i + \frac{1}{2}\gamma_{xy}m_i + \frac{1}{2}\gamma_{xz}n_i = 0 \tag{B.9}$$

$$\frac{1}{2}\gamma_{xy}l_i + \left(\varepsilon_y - \varepsilon_{p,i}\right)m_i + \frac{1}{2}\gamma_{yz}n_i = 0 \tag{B.10}$$

$$\frac{1}{2}\gamma_{xz}l_i + \frac{1}{2}\gamma_{yz}m_i + \left(\varepsilon_z - \varepsilon_{p,i}\right)n_i = 0 \tag{B.11}$$

where $i = 1,3$, $\varepsilon_{p,i}$ are the principal strains and l_i, m_i, n_i are the direction cosines of principal strain orientations.

The nontrivial solution of the equation systems ($[A]\{x\} = 0$) is obtained for nine direction cosines.

$$\begin{bmatrix} (\varepsilon_x - \varepsilon_{p,i}) & \frac{1}{2}\gamma_{xy} & \frac{1}{2}\gamma_{xz} \\ \frac{1}{2}\gamma_{xy} & (\varepsilon_y - \varepsilon_{p,i}) & \frac{1}{2}\gamma_{yz} \\ \frac{1}{2}\gamma_{xz} & \frac{1}{2}\gamma_{yz} & (\varepsilon_z - \varepsilon_{p,i}) \end{bmatrix} \begin{Bmatrix} l_i \\ m_i \\ n_i \end{Bmatrix} = 0 \qquad (B.12)$$

APPENDIX C: SHAPE OPTIMIZATION METHODS

Shape optimization methods are used to obtain the most appropriate geometry for a specified boundary of an engineering component by allowing the boundary shape to be varied. In shape optimization techniques, the objective function to be minimized for a specified boundary of the component is defined by considering the minimization of peak stresses, stress intensity factors, volume of the part, etc. In each iteration, the objective function is aimed to be minimized until no further improvement is obtained. Shape optimization methods increase the strength and the lifetime of parts under same loading conditions, they provide less weight structures without reducing the strength of them.

Global stochastic optimization methods are used to search the design space of the structure in which design variables are allowed to move any direction without considering the starting point. The simulated annealing (SA) is a well-known stochastic optimization method.

C.1. Simulated Annealing (SA) Algorithm

Simulated Annealing (SA) algorithm is one of the most preferred global stochastic algorithms. It was firstly proposed by Kirkpatrick *et al*. [72]. The algorithm is based on iterative process in which configurations in coordinate system are generated to improve the system. During the process, if a configuration that provides a better cost function is obtained, then the current configuration is accepted and replaced by the previous one. The process is randomly repeated starting from different configurations in a space until a further improvement is not obtained.

When a random configuration is generated by giving a random displacement to a design variable such as a nodal coordinate of system, the current cost function, f_c is obtained.

If the current configuration's cost function, f_c is equal to or less than the previous one, f_p $(f_c - f_p \leq 0)$, then the current one is accepted and the next iteration is started from the accepted one.

On the contrary, if $f_c - f_p > 0$, the acceptability depends on the situation described below.

$$P = \exp\left(-(f_c - f_p)/T_k\right) \tag{C.1}$$

where T_c is a temperature parameter which is associated with the physical meaning of it. The 'melting' phase is realized at high temperature and by decreasing it slowly, 'freezing' process takes place until a steady phase is reached. In optimization, at high temperature values, the likelihood of acceptance of current configuration will be high. After it is lowered to a specific value during iterations, there is not any improvement and the optimization process is stopped.

A randomly generated number between 0 and 1 is compared with P. If P is greater than that number, the current configuration will be accepted, otherwise the previous one will be used. Acceptability, A is given by the following equation.

$$A = \begin{cases} 1, & f_c - f_p \leq 0 \\ \exp\left(-(f_c - f_p)/T_k\right), & f_c - f_p > 0 \end{cases} \tag{C.2}$$

C.2. Direct Search Simulated Annealing (DSA) Algorithm

The DSA algorithm was presented by Ali *et al.* [63] as a modified version of simulated annealing algorithm. The main difference of DSA is that a set of current configurations rather than a single one as in SA are used for optimization. It is a memory-based global stochastic algorithm in which the best solution is kept.

C.2.1. Acceptability of current configuration

In the DSA algorithm, N different random configurations are initially generated and their cost function values are calculated and stored in an array A. The highest and lowest cost function values in A are stored as f_h and f_l, respectively. Then, a new configuration is again randomly generated by giving random displacements to nodes of a moving boundary as a starting point and its cost, f_c is calculated. The probability of acceptance, acceptability, A is given by the following equation.

$$A = \begin{cases} 1, & f_c - f_h \leq 0 \\ \exp\left(-(f_c - f_h)/T_k\right), & f_c - f_h > 0 \end{cases} \tag{C.3}$$

When $f_c - f_h \leq 0$, the current configuration is accepted and replaced by the worst configuration. After replacement, the cost functions are updated to obtain f_h and f_l for new condition. Iterations are repeated until the end of Markov chain. In this manner, the best configuration is always kept in array.

The current Markov chain (k th chain) will be ended if a generated configuration has a cost value less than the value of lowest cost, f_l of that chain and the next Markov chain will be started. During the execution of k th chain, if a cost value less than f_l is not obtained, then iterations are executed until the end of that chain.

C.2.2. The cooling schedule

The temperature parameter, T_k is kept constant during the execution of a chain. At the end of each chain, its value decreases. The initial temperature, T_0 value should be high to be performed an efficient process. At high values of initial temperature, this 'melting' process takes place in which the space is completely searched and nearly all current configurations are accepted. At low initial temperature, the algorithm may stick in a local minimum at the beginning of process.

C.2.3. Length of the Markov chains

It is assumed that the length of the Markov chains should be large enough to allow the algorithm to search all possible locations of the neighborhood of a point. Length of a k th Markov chain is determined by the following equation

$$L_k = L + L(1 - \exp(-(f_h - f_l))) \qquad \text{(C.4)}$$

where

$$L = 10 \; x \; n \qquad \text{(C.5)}$$

where n is the dimension of problem such as the number of design variables. If x and y coordinates of the nodes of a boundary to be optimized are selected as variables, then

$$n = 2 \; x \; m \qquad \text{(C.6)}$$

where m is the number of moving nodes. As can be seen in Equation (C.4), a Markov chain has a value between L and $2L$. When the difference between f_h and f_l is high, the iterations executed in a Markov chain will increase to allow the evaluations of more configurations unless a cost function which has a value less than f_l is obtained.

C.2.4. The temperature control parameter

The temperature parameter, T_k must be controlled with a parameter α_k by the following expression.

$$T_{k+1} = \alpha_{k+1} \; x \; T_k \qquad \text{(C.7)}$$

where α_{k+1} is a parameter used for the determination of the $(k + 1)$ th Markov chain's temperature parameter, T_{k+1}. There are three possible α_{k+1} values depending on the relation between Markov chain lengths.

$$\alpha_{k+1} = \alpha_{max}, \quad if \ L_{k+1} > L'_{k+1} \tag{C.8}$$

where L_{k+1} is the calculated $(k+1)$ th Markov chain length, L'_{k+1} is the number of configurations (trials) generated in the $(k+1)$ th Markov chain.

$$\alpha_{k+1} = \begin{cases} \alpha_k - (\alpha_k - \alpha_{min})(1 - \dfrac{L'_k}{L_{k+1}}), & L_{k+1} > L'_k \\ \alpha_{max} - (\alpha_{max} - \alpha_k)\dfrac{L_{k+1}}{L'_k}, & L_{k+1} \le L'_k \end{cases} \tag{C.9}$$

where α_{max} and α_{min} are two constants that were given as 0.90 and 0.80 in the paper, respectively. L'_k is the executed number of configurations in k th Markov chain. Initial value of α_k, $\alpha_{k,initial}$ is given as

$$\alpha_{k,initial} = \frac{(\alpha_{max} + \alpha_{min})}{2} \tag{C.10}$$

C.2.5. Stopping Criteria

The algorithm is ended when no considerable further development is obtained. There are two stopping criteria in which the temperature parameter and the difference between highest and lowest cost functions are evaluated.

$$T_k \le \varepsilon_1 \tag{C.11}$$

$$f_h - f_l \le \varepsilon_2 \tag{C.12}$$

where ε_1 and ε_2 are two constants both considered as 0.05 in the paper.